EFFECT OF VERTICAL GROUND MOTION ON THE PERFORMANCE OF HIGH-RISE BUILDINGS

A THESIS SUBMITTED TO
THE GRADUATE SCHOOL OF NATURAL AND APPLIED SCIENCES
OF
MIDDLE EAST TECHNICAL UNIVERSITY

BY

ENGİN KESKİN

IN PARTIAL FULFILLMENT OF THE REQUIREMENTS
FOR
THE DEGREE OF MASTER OF SCIENCE
IN
EARTHQUAKE STUDIES

APRIL 2020

Approval of the thesis:

EFFECT OF VERTICAL GROUND MOTION ON THE PERFORMANCE OF HIGH-RISE BUILDINGS

submitted by **ENGİN KESKİN** in partial fulfillment of the requirements for the degree of **Master of Science in Earthquake Studies, Middle East Technical University** by,

Prof. Dr. Halil Kalıpçılar
Dean, Graduate School of **Natural and Applied Sciences**

Prof. Dr. Ayşegül Askan Gündoğan
Head of the Department, **Earthquake Studies**

Prof. Dr. Murat Altuğ Erberik
Supervisor, **Earthquake Studies, METU**

Prof. Dr. Ayşegül Askan Gündoğan
Co-Supervisor, **Earthquake Studies, METU**

Examining Committee Members:

Prof. Dr. Erdem Canbay
Civil Eng, METU

Prof. Dr. Murat Altuğ Erberik
Earthquake Studies, METU

Prof. Dr. Ayşegül Askan Gündoğan
Earthquake Studies, METU

Assoc. Prof. Dr. Burcu Burak Bakır
Civil Eng., METU

Asst. Prof. Dr. Tuba Eroğlu Azak
Civil Eng., National Defence Uni

Date: 28.04.2020

I hereby declare that all information in this document has been obtained and presented in accordance with academic rules and ethical conduct. I also declare that, as required by these rules and conduct, I have fully cited and referenced all material and results that are not original to this work.

Name, Last name : Engin Keskin

Signature :

ABSTRACT

EFFECT OF VERTICAL GROUND MOTION ON THE PERFORMANCE OF HIGH-RISE BUILDINGS

Keskin, Engin
Master of Science, Earthquake Studies
Supervisor : Prof. Dr. Murat Altuğ Erberik
Co-Supervisor: Prof. Dr. Ayşegül Askan Gündoğan

April 2020, 159 pages

Throughout the history, the creation of new environments to support the needs of urban populations has been attained to a great extent through horizontal construction. When settlements with limited territories started to face rapid population growth, designers and government bodies started to give preference to vertical construction as it allowed urban growth within bounds. Vertical construction, also referred to as high-rise buildings, has quickly become an integral method for the development and expansion of settlements into urban areas, and cities into megacities. As the trend for construction moves from horizontal to vertical, there is a need for engineers to introduce new concepts and notions for the engineering of high-rise buildings that are safe and structurally sound. This study focuses on the effect of vertical components of ground motion records on the performance of a typical high-rise buildings. To see the effect of the vertical ground motion, 100 earthquake records are selected according to the source-to-site distance, site class, and earthquake magnitude. A generic high-rise reinforced concrete building designed according to Turkish Building Seismic Code (*TBSC18*) has been evaluated in terms of inter-story drift ratio, overturning moment, column axial force, and story shear force under the selected earthquake records. According to the nonlinear time history analysis, it was observed that the vertical ground motion has a very slighly effect in terms of inter-story drift ratio, overturning moment and base shear. However, it is observed that the vertical ground motion has a significant effect on the axial force on columns as expected. Results show that axial force (both compressive and tension) on a column, normalized with column axial capacity, is increased by 20% in the near-field zone. The observed maximum increase in compressive force is around 105%, 57%, and 68% of the column axial capacity for site classes A,B, anc C, respectively. When the results are examined in detail it is seen that the influence of vertical ground motion increases significantly when the contribution of horizontal ground motion is small. The above observations prove that the effect of vertical ground motion should be included during seismic design of high-rise structures.

Keywords: Vertical Ground Motion, High-Rise Buildings. Non-Linear Time History Analysis, Inter-story Drift Ratio, Story Shear Force, Column Axial Force

ÖZ

DÜŞEY DEPREM YER HAREKETİNİN YÜKSEK BİNALARIN PERFORMANSINA ETKİSİ

Keskin, Engin
Yüksek Lisans, Deprem Çalışmaları
Tez Yöneticisi: Prof. Dr. Murat Altuğ Erberik
Ortak Tez Yöneticisi: Prof. Dr. Ayşegül Askan Gündoğan

Nisan 2020, 159 sayfa

Kentsel nüfusun ihtiyaçlarını desteklemek için yeni ortamların yaratılması, tarih boyunca büyük ölçüde yatay mimari yoluyla elde edilmiştir. Sınırlı bölgeleri olan yerleşimler hızlı nüfus artışı ile karşı karşıya kalmaya başladığında, tasarımcılar ve hükümet organları belirli sınırlar içinde kentsel büyümeye izin verildiği için dikey mimariyi tercih etmeye başlamıştır. Yüksek binalar olarak da adlandırılan dikey mimari, hızlı bir şekilde yerleşimlerin kentleşmesi ve şehirlerin mega şehir haline gelmesi için tercih edilen bir yöntem haline gelmiştir. İnşa etme eğilimi yataydan dikeye doğru ilerledikçe, mühendislerin güvenli ve yapısal olarak sağlam yüksek katlı binaların mühendisliği için yeni bir boyut getirmeleri gerekmektedir. Bu çalışma, düşey deprem hareketlerinin tipik bir yüksek yapının performansına etkisi üzerine odaklanmıştır.

Düşey deprem hareketinin etkisini görmek için, kaynak-saha mesafesi, zemin sınıfı ve deprem büyüklüğüne göre 100 deprem kaydı seçilmiştir. Türkiye Bina Deprem Yönetmeliğine (*TBDY18*) göre tasarlanan betonarme bina, bu deprem kayıtları altında etkin göreli kat ötelemesi, devrilme momenti, kolon eksenel kuvveti ve kat kesme kuvveti açısından değerlendirilmiştir. Zaman tanım alanında doğrusal

olmayan analiz sonuçlarına göre, düşey deprem hareketinin göreli kat ötelemesi, devrilme momenti ve taban kesmesi açısından önemli bir etkisi olmadığı gözlenmiştir. Ayrıca, düşey deprem hareketinin kolonlar üzerindeki eksenel kuvvet üzerinde de önemli bir etkisi vardır. Kolon eksenel kapasitesi ile normalize edilen sonuçlar, kolon üzerindeki eksenel kuvvet (hem basınç hem çekme) değişiminin yakın alan bölgesinde %20 arttığını göstermektedir. Gözlenen maksimum basınç artışı, A, B, ve C zemin sınıflarına göre sırasıyla kolon eksenel kapasitesinin yaklaşık %105'i, %57'si, ve %68'idir. Sonuçlar ayrıntılı olarak incelendiğinde, yatay yer hareketinin katkısı az olduğunda düşey deprem hareketinin etkisinin önemli ölçüde arttığı görülmüştür. Yukarıda bahsi geçen tüm gözlemler, yüksek yapıların deprem tasarımı yapılırken düşey deprem hareketinin de dikkate alınması gerektiği yönündeki iddiayı kanıtlamaktadır.

Anahtar Kelimeler: Düşey Deprem Hareketi, Yüksek Bina, Zaman Tanım Alanında Doğrusal Olmayan Analiz, Kat Ötelemesi, Kat Kesme Kuvveti, Kolon Eksenel Kuvveti

To my family.

ACKNOWLEDGMENTS

I wish to express my deepest gratitude to my supervisor Prof. Dr. Murat Altuğ Erberik and co-supervisor Prof. Dr. Ayşegül Askan Gündoğan for supporting my interest in shaping this study into an opportunity of self-improvement. For this, and for their guidance throughout the research, I am extremely grateful.

I would like to acknowledge my colleagues Caner Soydaş, Can Karadeniz, and Gökberk Işık from Arup Ankara Office for their insights on the technical aspects of this research and for helping me improve my work with their suggestions and comments through each stage of the process.

I would like to express my appreciation to my friends for simply being there for me.

Finally, I would like to thank my family for their guidance, encouragement and moral support all through my life.

TABLE OF CONTENTS

LIST OF TABLES

TABLES

LIST OF FIGURES

FIGURES

LIST OF ABBREVIATIONS

ABBREVATIONS

AFAD	= Disaster and Emergency Management Presidency
EPOS	= European Plate Observing System
PEER	= Pacific Earthquake Engineering Research
TBSC18	= Turkish Building Seismic Code, 2018
TSC07	= Turkish Seismic Code, 2007
TS498	= Design Loads for Buildings, 1997
TS500	= Requirements for Design and Construction of Reinforced Concrete Structures, 2000

LIST OF SYMBOLS

SYMBOLS

A_c = Gross cross-sectional area of member

A_{ch} = Gross cross-sectional area of wall

A_s = Longitudinal reinforcement area

BKS = Building occupancy class

BYS = Building height class

D = Overstrength factor

DD-1 = Earthquake ground motion with 2% probability of exceeding in 50 years (Return period 2475 years)

DD-2 = Earthquake ground motion with 10% probability of exceeding in 50 years (Return period 475 years)

DD-3 = Earthquake ground motion with 50% probability of exceeding in 50 years (Return period 72 years)

DD-4 = Earthquake ground motion with 68% probability of exceeding in 50 years (Return period 43 years)

DGT = Force – based design principles

DTS = Earthquake design class

E_c = Elasticity modulus of concrete

E_s = Elasticity modulus of steel

EW = East – West component of earthquake ground motion record

F_S = Site coefficient at short period

F_1 = Site coefficient at 1 second period

f_c = Compressive stress on concrete

f_{cc} = Compressive strength of confined concrete

f_{cd} = Design compressive strength of concrete

f_{ck} = Characteristic compressive strength of concrete

f_{co} = Compressive strength of unconfined concrete

f_e = Effective confinement stress

f_s = Stress on steel

f_{sy} = Yield strength of steel

f_{yw} = Yield strength of transverse reinforcement

g = Gravitational acceleration [$g = 9.81$ m/s^2]

GÖ = Collapse prevention performance level

H_N = Total height of building [m]

h = Slab thickness

I = Importance factor

KH = Damage control performance level

KK = Immediate occupancy performance level

k_e = Confinement effectiveness factor

l_{sn} = Free opening length of slab in short direction

M_{DEV} = Overturning moment at the base of structural walls [kNm]

M_{ra} = Bearing moment at the lower end of the free height of column or wall

M_{ri} = Bearing moment on the face of column or wall at the left end of the beam

M_{rj} = Bearing moment on the face of column or wall at the right end of the beam

$M_{rü}$ = Bearing moment at the upper end of the free height of column or wall

M_w = Moment magnitude

M_0 = Overturning moment at the base of the structure [kNm]

m = Ratio of larger slab length to shorter slab length

m_t = Total weight of the structure [t]

N_{dm} = Maximum axial load on wall

NS = North – South component of earthquake ground motion record

n = Live load participation ratio

PGA = Peak ground acceleration

PGD = Peak ground displacement

PGV = Peak ground velocity

R = Response modification coefficient

R_{jb} = Closest distance to the horizontal projection of the fault rupture

S_a = Spectral acceleration

$S_{ae}(T)$ = Horizontal elastic design spectral acceleration [g]

S_{DS} = Short period design spectral acceleration coefficient [unitless]

S_{D1} = [unitless]

SH = Limited damage performance level

S_S = Mapped spectral acceleration coefficient at short period [unitless]

S_1 = Mapped spectral acceleration coefficient at a 1 second period [unitless]

s = Spacing of stirrups

ŞGDT = Displacement – based design principles

T = Natural vibration period [s]

T_A = $0.2\ S_{D1} / S_{DS}$

T_B = S_{D1} / S_{DS}

T_L = Long – period transition period

UD = Up – Down component of earthquake ground motion record

V_d = Shear force on beam

V_e = Shear force on wall

V_{s30} = The average shear – wave velocity between 0 and 30 – meters depth [m/s]

$V_{t,min}$ = Base shear force [kN]

α_H = Empirical coefficient depending on height of the structure

α_s = Ratio of sum of continuous edge lengths of slab to total edge length of slab

ε_c = Strain on concrete

$\varepsilon_c^{(GÖ)}$ = Allowable strain limit of confined concrete for collapse prevention performance level

$\varepsilon_s^{(GÖ)}$ = Allowable strain limit of steel for collapse prevention performance level

ε_s = Strain on steel

ε_{su} = Strain of steel corresponding to maximum strength

ε_{sy} = Yield strain of steel

ρ_x, ρ_x = Volumetric ratio of transverse reinforcement

ω_{we} = Mechanical reinforcement ratio of effective transverse reinforcement

CHAPTER 1

INTRODUCTION

Outlining the effects of ground motion due to earthquakes on buildings has historically been a challenge for designers and engineers. This task has become even more difficult when buildings started to get increasingly taller. Seismic design regulations created for various types of buildings are needed to be expanded to include specialized provisions for its effect on high-rise buildings. Some regulations around the world have seen recent improvements when the vertical component of ground motion along with the horizontal component has started to be considered for the design of buildings. This, however, is used as a holistic method and applies to the design of all types of buildings. The aim of this study is to examine the effect of the vertical component of ground motion on high-rise buildings specifically to understand if better descriptions of design specifications can be introduced.

1.1 Horizontal and Vertical Components of Ground Motion

Waves of energy released by an earthquake traveling through a medium are called seismic waves. Ground shaking caused by seismic waves results in ground acceleration when they reach the site of a built structure. Ground acceleration, also referred to as ground motion, is composed of two components: horizontal and vertical. Some recent studies suggest the ratio of vertical to horizontal components of ground motion can provide useful data for the seismic design of built structures.

1.2 Literature Review

One of the first studies related to vertical ground motion is carried out with the aim of to create both vertical and separate horizontal response spectra of certain earthquakes to be able to make a comparison of these spectra, to determine the shape of spectra depending on frequency, and finally to make a procedure suggestion regarding horizontal and vertical responses. In that study, it is suggested that approximately 2/3 of the horizontal spectrum should be considered for the vertical spectrum (Newmark et al., 1973). In some other studies, this ratio is suggested lower than 2/3. For example, it is concluded that the ratio is approximately 1/3 (Kawashima et al., 1985). Moreover, it is stated that almost there is no correlation between this ratio and the earthquake magnitude and epicentral distance. In some studies, this ratio is suggested bigger than 2/3. For instance, it is stated that the ratio of peak vertical ground acceleration to peak horizontal ground motion is fault type dependent and it is independent of distance. Moreover, it is stated that the ratio exceeds 1 in short periods whilst it is lower than 1 in intermediate and long periods (Ambraseys, Simpson, & Bommer, 1996).

Through time, several codes have started to include the effect of vertical ground motion. In Turkey, the effect of vertical ground motion is started to be considered with the new seismic code, *TBSC18 (Turkish Building Seismic Code, 2018).* The vertical elastic design spectrum along with the horizontal elastic design spectrum defined in *TBSC18* is presented in *Figure 1.1*. In the Code, it is stated that the effect of the vertical ground motion can be taken as $(2/3)S_{DS}G$ under certain conditions. In the statement, S_{DS} denotes short period design spectral acceleration coefficient, and G denotes dead load.

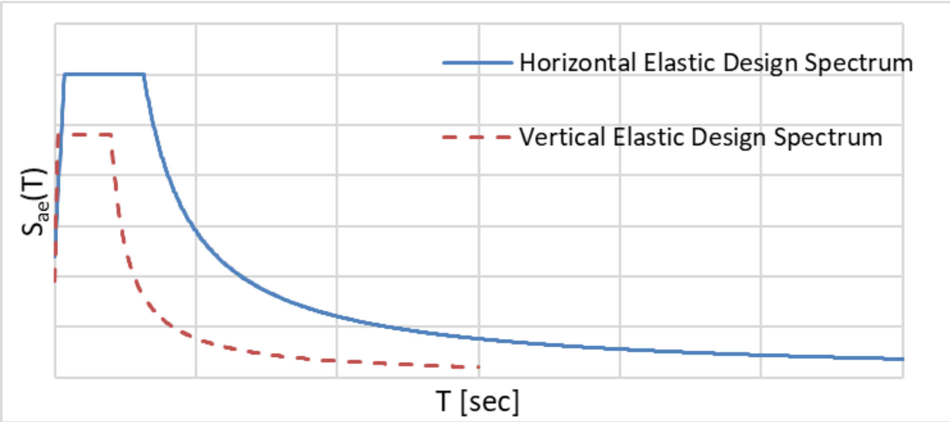

Figure 1.1. Spectral Acceleration vs Period Graphs of Vertical and Horizontal Design Spectrum (TBSC18)

1.3 Identifying the Major Factors Defining the Effect of Vertical Component of Ground Motion on Built Structures

The vertical and horizontal components of ground motion can be analyzed in terms of local site conditions, source-to-site distance, and earthquake magnitude (Bozorgnia & Campbell, 2004). The vertical-to-horizontal ratio of ground motion (V/H) exhibits different behaviors at different soil types (Silva, 1997), differs based on source-to-site distance and its effect is dependent on earthquake magnitude (Collier & Elnashai, 2001). In some studies, local site conditions, source-to-site distance, and earthquake magnitude are used to identify the effects of the vertical component of ground motion on specialized structures (nuclear power plants, dams, bridges, etc.). Site class, source-to-site distance, and earthquake magnitude are utilized in this study to outline the effect of the vertical component of ground motion on high-rise buildings.

1.4 Scope and Outline

In this chapter, horizontal and vertical components of ground motion have been explained briefly. The aim is to bring attention to the fact that there are no generalized specifications that help explain the effects of vertical ground motion on high-rise buildings. A brief overview of major factors defining the effect of the vertical component of ground motion on built structures is presented to shape the discussion towards finding better descriptions of seismic design specifications.

In *Chapter 2*, a model reinforced concrete structure building designed with a symmetric plan layout is presented as a case study. The composition of the building is in accordance with the definition of a high-rise structure as outlined in the Turkish Building Seismic Code 2018 (*TBSC18*).

Chapter 3 covers the selection and processing stage of actual earthquake records that are used to realistically observe the effect of the vertical component of ground motion on the model building. Earthquake magnitude (M_w), soil type and source-to-site distance are considered in the selection of these records.

Non-linear time history analysis method is used to observe the behavior of the structure under time series. Non-linear modeling of the case study building is presented in *Chapter 4*.

Chapter 5 covers the results of non-linear time-history analyses and its interpretation based on inter-story drift ratio, overturning moment, axial force on columns, and story shear force.

In *Chapter 6*, a brief summary of this study is given. Moreover, the results of this study are interpreted, and the conclusions of the study are presented. Finally, some future studies are recommended.

CHAPTER 2

DESIGN OF THE MODEL HIGH-RISE BUILDING

2.1 General Information About the Building

A reinforced concrete building designed according to the New Turkish Building Seismic Code *(TBSC18)* is used to represent a model high-rise building in the current study. The building has 30 floors with a typical floor height of 4 m. The total height of the building is 120 m.

Ten different tall office buildings around the world have been investigated to represent the characteristics of floor plan layouts and structural systems of contemporary high-rise reinforced concrete buildings (*Figure 2.1*). Based on the information gathered by this investigation, a floor plan with perimeter columns and a central core with I-shaped structural walls is selected for the model building. The reason for selecting the I-shaped structural wall is to satisfy minimum wall requirements according to design code as well as to provide free space as much as possible. The plan is aimed to be symmetrical to reduce analysis time by eliminating direction effect. Therefore, the columns are located symmetrically in the plan. The structural walls, on the other hand, are symmetric in both principal directions separately. It is not possible to choose a symmetrical structural wall layout in both principal directions at the same time due to architectural reasons. In addition, the horizontal structural members are designed with the same cross-sectional properties for all floors while the vertical structural members are reduced in cross-sectional size at every 10 floors for a more optimal design. The typical floor plan is presented in *Figure 2.2.*

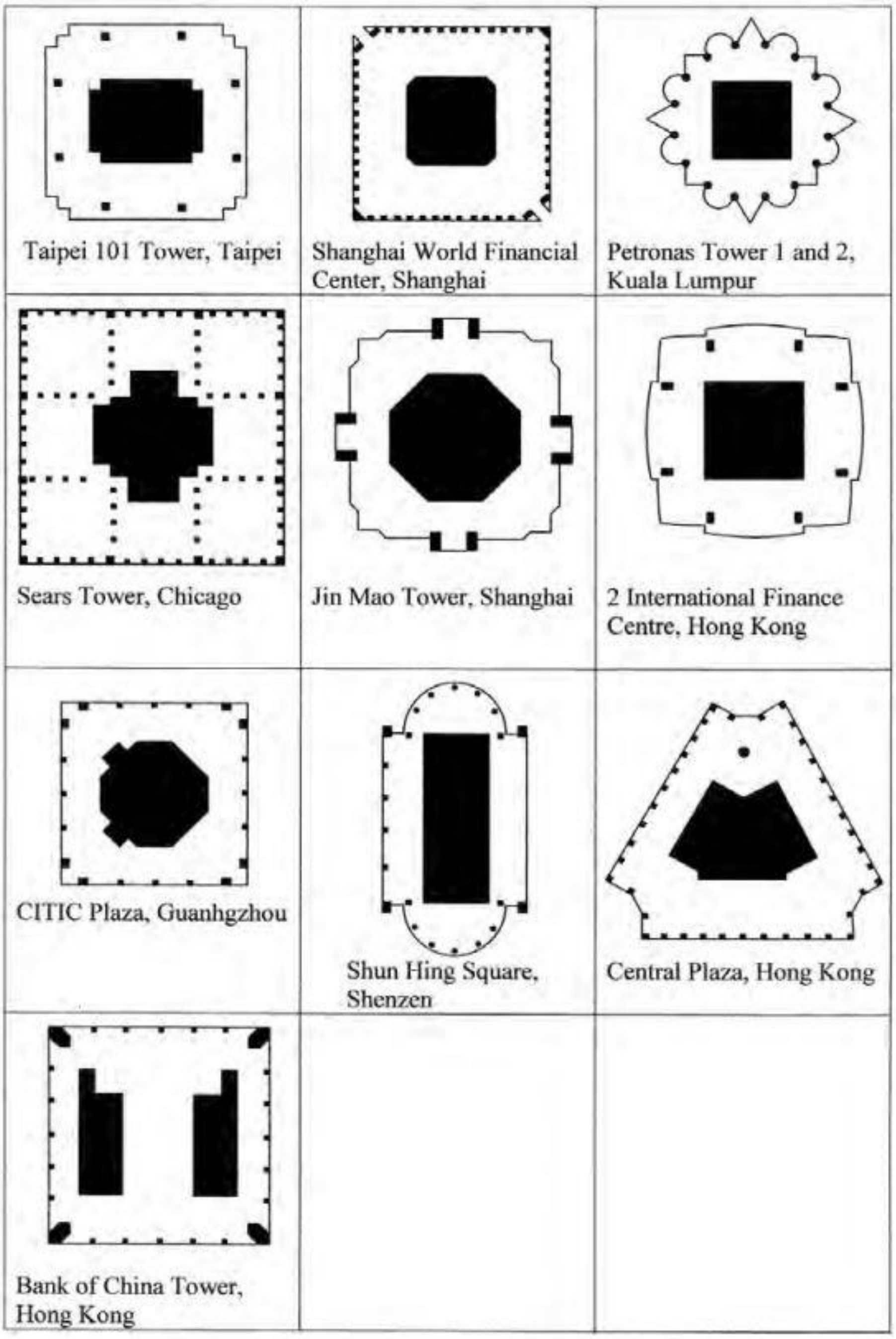

Figure 2.1. Geometry of typical floor plans of ten tall office buildings around the world (Sev & Özgen, 2009)

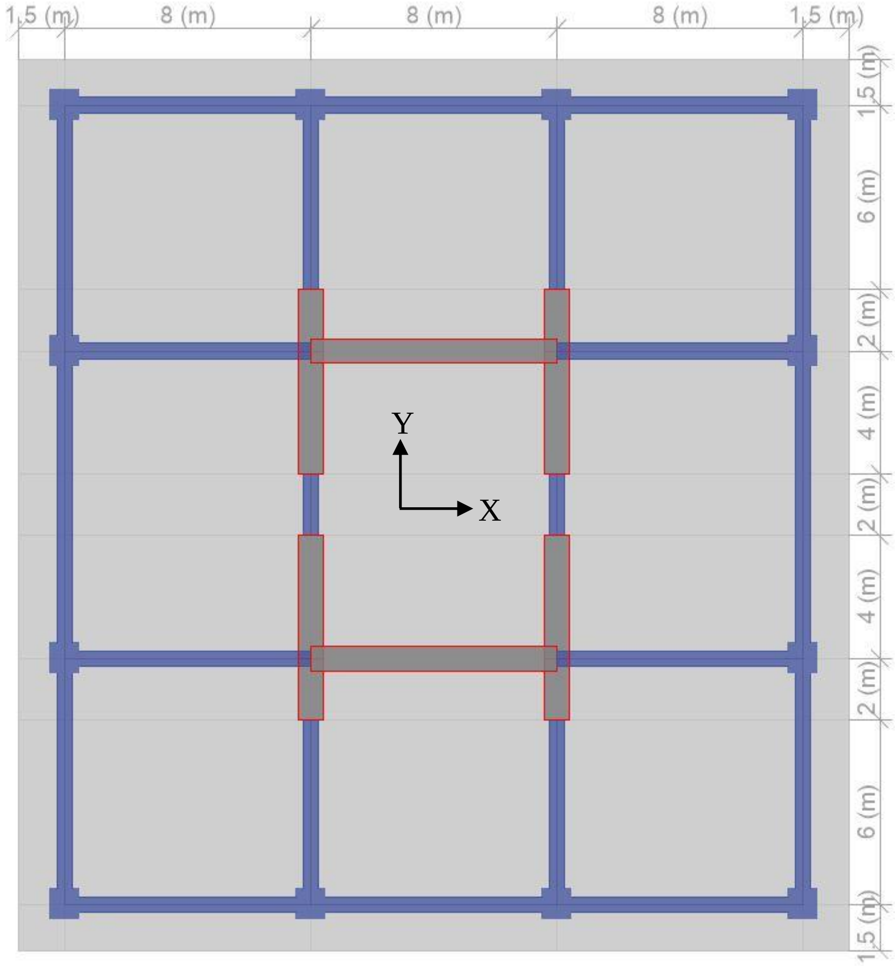

Figure 2.2. Typical Floor Plan

Since the total height of the model building is 120 m., it is classified as "high-rise building" according to the new Turkish Building Seismic Code (*Table 3.3 in TBSC18*). Building height class *(BYS in the Code)* is specified as *BYS = 1* for high-rise buildings. Building height ranges according to building height class and earthquake design class are presented in *Table 2.1*.

Table 2.1. Building Height Classes and Building Height Ranges Defined Per Earthquake Design Classes (*Table 3.3* of *TBSC18*)

Building Height Class	Building Height Classes and Building Height Ranges Defined per Earthquake Design Classes [m]		
	DTS = 1, 1a, 2, 2a	DTS = 3, 3a	DTS = 4, 4a
BYS = 1	$H_N > 70$	$H_N > 91$	$H_N > 105$
BYS = 2	$56 < H_N \leq 70$	$70 < H_N \leq 91$	$91 < H_N \leq 105$
BYS = 3	$42 < H_N \leq 56$	$56 < H_N \leq 70$	$56 < H_N \leq 91$
BYS = 4	$28 < H_N \leq 42$	$42 < H_N \leq 56$	
BYS = 5	$17.5 < H_N \leq 28$	$28 < H_N \leq 42$	
BYS = 6	$10.5 < H_N \leq 17.5$	$17.5 < H_N \leq 28$	
BYS = 7	$7 < H_N \leq 10.5$	$10.5 < H_N \leq 17.5$	
BYS = 8	$H_N \leq 7$	$H_N \leq 10.5$	

Even if the building is classified as a high-rise building regardless of its design class, it should be designed according to one of the earthquake design classes *(DTS in the Code)* as given in *Table 3.2* of *TBSC18.*

Table 2.2. Earthquake Design Classes (*Table 3.2 of TBSC18*)

Short Period Design Spectrum Acceleration Coefficient in DD-2 Earthquake Ground Motion (S_{DS})	Building Occupancy Class	
	BKS =1	BKS = 2, 3
$S_{DS} < 0.33$	DTS = 4a	DTS = 4
$0.33 \leq S_{DS} < 0.50$	DTS = 3a	DTS = 3
$0.50 \leq S_{DS} < 0.75$	DTS = 2a	DTS = 2
$0.75 \leq S_{DS}$	DTS = 1a	DTS = 1

In order to determine the *BYS* of the building, building occupancy class *(BKS in the Code)* and short period design spectral acceleration coefficient *(S_{DS} in the Code)* should be determined first. According to *Table 3.1* of *TBSC18,* building occupancy class can be chosen as *BKS=3* for high-rise buildings. In this study, *BKS* is chosen as 3.

Table 2.3. Building Occupancy Classes and Importance Factors (*Table 3.1 of TBSC18*)

Building Occupancy Class	Purpose of Occupancy	Importance Factor (I)
BKS = 1	**Buildings required to be utilized after the earthquake, intensively and long-term occupied buildings, buildings preserving valuable goods and buildings containing hazardous materials** a) Buildings required to be utilized immediately after the earthquake (Hospitals, dispensaries, health wards, firefighting buildings and facilities, PTT and other telecommunication facilities, transportation stations and terminals, power generation and distribution facilities; governorate, county and municipality administration buildings, first aid and emergency planning stations) b) Schools, other educational buildings and facilities, dormitories and hostels, military barracks, prisons, etc. c) Museums d) Buildings containing or storing toxic, explosive and flammable materials, etc.	1.5
BKS = 2	**Intensively but short-term occupied buildings** Malls, sport facilities, cinema, theatre and concert halls, etc.	1.2
BKS = 3	**Other Buildings** Buildings other than above defined buildings for BKS=1 and BKS=2. (Residential and office buildings, hotels, building-like industrial structures, etc.)	1

There were four seismic zones defined in the former version of the Turkish Seismic Code (2007) or in short *TSC07*. Peak ground acceleration (*PGA*) was dependent on these seismic zones. However, in *TBSC18*, there are no such seismic zones. *PGA* and spectral acceleration (S_a) are dependent on the location, where the building is going to be designed and constructed. Eventually, the S_{DS}, S_1, and *PGA* values vary with the distance between building location and the nearest fault. To use consistent spectral values with *TSC07*, S_S and S_1 are chosen as 1.0 and 0.276, respectively for a building location of 41.017808 ° N and 28.896445 ° E (Güngören district of Istanbul) (These values are taken from the website of AFAD *(Disaster and Emergency Management Presidency)* that provides Seismic Hazard Maps for Turkey (https://tdth.afad.gov.tr/TDTH/main.xhtml)). Horizontal elastic design spectrum in *TBSC18* is presented in *Figure 2.3*.

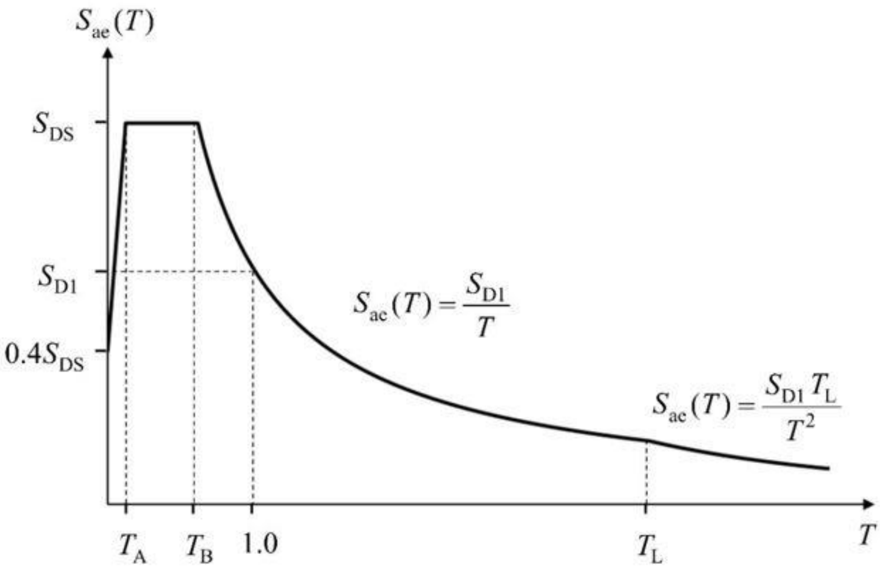

Figure 2.3. Horizontal Elastic Design Spectrum (*Figure 2.1 in TBSC18*)

Spectral acceleration is defined in terms of S_{DS} after obtaining the S_S values from the map. The relationship between S_S and S_{DS} is given in *Equation 2.1*. A similar relationship exists between spectral acceleration values at short period, i.e S_1 and S_{D1}, as given in *Equation 2.2*. Site coefficients at short period (i.e F_S in the Code) and Site coefficients at 1 second period (i.e F_1 in the Code) are presented in *Table 2.4 – 2.5*, respectively.

$$S_{DS} = S_S F_S \quad \text{------------------------} \quad (2.1)$$

$$S_{D1} = S_1 F_1 \quad \text{------------------------} \quad (2.2)$$

Table 2.4. Site Coefficients at Short Period *(Table 2.1 in TBSC18)*

Site Class	Site Coefficients at Short Period, F_S					
	$S_S \leq 0.25$	$S_S = 0.50$	$S_S = 0.75$	$S_S = 1.00$	$S_S = 1.25$	$S_S \geq 1.50$
ZA	0.8	0.8	0.8	0.8	0.8	0.8
ZB	0.9	0.9	0.9	0.9	0.9	0.9
ZC	1.3	1.3	1.2	1.2	1.2	1.2
ZD	1.6	1.4	1.2	1.1	1.0	1.0
ZE	2.4	1.7	1.3	1.1	0.9	0.8
ZF	Site-specific soil behavior analysis will be performed.					

Table 2.5. Site Coefficients at 1 Second Period *(Table 2.2 in TBSC18)*

Site Class	Site Coefficients at 1 Second Period, F_1					
	$S_1 \leq 0.10$	$S_1 = 0.20$	$S_1 = 0.30$	$S_1 = 0.40$	$S_1 = 0.50$	$S_1 \geq 0.60$
ZA	0.8	0.8	0.8	0.8	0.8	0.8
ZB	0.8	0.8	0.8	0.8	0.8	0.8
ZC	1.5	1.5	1.5	1.5	1.5	1.4
ZD	2.4	2.2	2.0	1.9	1.8	1.7
ZE	4.2	3.3	2.8	2.4	2.2	2.0
ZF	Site-specific soil behavior analysis will be performed.					

Design spectrum for the case study building is developed by considering soil type C since it is the most critical case according to *Table 2.4*. After determining building occupancy class *(BKS)* and short period design spectral acceleration coefficient

(S_{DS}), earthquake design class is specified as *DTS = 1*. Horizontal elastic design spectrum of the selected location is presented in *Figure 2.4.*

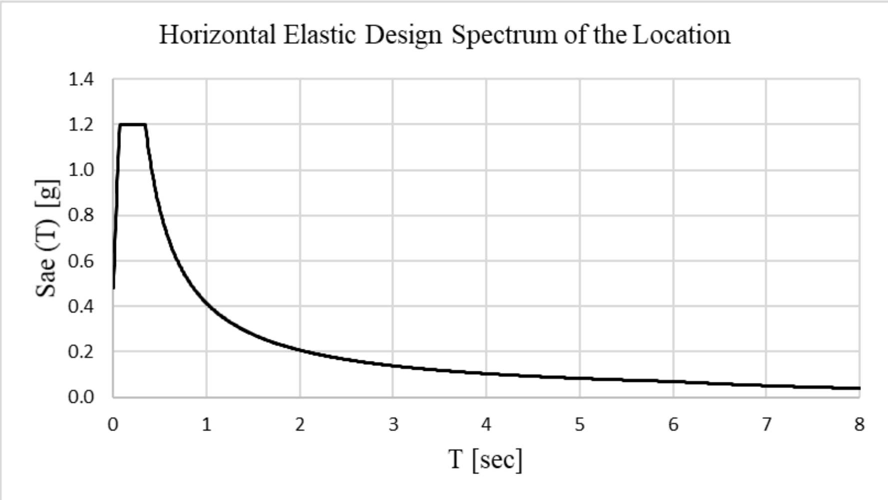

Figure 2.4. Horizontal Elastic Design Spectrum of the Location

2.2 Design of the Case Study Building

According to *Chapter 13* of *TBSC18*, design of high-rise buildings should be conducted in 3 phases.

1. Design phase 1: Preliminary design with *DD-2* earthquake ground motion – Dimensioning
2. Design phase 2: Assessment for uninterrupted use or limited damage performance target with *DD-4* or *DD-3* earthquake ground motion – Design enhancement
3. Design phase 3: Assessment for failure prevention or controlled damage performance target with *DD-1* earthquake ground motion – Final design

2.2.1 Design Phase 1

According to *Table 3.4.b* in *TBSC18,* design of the building must be conducted according to strength design principles (i.e *DGT* in the Code).

Table 2.6. New Buildings or Existing Tall Buildings (BYS = 1) *(Table 3.4.b in TBSC18)*

	DTS = 1, 2, 3, 3a, 4, 4a		DTS = 1a, 2a	
	Normal Performance Level	Design Approach	High Performance Level	Design Approach
DD-4	KH	DGT	-	-
DD-3	-	-	SH	ŞGDT
DD-2	KH	DGT [3]	KH	DGT [3,4]
DD-1	GÖ	ŞGDT	KH	ŞGDT

[3] Shall be conducted as preliminary design.

[4] I shall be taken 1.5.

At this stage, the preliminary design of the building is conducted under *DD-2* earthquake ground motion which is called standard design earthquake ground motion. The design is carried out as per design principles of strength design according to *Table 3.4.b* of *TBSC18*.

2.2.1.1 Modeling of the Case Study Building

The case study building has been modeled as a 3D model in structural analysis software, ETABS (COMPUTERS AND STRUCTURES, INC. version 17.2.1). Modeling is carried out according to the specifications given in *Section 4.5 of TBSC18*. Since the focus of this study is not the design of high-rise buildings, full design process will not be presented. Some key points will be presented instead.

- Damping ratio is selected as 5% for preliminary design.
- Effective section rigidity is considered in design according to *Table 4.2* of the *TBSC18*. Effective section rigidity is considered in load combinations with earthquake effect only (see *Table 2.7*).
- ± 5 % eccentricity is considered in design.
- Live load participation ratio is considered as 0.3 as per *Table 4.3 of the TBSC18 (*see *Table 2.8).*
- Concrete class is chosen as C50.
- Steel material is chosen as S420.

Table 2.7. Effective Section Rigidity Coefficients of Load Bearing Concrete Members (*Table 4.2 in TBSC18*)

Load Bearing Reinforced Concrete Member	Effective Section Rigidity Coefficient	
Shear Wall - Slab (In Plane)	**Axial**	**Shear**
Shear Wall	0.50	0.50
Basement Wall	0.80	0.50
Slab	0.25	0.25
Shear Wall - Slab (Out of Plane)	**Bending**	**Shear**
Shear Wall	0.25	1.00
Basement Wall	0.50	1.00
Slab	0.25	1.00
Frame Member	**Bending**	**Shear**
Coupling Beam	0.15	1.00
Frame Beam	0.35	1.00
Frame Column	0.70	1.00
Shear Wall (Equivalent frame)	0.50	0.50

Table 2.8. Live Load Participation Ratio (*Table 4.3 in TBSC18*)

Purpose of Occupancy Class of Building	*n*
Depot, warehouse, etc.	0.80
School, dormitory, sport facility, cinema, theatre, concert hall, car park, restaurant, shop, etc.	0.60
Residence, office, hotel, hospital, etc	0.30

2.2.1.2 Load Combinations to be Considered in Design

Load combinations to be used in the design of the case study model are given in *Table 2.9*. These combinations are taken from *TBSC18* and *TS500 (Requirements for Design and Construction of Reinforced Concrete Structures, 2000)*. The purpose of each load combination is also given in the last column of the table. For the load combinations with earthquake load, directional effect is considered.

Table 2.9. Load Combinations

Combination Name	*Case Components of Combination*	*Explanation*
C100	1.0G + 1.0Q	Service load combination.
C101	1.0G + 0.5Q	Service load combination.
C200	1.4G + 1.6Q	Factored vertical load combination.
C250	0.9G	Factored vertical load combination.
C300 ~ C303	1.0G + 1.3Q ± 1.3W	Wind load combination.
C304 ~ C307	0.9G ± 1.3W	Wind load combination.
C400 ~ C401	1.0G + 1.2Q ± 1.2T	Temperature combination.
C600 ~ C601	$(1.0 + 0.2S_{DS})$G + 1.0Q + 1.0SPEC	Combination for moment.
C602 ~ C603	$(0.9 - 0.2S_{DS})$G + 1.0SPEC	Combination for moment.
C650 ~ C651	$(1.0 + 0.2S_{DS})$G + 1.0Q + D*SPEC	Combination for shear on columns and beams.
C652 ~ C653	$(0.9 - 0.2S_{DS})$G + D*SPEC	Combination for shear on columns and beams.

Table 2.9 Load Combinations (Cont.)

Combination Name	*Case Components of Combination*	*Explanation*
C850 ~ C851	$(1.0 + 0.2S_{DS})G + 1.0Q + 1.2*D*SPEC$	Combination for shear on solid structural walls.
C852 ~ C853	$(0.9 - 0.2S_{DS})G + 1.2*D*SPEC$	Combination for shear on solid structural walls.
C875 ~ C876	$(1.0 + 0.2S_{DS})G + 1.0Q + 1.4*D*SPEC$	Combination for shear on coupled structural walls.
C877 ~ C878	$(0.9 - 0.2S_{DS})G + 1.4*D*SPEC$	Combination for shear on coupled structural walls.

In *Table 2.9,* some abbreviations have been used for different load parameters. Accordingly, G denotes dead load, Q denotes live load, W denotes wind load, T denotes temperature load, and SPEC denotes earthquake load. Also, D denotes overstrength factor.

2.2.1.3 Earthquake Load Calculations

Structural system behavior factor *(R)* and overstrength factor *(D)* should be determined per the requirements of *Section 4.3* in *TBSC18*. The model building consists of high ductile structural walls and high ductile frame members. Hence *Equation 4.2* in *TBSC18,* which is also provided in *Equation 2.3* below, is checked and verified. According to *Section 4.5.4.3* in *TBSC18,* walls in Y direction are determined as coupled walls. As a result of this, it should be considered that seismic loads are jointly resisted by high ductile frames and high ductile solid structural walls in X direction (A15 in *Table 4.1* of the *TBSC18*) and seismic loads are jointly resisted by high ductile frames and high ductile coupled structural walls in Y direction (A14 in *Table 4.1* of *TBSC18*). (Although there is no statement for *BYS = 1* in the Code) R and D factors are chosen according to *Table 2.10* (*Table 4.1* in *the Code)*. M_o and M_{DEV} values used in *Equation 2.3* are presented in Table *2.11.*

$$0.40M_0 < \sum M_{DEV} < 0.75M_0 \quad \text{-----------------------} \ (2.3)$$

In *Equation 2.3*, M_o and M_{DEV} are defined as overturning moment at the base of whole structure and overturning moment at the base of structural walls, respectively.

Table 2.10. Structural System Behavior Factors, Overstrength Factors and Allowable Building Height Classes *(Table 4.1 in TBSC18)*

Building Structural System	Systems of High Ductility Level R	Overstrength Factor D	Allowable Building Height Class
Cast-in-site Reinforced Concrete Buildings			
A1. Buildings with high ductility level			
A11. Buildings in which seismic loads are fully resisted by high ductile frames	8	3	BYS ≥ 3
A12. Buildings in which seismic loads are fully resisted by high ductile coupled structural walls	7	2.5	BYS ≥ 2
A13. Buildings in which seismic loads are fully resisted by high ductile solid structural walls	6	2.5	BYS ≥ 2
A14. Buildings in which seismic loads are jointly resisted by high ductile frames and high ductile coupled structural walls	8	2.5	BYS ≥ 2
A15. Buildings in which seismic loads are jointly resisted by high ductile frames and high ductile solid structural walls	7	2.5	BYS ≥ 2

Table 2.11. M_o and M_{DEV} values

	X direction	Y direction
M_o (kN.m)	880,000	680,000
M_{DEV} (kN.m)	550,000	470,000

According to *Equation 2.4* (*Equation 13.1* in the Code) minimum earthquake force should be determined as follows

$$V_{t,min} = 0.04\alpha_H m_t S_{DS} g \quad \text{- -} \quad (2.4)$$

where $V_{t,min}$, α_H, m_t and are defined as base shear force, empirical coefficient depending on height of the structure, and total weight of the structure, respectively.

Base shear forces obtained from response spectrum load cases are compared with minimum base shear force defined in *Equation 2.4.* It is observed that base shear forces under response spectrum load cases do not meet the requirement of minimum base shear.Thus, scale factors of response spectrums are modified per minimum base shear force in order to satisfy *Equation 2.4*.

2.2.1.4 Other Loads

According to *TS498 (Design Loads for Buildings, 1997)*, wind pressure changes through the height of the building. Wind pressure is considered in design according to *Table 2.12* (*Table 5* in *TS498*).

Table 2.12. Wind Speed and Absorption Depending on Height

Height [m]	Wind Speed [m/s]	Absorption [kN/m^2]
0 – 8	28	0.5
0 – 8	36	0.8
0 – 8	42	1.1
> 100	46	1.3

Since the focus of this study does not cover temperature load, detailed calculations are not carried out for temperature load. Annual mean, maximum and minimum temperature of the building location are examined. Depending on this examination it is decided to include temperature change as ± 30^o.

2.2.1.5 Section Control

Slab thickness is determined according to *Equation 2.5* (*Equation 11.1* in *TS500)*

$$h \geq \frac{l_{sn}}{15+\frac{20}{m}}\left(1-\frac{\alpha_s}{4}\right) and\ h \geq 80\ mm \quad \text{------------ (2.5)}$$

where *h*, l_{sn}, *m*, and α_s are defined as slab thickness, free opening length of slab in short direction, ratio of larger slab length to shorter slab length, and ratio of sum of continuous edge lengths of slab to total edge length of slab, respectively. In this study slab thickness is chosen as 200 mm.

Axial load on shear wall is checked according to *Equation 2.6*

$$A_c \geq N_{dm}/(0.35 f_{ck}) \quad \text{---------------------- (2.6)}$$

where A_c, N_{dm}, f_{ck} and are defined as gross cross-sectional area of structural wall, maximum axial load of gravity load and combination of gravity load and earthquake load, and characteristic compressive strength of structural wall material, respectively.

For solid shear walls, shear force is checked according to *Equation 2.7* (*Equation 7.17* of the Code) whereas for coupled shear walls, shear force is checked according to *Equation 2.8* (*Equation 7.17* of the Code).

$$V_e \leq 0.85 A_{ch}\sqrt{f_{ck}} \quad \text{------------------- (2.7)}$$

$$V_e \leq 0.65 A_{ch}\sqrt{f_{ck}} \quad \text{------------------- (2.8)}$$

In these equations, V_e and A_{ch} are defined as shear force on structural wall and gross cross-sectional area of structural wall, respectively.

The detailing of the longitudinal reinforcement in the shear wall is carried out by using the design principles in the code and varying with the height of the structure. *Figure 2.5* - *Figure* 2.7 show the reinforcement details of the shear wall for stories between 1 – 10, 11 – 20, and 21 – 30, respectively.

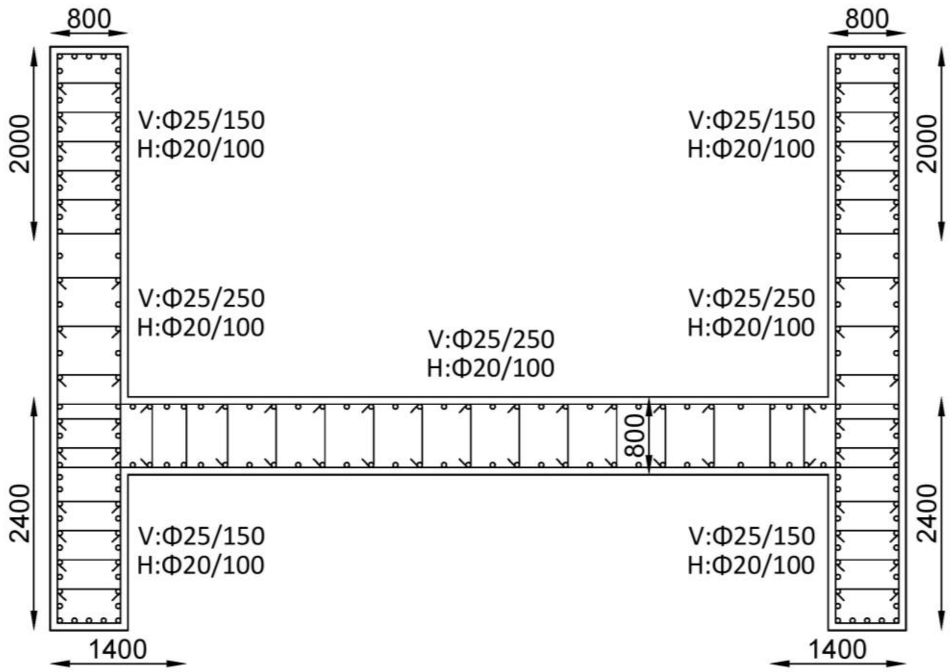

Figure 2.5. Shear Wall Longitudinal Reinforcement for Stories Between 1 - 10

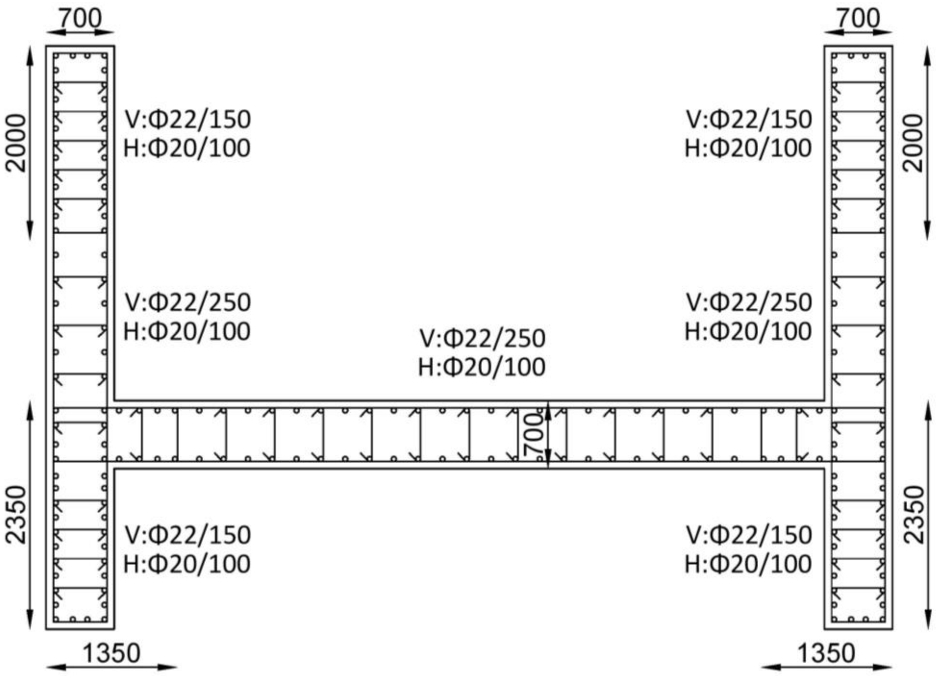

Figure 2.6. Shear Wall Longitudinal Reinforcement for Stories Between 11 - 20

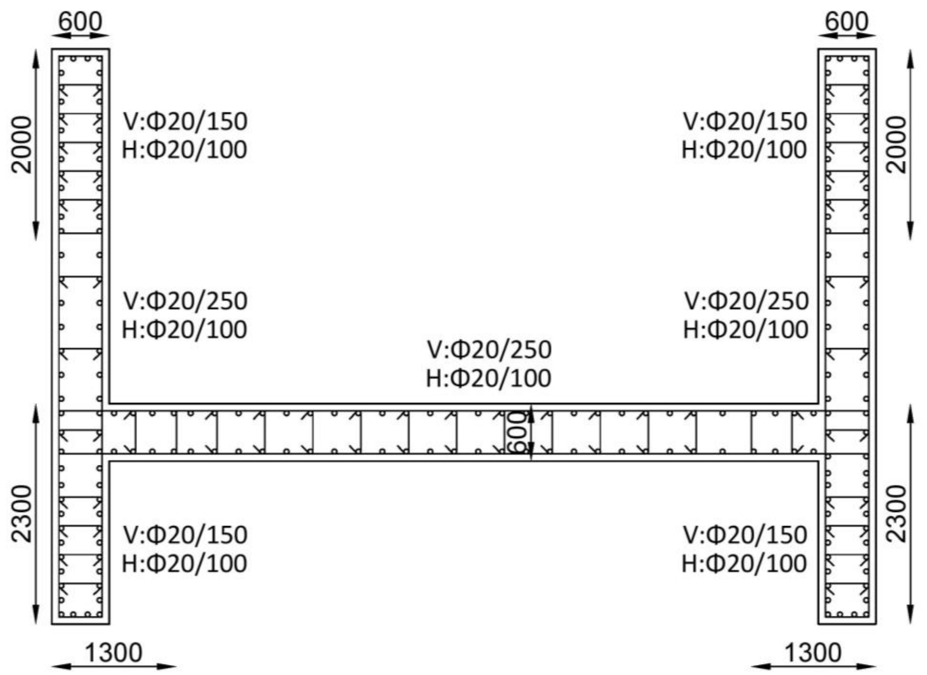

Figure 2.7. Shear Wall Longitudinal Reinforcement for Stories Between 21 - 30

Whilst axial force on column is checked according to *Equation 2.9* under combination of gravity load and earthquake load, axial force on column is checked according to *Equation 2.10* (Equation 7.7 of TS500) under gravity load only.

$$A_c \geq N_{dm}/(0.40 f_{ck}) \quad \text{------------------} \quad (2.9)$$

$$A_c \geq N_{dm}/(0.90 f_{cd}) \quad \text{-----------------} \quad (2.10)$$

Dimensions and longitudinal reinforcement details of columns for stories between 1 – 10, 11 – 20, and 21 – 30 are shown in *Figure 2.8* - *Figure 2.10*, respectively.

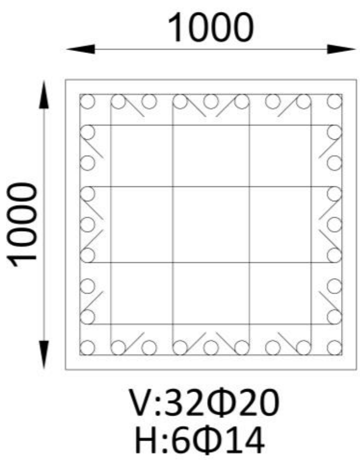

Figure 2.8. Column Longitudinal Reinforcement for Stories Between 1 - 10

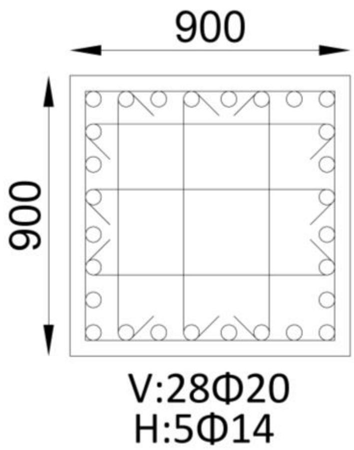

Figure 2.9. Column Longitudinal Reinforcement for Stories Between 11 - 20

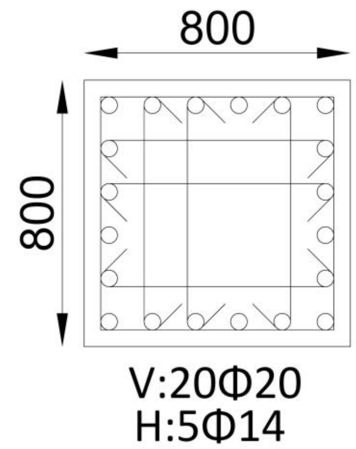

Figure 2.10. Column Longitudinal Reinforcement for Stories Between 21 - 30

Shear force on beam is checked by following statement given on *TS500*.

$$V_d \leq 0.2 f_{cd} A_c \quad \text{- - - - - - - - - - - - - - - -} \quad (2.11)$$

Dimensions and longitudinal reinforcement details of beams is given in *Figure 2.11* which are the same throughout the building. *Figure 2.12* shows the size and the reinforcement of the coupling beams.

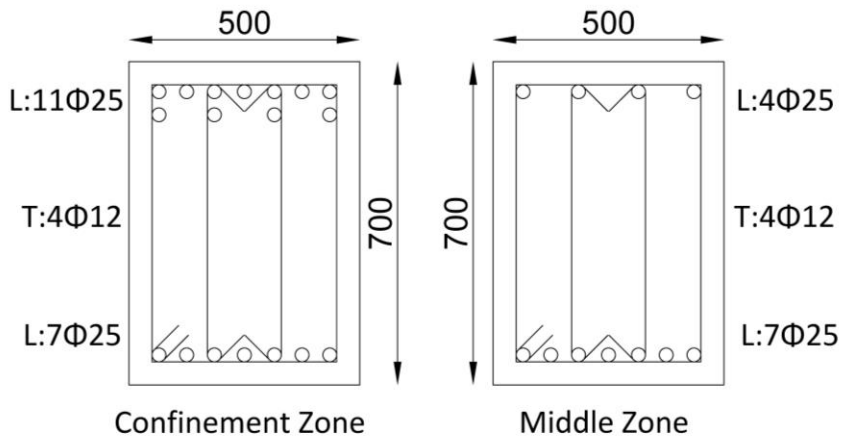

Figure 2.11. Typical Beam Longitudinal Reinforcement

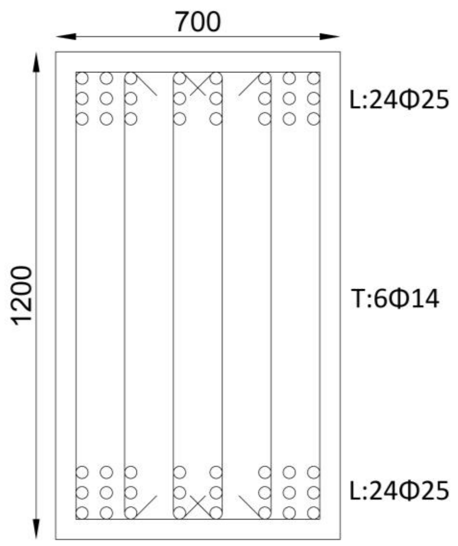

Figure 2.12. Coupling Beam Longitudinal Reinforcement

Strong column – weak beam requirement is checked and verified by *Equation 2.12 (Equation 7.3 of TBSC18)*

$$(M_{ra} + M_{rü}) \geq 1.2(M_{ri} + M_{rj}) \quad \text{---------------} \ (2.12)$$

where M_{ra}, $M_{rü}$, M_{ri}, M_{rj} and are defined as moment at bottom of the column, moment at top of the column, moment at left side of the beam, and moment at right side of the beam, respectively.

2.2.2 Design Phase 2

Since the building is classified as *DTS = 1* per *Table 2.6* (*Table 3.4.b in TBSC18*), it should be verified that the building meets the *Immediate Occupancy* (KK in the Code) performance level under *DD-4* earthquake ground motion. Evaluation should be conducted with forced-based design requirements per *Chapter 4* in *TBSC18*.

2.2.2.1 Modeling of the Case Study Building

The case study building is modelled as described in *Section 2.2.1.1.* There are two points that differ from *Design Phase 1*. The first difference is that damping ratio is taken as 2.5% for *Design Phase 2*. The second difference is that effective section rigidity values are taken from *Table 13.1* in *TBSC18* (see *Table 2.13*).

Table 2.13. Effective Section Rigidity Coefficients of Load Bearing Concrete Members (*Table 13.1 in TBSC18*)

Load Bearing Reinforced Concrete Member	Effective Section Rigidity Coefficient	
Shear Wall - Slab (In Plane)	**Axial**	**Shear**
Shear Wall	0.75	1.00
Basement Wall	1.00	1.00
Slab	0.50	0.80
Shear Wall - Slab (Out of Plane)	**Bending**	**Shear**
Shear Wall	1.00	1.00
Basement Wall	1.00	1.00
Slab	0.50	1.00
Frame Member	**Bending**	**Shear**
Coupling Beam	0.30	1.00
Frame Beam	0.70	1.00
Frame Column	0.90	1.00
Shear Wall (Equivalent frame)	0.80	1.00

2.2.2.2 Load Combinations to be Considered in Design

The same load combinations as considered in *Section 2.2.1.2* are employed in *Design Phase 2*.

2.2.2.3 Earthquake Load Calculations

In this phase, the following conditions are applied:

- The conditions R/I = 1 and D = 1 are applied during internal force calculations.
- Minimum base shear statement is not applied for this design phase.
- Acceleration values specified in *TBSC18* for horizontal elastic spectrum are multiplied by 1.25 to get corresponding accelerations for 2.5 % damping ratio since the spectrum has been created with 5 % damping ratio.

2.2.2.4 Section Control

In this phase, structural members in the building are checked considering their demand / capacity ratio that shall not be exceed 1.5 per statement in *Section 13.5.5.2* in *TBSC18*. All members should satisfy this requirement.

2.2.3 Design Phase 3

In this design phase, the building whose preliminary design has been completed in *Phase 1* and shown to satisfy the performance target in *Phase 2* is verified to have adequate capacity to meet requirement of *Collapse Prevention* (GÖ in the Code) performance target under the *DD-1* earthquake ground motion, which is considered as the largest earthquake with a probability of exceedance 2% in 50 years.

Requirements of *Section 13.6* in *TBSC18* are followed in this phase. According to the statement in this section, at least 11 x 2 = 22 ground motion shall be used in calculations. 11 ground motion records are chosen from PEER website (https://ngawest2.berkeley.edu/spectras/250229/searches/new). Each of these records are scaled according to the *DD-1* design spectrum and applied to building in both *X* and *Y* directions. Key properties of these ground motion records are presented in *Table 2.14*. Scaled response spectra of selected records are presented in loglog scale in *Figure 2.13.*

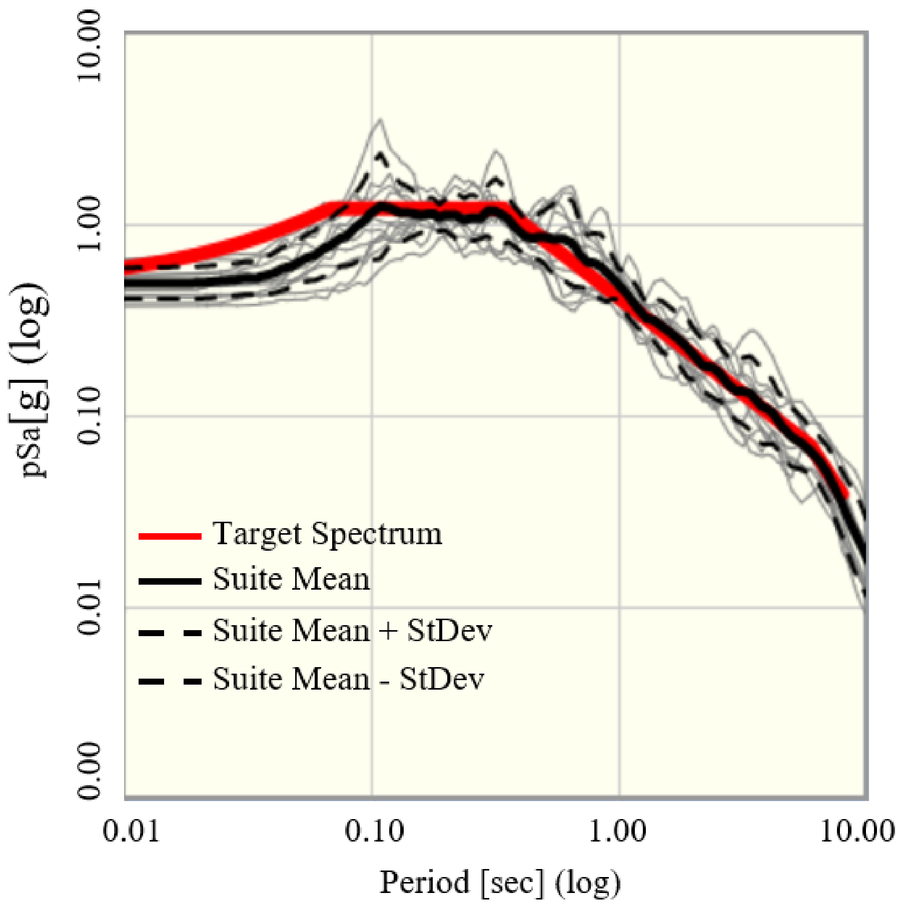

Figure 2.13. Scaled Spectra of Selected Records

Table 2.14. 11 Ground Motion Records Used in Phase 3

Earthquake Name	**Fault Mechanism**	**Magnitude**	**Station**	**R_{jb} (km)**
Parkfield (1966)	Strike Slip	6.19	Cholame - Shandon Array #12	17.64
San Fernando (1971)	Reverse	6.61	Santa Felita Dam (Outlet)	24.69
Imperial Valley (1979)	Strike Slip	6.53	Cerro Prieto	15.19
Loma Prieta (1989)	Reverse Oblique	6.93	Coyote Lake Dam - Southwest Abutment	19.97
Duzce (1999)	Strike Slip	7.14	Lamont 1061	11.46
Manjil (1990)	Strike Slip	7.37	Abbar	12.55
Chi-Chi (1999)	Reverse	6.2	CHY074	27.84
Cape Mendocino (1992)	Reverse	7.01	Loleta Fire Station	23.46
Landers (1992)	Strike Slip	7.28	Whitewater Trout Farm	27.05
Chuetsu-Oki (2007)	Reverse	6.8	Matsushiro Tokamachi	18.16
Iwate-Miyagi (2008)	Reverse	6.9	Tamati Ono	28.9

Critical internal forces for concrete members are obtained, with respected to force-based design requirements, considering internal forces as mean of maximum absolute values obtained from each of 2 x 11 structural analyses.

According to *Section 13.6.5* in *TBSC18*, high ductile concrete members shall meet the requirements of *Section 5.8.1* (strain limitations). Also, relative story drift ratios obtained from the conducted nonlinear time history analyses shall satisfy following conditions: Mean relative story drift ratio shall not exceed 0.03 and maximum relative story drift ratio shall not exceed 0.045.

For *Collapse Prevention* performance level, strain in structural members shall satisfy *Equation 2.13* and *Equation 2.14*.

For rectangular column, beam and shear wall; concrete and steel strains at *Collapse Prevention* performance level together with the ultimate steel strain are given as

$$\varepsilon_c^{(GÖ)} = 0.0035 + 0.04\sqrt{\omega_{we}} \leq 0.018 \quad \text{------------- (2.13)}$$

$$\varepsilon_s^{(GÖ)} = 0.4\,\varepsilon_{su} \quad \text{------------- (2.14)}$$

$$\varepsilon_{su} = 0.08 \quad \text{------------- (2.15)}$$

Strain results for maximum tension and compression states are presented in *Table 2.15*. According to *Equation 2.13*, maximum compression strain should not exceed 0.018. Maximum compression strain obtained from the conducted nonlinear time history analyses is 0.00244 (see *Table 2.15*). Similarly, according to *Equation 2.14*, maximum tension strain should not exceed 0.032 which is calculated by using ultimate steel strain given in *Equation 2.15*. Maximum tension strain obtained from the analyses is 0.01853 (see *Table 2.15*). According to these results the structure meets the strain requirements. In *Table 2.15*, H1 and H2 are Horizontal – 1 and Horizontal – 2 components of the corresponding ground motion records, respectively.

Table 2.15. Strain Results of Phase 3

Direction	**Earthquake Name**	**Tension Strain**	**Compression Strain**
H1 = X & H2 = Y	Parkfield (1966)	0.00785	0.00156
	San Fernando (1971)	0.00565	0.00128
	Imperial Valley (1979)	0.00989	0.00149
	Loma Prieta (1989)	0.01109	0.00119
	Duzce (1999)	0.00466	0.00130
	Manjil (1990)	0.00517	0.00147
	Chi-Chi (1999)	0.01131	0.00176
	Cape Mendocino (1992)	0.00897	0.00151
	Landers (1992)	0.01032	0.00156
	Chuetsu-oki (2007)	0.01069	0.00162
	Iwate-Miyagi (2008)	0.01196	0.00201
H1 = Y & H2 = X	Parkfield (1966)	0.00550	0.00129
	San Fernando (1971)	0.00368	0.00093
	Imperial Valley (1979)	0.00899	0.00156
	Loma Prieta (1989)	0.00850	0.00157
	Duzce (1999)	0.00771	0.00135
	Manjil (1990)	0.00391	0.00124
	Chi-Chi (1999)	0.01853	0.00244
	Cape Mendocino (1992)	0.00811	0.00148
	Landers (1992)	0.01414	0.00169
	Chuetsu-oki (2007)	0.00598	0.00136
	Iwate-Miyagi (2008)	0.01524	0.00217
Maximum Strain		0.01853 < 0.032	0.00244 < 0.018

Drift ratio results are presented in X and Y directions in *Table 2.16.* According to the *Code (TBSC18)*, mean drift ratio value should not exceed 0.03. Also, maximum drift ratio should not exceed 0.045. According to *Table 2.16*, maximum drift ratio is 0.01472 and mean drift ratio is 0.00921, meaning that the structure meets drift ratio requirements.

Table 2.16. Drift Ratio Results of Phase 3

Direction	**Earthquake Name**	**X Dir. Drift Ratio**	**Y Dir. Drift Ratio**
H1 = X & H2 = Y	Parkfield (1966)	0.01158	0.00981
	San Fernando (1971)	0.00858	0.00767
	Imperial Valley (1979)	0.00549	0.00953
	Loma Prieta (1989)	0.00698	0.00842
	Duzce (1999)	0.01109	0.00889
	Manjil (1990)	0.00672	0.00871
	Chi-Chi (1999)	0.00937	0.00963
	Cape Mendocino (1992)	0.01472	0.00602
	Landers (1992)	0.00507	0.00654
	Chuetsu-oki (2007)	0.00798	0.00891
	Iwate-Miyagi (2008)	0.01179	0.01096
H1 = Y & H2 = X	Parkfield (1966)	0.01187	0.01123
	San Fernando (1971)	0.00737	0.00657
	Imperial Valley (1979)	0.01005	0.00654
	Loma Prieta (1989)	0.01093	0.00585
	Duzce (1999)	0.00959	0.00824
	Manjil (1990)	0.00825	0.00533
	Chi-Chi (1999)	0.00912	0.00937
	Cape Mendocino (1992)	0.00673	0.01448
	Landers (1992)	0.00857	0.00449
	Chuetsu-oki (2007)	0.00923	0.00573
	Iwate-Miyagi (2008)	0.01148	0.01267
Maximum Drift Ratio		0.01472 < 0.045	0.01448 < 0.045
Mean Drift Ratio		0.00921 < 0.03	0.00844 < 0.03

CHAPTER 3

EARTHQUAKE GROUND MOTION DATA SELECTION AND PROCESSING

3.1 Data Selection

Philosophy behind the seismic design of structural systems mainly depends on Newton's second law. Structures must have adequate capacity to resist inertial forces acting on the structures as a result of strong ground shaking during earthquakes. These inertial forces are due to the earthquake ground motion accelerations. When an earthquake occurs, a huge amount of energy is released. This suddenly released energy dissipates by wave propagation. Generated seismic waves from a seismic source travel through the bedrock and soil media up to the surface where they are recorded by a seismogram at a station (Stein & Wysession, 2009). *Figure 3.1* shows the schematic geometry of wave propagation recording.

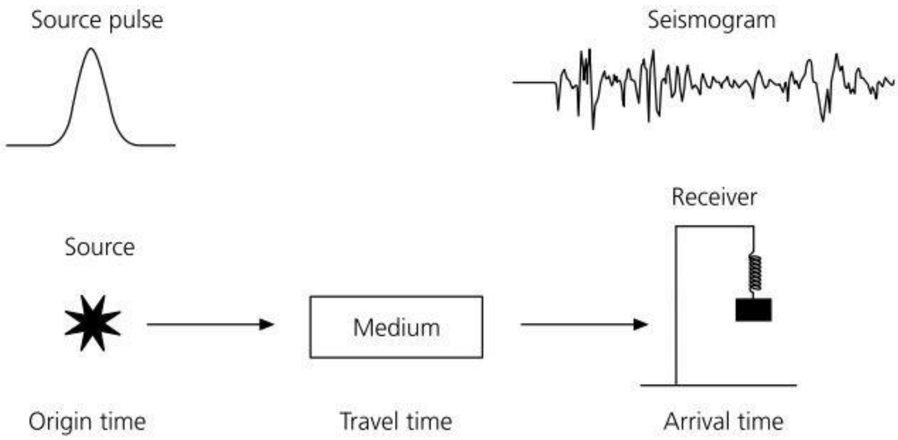

Figure 3.1. Schematic Geometry of Wave Propagation (Stein & Wysession, 2009)

The main reason of recording different ground motion accelerations of the same earthquake at two different stations is due to change in medium properties and different source-to-site distances. It can be summarized that the magnitude of earthquake, soil beneath structure and source-to-site distances are the main effects that change the amplitude and frequency content of the recorded accelerations. Since the effect of earthquakes on buildings mainly depend on these factors, they are also the main factors considered in data selection. In this study, the following limitations are considered during data selection: Earthquake magnitude, M_w, is aimed to be between 5.5 and 7.5. Epicentral distance is limited to be less than or equal to 50 km. Furthermore, the distance values are divided into two classes to observe near-field and intermediate-field effects: 0 – 15 km and 15 km – 50 km, respectively. In *Disaster and Emergency Management Presidency (AFAD)* ground motion database, records are provided without R_{jb}. Therefore, *Italian Accelerometric Archive (ITACA)* ground motion database which provides R_{jb} is aimed to be used during the selection of the records. Initially, all site classes are aimed to be included. However, there is not sufficient number of earthquake ground motion records with site class of D and E, which fulfill the selection criteria since Italy is consist of generally rock and dense soil. Hence, only site classes of A (Rock), B (Very dense sand) and C (Dense or medium-dense sand) are considered. A total of 30 ground motion records for site class of A, 41 ground motion records for site class of B and 29 ground motion records for site class C have been selected from *European Plate Observing System (EPOS (https://www.orfeus-eu.org/data/strong/))* which contains *ITACA* ground motion database. Seismological and intensity-based parameters of the selected data are presented in *Table 3.1* and *Table 3.2,* respectively. In *Table 3.2*, EW, NS, and UD represent East-West, North-South, and Up-Down components of the records. To have a better understanding, distribution of ground motions in terms of M_w, peak ground acceleration, and R_{jb} are presented in *Figure 3.2 - Figure 3.4.* Also, acceleration time histories, Fourier Amplitude Spectra and Response Spectra of the selected data are presented in *Appendix A*.

Table 3.1 Seismological Parameters of Selected Ground Motion Records

Record ID (In this Study)	Event Name	M_w	Source Mechanism	Site Class	Ep. Dist. (km)	R_{jb} (km)	V_{s30} (m/s)
A1	L' Aquila (2009) (Central Italy)	5.5	Normal	A	3.6	1.89	NA
A2	Macerata (2016) (Central Italy)	5.9	Normal	A	10.8	3.60	NA
A3	Umbria – Marche 3rd Shock (1997)	5.6	Normal	A	8.7	6.20	NA
A4	Abruzzo (1984)	5.9	Normal	A	10.1	12.28	NA
A5	L' Aquila (2009) (Central Italy)	5.5	Normal	A	13.2	9.58	836
A6	L' Aquila (2009) (Central Italy)	5.5	Normal	A	3.4	0.26	NA
A7	Macerata (2016) (Central Italy)	5.9	Normal	A	14.4	11.20	NA
A8	Perugia (2016) (Central Italy)	6.5	Normal	A	11	0.00	NA
A9	Perugia (2016) (Central Italy)	6.5	Normal	A	12	4.41	NA
A10	Perugia (2016) (Central Italy)	6.5	Normal	A	7.8	0.00	NA

Table 3.1 Seismological Parameters of Selected Ground Motion Records (Cont.)

Record ID (In this Study)	Event Name	M_w	Source Mechanism	Site Class	Ep. Dist. (km)	R_{jb} (km)	V_{s30} (m/s)
A11	Perugia (2016) (Central Italy)	6.5	Normal	A	10.5	8.77	NA
A12	Macerata (2016) (Central Italy)	5.9	Normal	A	16.2	10.40	NA
A13	L’ Aquila (2009) (Central Italy)	5.5	Normal	A	15.6	12.29	NA
A14	Macerata (2016) (Central Italy)	5.9	Normal	A	17.4	6.84	NA
A15	Sicily (1990)	5.6	Strike-slip	A	36.9	24.58	871
A16	Macerata (2016) (Central Italy)	5.9	Normal	A	30.4	22.82	NA
A17	Sicily (1990)	5.6	Strike-slip	A	48.3	49.35	NA
A18	Macerata (2016) (Central Italy)	5.9	Normal	A	25.4	18.05	NA
A19	Perugia (2016) (Central Italy)	6.5	Normal	A	18.6	2.19	NA
A20	Perugia (2016) (Central Italy)	6.5	Normal	A	22.6	6.88	NA

Table 3.1 Seismological Parameters of Selected Ground Motion Records (Cont.)

Record ID (In this Study)	Event Name	M_w	Source Mechanism	Site Class	Ep. Dist. (km)	R_{jb} (km)	V_{s30} (m/s)
A21	Perugia (2016) (Central Italy)	6.5	Normal	A	30.6	13.61	NA
A22	Perugia (2016) (Central Italy)	6.5	Normal	A	24.8	8.00	NA
A23	Perugia (2016) (Central Italy)	6.5	Normal	A	19.2	9.78	NA
A24	Perugia (2016) (Central Italy)	6.5	Normal	A	26	12.55	NA
A25	Perugia (2016) (Central Italy)	6.5	Normal	A	31.8	31.26	NA
A26	Perugia (2016) (Central Italy)	6.5	Normal	A	20.1	18.61	NA
A27	Perugia (2016) (Central Italy)	6.5	Normal	A	39.3	34.29	NA
A28	L’ Aquila (2009)	6.1	Normal	A	23.1	16.95	1024
A29	Irpinia (1980)	6.9	Normal	A	28.3	17.98	972
A30	Irpinia (1980)	6.9	Normal	A	23.4	18.27	1018

Table 3.1 Seismological Parameters of Selected Ground Motion Records (Cont.)

Record ID (In this Study)	Event Name	M_w	Source Mechanism	Site Class	Ep. Dist. (km)	R_{jb} (km)	V_{s30} (m/s)
B1	L' Aquila (2009) (Central Italy)	5.5	Normal	B	13.4	10.15	492
B2	Friuli (1976)	5.6	Thrust	B	9.4	8.82	445
B3	Macerata (2016) (Central Italy)	5.9	Normal	B	14	4.21	NA
B4	Macerata (2016) (Central Italy)	5.9	Normal	B	13.2	5.92	498
B5	Macerata (2016) (Central Italy)	5.9	Normal	B	8.4	5.91	NA
B6	Friuli 2nd Shock (1976)	5.9	Thrust	B	6.2	3.25	445
B7	Rieti (2016) (Central Italy)	6.0	Normal	B	8.5	1.38	670
B8	L' Aquila (2009)	6.1	Normal	B	5	0.00	696
B9	L' Aquila (2009)	6.1	Normal	B	5	0.00	549
B10	L' Aquila (2009)	6.1	Normal	B	1.8	0.00	705

Table 3.1 Seismological Parameters of Selected Ground Motion Records (Cont.)

Record ID (In this Study)	Event Name	M_w	Source Mechanism	Site Class	Ep. Dist. (km)	R_{jb} (km)	V_{s30} (m/s)
B11	L' Aquila (2009)	6.1	Normal	B	4.9	0.00	474
B12	L' Aquila (2009)	6.1	Normal	B	2.2	0.00	NA
B13	Perugia (2016) (Central Italy)	6.5	Normal	B	4.7	3.14	423
B14	Perugia (2016) (Central Italy)	6.5	Normal	B	4.6	2.84	498
B15	Perugia (2016) (Central Italy)	6.5	Normal	B	8.2	2.65	NA
B16	Perugia (2016) (Central Italy)	6.5	Normal	B	11.4	0.00	NA
B17	Perugia (2016) (Central Italy)	6.5	Normal	B	9.9	3.06	NA
B18	Friuli 3rd Shock (1976)	6.0	Thrust	B	16.2	11.22	454
B19	Friuli 2nd Shock (1976)	5.9	Thrust	B	17.4	13.06	454
B20	Macerata (2016) (Central Italy)	5.9	Normal	B	39.1	28.18	579

Table 3.1 Seismological Parameters of Selected Ground Motion Records (Cont.)

Record ID (In this Study)	Event Name	M_w	Source Mechanism	Site Class	Ep. Dist. (km)	R_{jb} (km)	V_{s30} (m/s)
B21	Friuli (1976)	5.6	Thrust	B	18.6	17.36	454
B22	Umbria – Marche 2nd Shock (1997)	6.0	Normal	B	21.6	13.21	NA
B23	Macerata (2016) (Central Italy)	5.9	Normal	B	17.8	10.48	NA
B24	Macerata (2016) (Central Italy)	5.9	Normal	B	30.7	23.40	541
B25	Macerata (2016) (Central Italy)	5.9	Normal	B	35.1	27.71	NA
B26	Perugia (2016) (Central Italy)	6.5	Normal	B	26.9	10.57	NA
B27	Perugia (2016) (Central Italy)	6.5	Normal	B	27.6	11.05	NA
B28	Perugia (2016) (Central Italy)	6.5	Normal	B	26.4	10.12	670
B29	Perugia (2016) (Central Italy)	6.5	Normal	B	26.4	10.12	670
B30	Perugia (2016) (Central Italy)	6.5	Normal	B	27.2	10.88	452

Table 3.1 Seismological Parameters of Selected Ground Motion Records (Cont.)

Record ID (In this Study)	Event Name	M_w	Source Mechanism	Site Class	Ep. Dist. (km)	R_{jb} (km)	V_{s30} (m/s)
B31	Perugia (2016) (Central Italy)	6.5	Normal	B	22.6	6.30	NA
B32	Perugia (2016) (Central Italy)	6.5	Normal	B	26.1	9.79	NA
B33	Perugia (2016) (Central Italy)	6.5	Normal	B	17.4	1.05	NA
B34	Perugia (2016) (Central Italy)	6.5	Normal	B	27.7	11.37	590
B35	Perugia (2016) (Central Italy)	6.5	Normal	B	28.4	11.85	562
B36	Irpinia (1980)	6.9	Normal	B	33.3	3.91	382
B37	Irpinia (1980)	6.9	Normal	B	42.6	37.70	403
B38	Irpinia (1980)	6.9	Normal	B	21.9	6.87	498
B39	Irpinia (1980)	6.9	Normal	B	18.9	13.05	557
B40	Irpinia (1980)	6.9	Normal	B	47.1	29.37	452

Table 3.1 Seismological Parameters of Selected Ground Motion Records (Cont.)

Record ID (In this Study)	Event Name	M_w	Source Mechanism	Site Class	Ep. Dist. (km)	R_{jb} (km)	V_{s30} (m/s)
B41	Irpinia (1980)	6.9	Normal	B	35.5	29.22	539
C1	Macerata (2016) (Central Italy)	5.9	Normal	C	7.1	2.53	NA
C2	Macerata (2016) (Central Italy)	5.9	Normal	C	2.5	0.00	NA
C3	Emilia – Romagna 2nd Shock (2012)	6.0	Thrust	C	9.3	5.30	NA
C4	Emilia – Romagna 2nd Shock (2012)	6.0	Thrust	C	0.5	0.00	NA
C5	Emilia – Romagna 2nd Shock (2012)	6.0	Thrust	C	13	5.37	NA
C6	Emilia – Romagna 2nd Shock (2012)	6.0	Thrust	C	11.3	0.67	NA
C7	Emilia – Romagna 2nd Shock (2012)	6.0	Thrust	C	14.4	4.86	NA
C8	Emilia – Romagna 2nd Shock (2012)	6.0	Thrust	C	11.2	5.92	NA
C9	Emilia – Romagna 2nd Shock (2012)	6.0	Thrust	C	9.9	0.00	NA

Table 3.1 Seismological Parameters of Selected Ground Motion Records (Cont.)

Record ID (In this Study)	Event Name	M_w	Source Mechanism	Site Class	Ep. Dist. (km)	R_{jb} (km)	V_{s30} (m/s)
C10	Emilia – Romagna 2nd Shock (2012)	6.0	Thrust	C	4.1	0.00	208
C11	Perugia (2016) (Central Italy)	6.5	Normal	C	7.7	0.00	NA
C12	Macerata (2016) (Central Italy)	5.9	Normal	C	23	13.55	NA
C13	Emilia – Romagna 2nd Shock (2012)	6.0	Thrust	C	21.9	13.92	NA
C14	Emilia – Romagna 2nd Shock (2012)	6.0	Thrust	C	15.8	10.62	NA
C15	Emilia – Romagna 2nd Shock (2012)	6.0	Thrust	C	22	11.37	NA
C16	Emilia – Romagna 2nd Shock (2012)	6.0	Thrust	C	15.8	3.56	NA
C17	Emilia – Romagna 2nd Shock (2012)	6.0	Thrust	C	17.5	8.15	NA
C18	Macerata (2016) (Central Italy)	5.9	Normal	C	31	23.63	348
C19	Macerata (2016) (Central Italy)	5.9	Normal	C	19.8	15.49	NA

Table 3.1 Seismological Parameters of Selected Ground Motion Records (Cont.)

Record ID (In this Study)	Event Name	M_w	Source Mechanism	Site Class	Ep. Dist. (km)	R_{jb} (km)	V_{s30} (m/s)
C20	Emilia – Romagna 2nd Shock (2012)	6.0	Thrust	C	15.5	8.40	NA
C21	Perugia (2016) (Central Italy)	6.5	Normal	C	24.5	7.99	348
C22	Perugia (2016) (Central Italy)	6.5	Normal	C	23.1	6.39	355
C23	Perugia (2016) (Central Italy)	6.5	Normal	C	25.6	9.16	NA
C24	Perugia (2016) (Central Italy)	6.5	Normal	C	27.8	18.13	NA
C25	Perugia (2016) (Central Italy)	6.5	Normal	C	26.8	12.54	NA
C26	Perugia (2016) (Central Italy)	6.5	Normal	C	25.5	15.85	NA
C27	Emilia – Romagna 1st Shock (2012)	6.1	Thrust	C	16.1	4.34	208
C28	Perugia (2016) (Central Italy)	6.5	Normal	C	31	25.81	NA
C29	Perugia (2016) (Central Italy)	6.5	Normal	C	36.6	29.06	NA

Table 3.2 Intensity-based Parameters of Selected Ground Motion Records

Record ID (In this Study)	Low Cut Freq. / High Cut Freq. (Hz)	Arias Intensity Duration / Total duration (sec)	PGA (cm/s^2)			PGV (cm/s)			PGD (cm)		
			EW	NS	UD	EW	NS	UD	EW	NS	UD
A1	0.10 / 30.00	19.45 / 53.91	651.51	-23.58	1.59	304.10	-14.93	0.83	-247.16	4.93	-0.55
A2	0.07 / 40.00	9.98 / 39.26	-179.96	12.32	-1.87	-189.39	12.81	2.92	-215.13	8.57	-1.40
A3	0.10 / 40.00	7.44 / 36.00	94.06	3.61	-0.73	-175.51	6.74	-1.03	-43.21	2.66	0.61
A4	0.25 / 27.00	10.46 / 30.68	109.84	3.61	0.57	98.25	-3.78	0.79	61.88	-2.97	-0.56
A5	0.10 / 40.00	9.855/ 90.00	92.14	4.27	-0.67	74.60	-2.77	-0.41	-42.29	1.43	-0.16
A6	0.05 / 40.00	5.62 / 75.00	90.90	4.65	-0.70	70.87	3.18	0.34	102.32	-1.72	-0.50
A7	0.07 / 40.00	14.96 / 59.98	57.57	4.10	-1.53	-63.75	4.35	-1.29	53.53	-3.25	-1.06
A8	0.10 / 40.00	6.75 / 45.00	-931.14	843.73	893.50	77.26	-37.80	-44.33	-9.71	14.96	-20.22
A9	0.04 / 50.00	7.00 / 53.15	779.27	-60.73	-12.42	-849.97	-30.54	-7.69	868.89	-32.63	-9.28
A10	0.10 / 30.00	9.85 / 60.00	-418.62	52.23	-14.13	571.42	-66.08	14.92	782.02	-68.62	-37.08

Table 3.2 Intensity-based Parameters of Selected Ground Motion Records (Cont.)

Record ID (In this Study)	Low Cut Freq. / High Cut Freq. (Hz)	Arias Intensity Duration / Total duration (sec)	PGA (cm/s^2)			PGV (cm/s)			PGD (cm)		
			EW	NS	UD	EW	NS	UD	EW	NS	UD
A11	0.04 / 50.00	10.33 / 61.92	274.43	27.71	-14.85	273.15	24.66	-12.76	163.57	-8.90	4.10
A12	0.10 / 30.00	9.33 / 43.45	166.93	7.31	-1.11	-164.77	13.50	2.20	-86.76	-5.70	-0.97
A13	0.04 / 40.00	9.58 / 64.89	88.03	2.37	-0.36	130.92	-4.50	0.52	-16.79	-1.06	-0.29
A14	0.03 / 50.00	7.63 / 35.26	-118.54	8.25	3.03	-83.53	-9.68	2.76	86.31	7.98	-3.49
A15	0.30 / 28.00	12.75 / 40.35	105.36	7.07	-1.17	61.25	-3.28	0.54	40.32	-2.42	0.31
A16	0.05 / 30.00	15.27 / 94.53	-93.88	3.86	0.91	-72.13	3.63	-0.72	36.22	-2.06	0.66
A17	0.30 / 26.00	24.95 / 57.04	88.65	-5.58	-0.95	-61.59	3.33	0.56	-37.17	2.37	-0.27
A18	0.04 / 40.00	14.82 / 64.91	88.32	4.35	1.09	-49.27	2.93	0.82	-38.63	1.95	0.88
A19	0.06 / 30.00	6.42 / 35.00	425.86	-44.11	-14.16	384.70	-39.41	-10.51	-546.90	-23.91	-10.55
A20	0.04 / 70.00	8.08 / 50.75	-356.09	-34.60	-12.56	-395.56	21.57	-5.47	204.44	-20.66	4.90

Table 3.2 Intensity-based Parameters of Selected Ground Motion Records (Cont.)

Record ID (In this Study)	Low Cut Freq. / High Cut Freq. (Hz)	Arias Intensity Duration / Total duration (sec)	PGA (cm/s^2)			PGV (cm/s)			PGD (cm)		
			EW	NS	UD	EW	NS	UD	EW	NS	UD
A21	0.04 / 70.00	8.08 / 50.75	214.93	-6.92	2.74	-252.61	-9.41	-3.95	-107.20	8.10	3.13
A22	0.04 / 70.00	9.97 / 65.41	-165.74	15.43	4.94	-195.11	41.97	-13.87	-86.08	14.75	-5.50
A23	0.03 / 30.00	11.00 / 54.17	-185.32	8.92	6.56	-185.09	-11.42	9.16	136.91	-11.45	-5.57
A24	0.05 / 30.00	14.85 / 60.00	-130.68	6.43	3.30	114.30	-6.17	-3.32	109.73	-5.73	-1.82
A25	0.03 / 50.00	11.10 / 46.38	-92.68	-6.80	-1.99	76.93	-4.62	-1.66	-45.40	3.64	-2.23
A26	0.10 / 30.00	17.05 / 48.26	73.46	6.57	-5.05	-87.24	-5.86	-1.40	-63.96	5.35	3.35
A27	0.04 / 30.00	14.35 / 84.68	-59.27	3.82	-3.70	-74.16	-5.53	-2.73	23.57	2.61	-2.69
A28	0.02 / 30.00	16.05 / 54.96	42.92	-3.54	-0.77	61.37	2.89	0.63	22.61	3.26	-0.94
A29	0.08 / 40.00	19.35 / 100.00	-80.96	-13.93	-7.78	-94.49	21.42	11.84	-53.06	13.23	8.30
A30	0.10 / 30.00	52.77 / 76.21	56.32	6.28	-2.55	54.71	-5.05	2.01	33.89	3.40	-1.46

Table 3.2 Intensity-based Parameters of Selected Ground Motion Records (Cont.)

Record ID (In this Study)	Low Cut Freq. / High Cut Freq. (Hz)	Arias Intensity Duration / Total duration (sec)	PGA (cm/s^2)			PGV (cm/s)			PGD (cm)		
			EW	NS	UD	EW	NS	UD	EW	NS	UD
B1	0.10 / 50.00	6.62 / 70.00	-276.52	16.34	1.38	-246.85	9.80	1.45	91.44	-3.44	-0.56
B2	0.20 / 25.00	3.50 / 9.45	-293.50	-20.32	3.63	-321.91	-36.68	4.04	232.59	13.45	1.86
B3	0.15 / 40.00	5.50 / 30.00	377.21	-12.70	-1.48	-538.79	17.13	2.50	474.88	6.46	0.88
B4	0.04 / 30.00	12.30 / 57.71	248.28	-16.24	-2.75	-366.36	-14.56	-2.14	208.84	-7.93	1.22
B5	0.07 / 40.00	9.10 / 83.68	-253.55	-10.55	-1.76	-223.23	-9.49	-2.60	-150.49	-5.19	-1.66
B6	0.30 / 25.00	5.05 / 19.42	-631.78	-68.44	-11.54	-318.47	-33.74	-8.09	476.99	-20.59	-4.38
B7	0.06 / 40.00	4.80 / 27.89	-850.80	43.55	-3.27	368.39	-41.50	8.54	391.37	-33.70	-8.87
B8	0.10 / 40.00	9.30 / 100.00	-437.43	-30.96	6.00	-479.27	-35.76	4.37	234.62	-10.41	-1.93
B9	0.10 / 40.00	8.12 / 40.00	394.75	-31.92	5.45	-433.85	-26.67	3.64	435.39	-9.38	-1.72
B10	0.10 / 40.00	12.85 / 100.00	323.73	-32.22	-7.19	-346.78	-35.80	11.64	355.46	-20.07	4.14

Table 3.2 Intensity-based Parameters of Selected Ground Motion Records (Cont.)

Record ID (In this Study)	Low Cut Freq. / High Cut Freq. (Hz)	Arias Intensity Duration / Total duration (sec)	PGA (cm/s^2)			PGV (cm/s)			PGD (cm)		
			EW	NS	UD	EW	NS	UD	EW	NS	UD
B11	0.10 / 40.00	8.82 / 100.00	644.25	-40.21	6.79	-535.20	-42.72	3.31	486.65	12.44	-2.45
B12	0.15 / 40.00	8.80 / 90.00	-255.27	-20.95	3.34	-301.88	-29.13	8.12	306.43	-21.24	-6.32
B13	0.05 / 60.00	15.45 / 60.00	-305.74	56.24	-23.02	-288.12	48.15	10.56	283.36	-23.49	7.42
B14	0.10 / 50.00	11.15 / 50.00	476.43	-48.29	-17.98	365.05	41.45	8.14	-367.53	25.60	6.41
B15	0.05 / 30.00	12.92 / 70.00	-244.71	-14.20	-6.16	305.01	12.73	-5.57	180.11	-7.57	-2.96
B16	0.04 / 30.00	7.30 / 76.24	-593.20	53.95	-21.28	-412.96	-34.19	18.76	632.91	-30.63	-21.13
B17	0.04 / 30.00	13.10 / 125.52	259.80	-15.43	-5.51	-277.30	-16.48	-5.10	-157.62	-6.48	-2.97
B18	0.15 / 29.00	4.85 / 24.59	-326.85	23.66	-5.31	341.51	23.66	3.55	-188.38	9.94	3.50
B19	0.20 / 29.00	6.90 / 21.99	210.13	9.79	-1.95	258.81	-9.04	1.30	-96.16	-6.49	1.66
B20	0.04 / 30.00	13.05 / 57.80	-122.18	-6.09	-1.27	-240.47	-11.68	1.69	-77.86	5.46	1.34

Table 3.2 Intensity-based Parameters of Selected Ground Motion Records (Cont.)

Record ID (In this Study)	Low Cut Freq. / High Cut Freq. (Hz)	Arias Intensity Duration / Total duration (sec)	PGA (cm/s^2)			PGV (cm/s)			PGD (cm)		
			EW	NS	UD	EW	NS	UD	EW	NS	UD
B21	0.20 / 29.00	5.42 / 18.56	-229.36	11.80	-0.86	-126.72	9.04	0.93	-116.01	3.79	0.46
B22	0.30 / 35.00	6.05 / 29.42	184.35	-10.23	-0.82	164.14	7.84	-0.63	75.05	-2.63	0.21
B23	0.07 / 30.00	10.05 / 106.18	184.08	5.16	0.96	109.80	-5.46	1.24	53.60	3.97	-0.97
B24	0.04 / 30.00	10.37 / 73.06	179.12	-11.22	1.36	-124.20	-9.02	1.05	69.75	-5.43	-0.76
B25	0.05 / 30.00	15.30 / 73.28	179.01	-13.79	1.24	-110.49	-8.51	-0.69	37.64	2.62	0.98
B26	0.04 / 70.00	9.95 / 89.79	-675.65	-33.58	-5.24	404.77	-35.92	-7.33	218.47	-21.96	4.16
B27	0.04 / 70.00	7.95 / 61.71	312.63	20.81	3.27	534.23	-38.10	-8.10	-270.94	-18.06	4.75
B28	0.04 / 70.00	6.95 / 84.49	-526.75	-36.95	-7.02	427.39	-39.10	-6.99	321.39	-31.93	4.36
B29	0.04 / 40.00	6.62 / 40.19	521.62	-37.92	-6.02	393.63	-33.52	7.46	317.82	-31.40	4.42
B30	0.04 / 70.00	9.40 / 93.76	453.45	-42.70	-7.73	-474.23	-48.93	-8.46	297.32	-35.73	4.55

Table 3.2 Intensity-based Parameters of Selected Ground Motion Records (Cont.)

Record ID (In this Study)	Low Cut Freq. / High Cut Freq. (Hz)	Arias Intensity Duration / Total duration (sec)	PGA (cm/s^2)			PGV (cm/s)			PGD (cm)		
			EW	NS	UD	EW	NS	UD	EW	NS	UD
B31	0.04 / 30.00	8.75 / 60.48	339.25	-20.42	-9.71	473.69	-83.03	12.33	229.19	-16.60	4.82
B32	0.04 / 30.00	8.55 / 45.04	-444.87	18.70	-6.08	435.95	-32.39	6.97	288.77	-21.93	3.56
B33	0.06 / 40.00	5.60 / 77.15	365.20	43.45	-14.26	-397.23	-48.08	-17.78	312.38	-34.19	-16.24
B34	0.04 / 70.00	8.42 / 60.25	312.85	-26.86	4.97	390.02	-43.23	-7.73	225.07	17.16	4.52
B35	0.04 / 70.00	11.02 / 75.29	-239.36	-13.44	2.69	377.01	-31.32	-7.71	109.46	12.80	4.59
B36	0.10 / 30.00	40.00 / 70.76	314.18	70.05	27.79	-220.80	-36.62	-13.00	226.01	-23.48	-11.11
B37	0.15 / 30.00	32.22 / 78.83	-174.82	-9.71	2.67	-214.40	-12.72	-3.40	-178.88	4.98	-2.53
B38	0.10 / 30.00	41.15 / 79.15	183.59	-34.44	-11.76	126.93	22.44	10.78	98.99	-15.32	-7.31
B39	0.10 / 30.00	49.62 / 86.10	-171.50	-29.07	-9.39	-154.98	26.01	-9.23	162.55	-23.25	-14.86
B40	0.15 / 30.00	47.50 / 79.85	138.24	13.29	-3.25	104.79	-7.91	1.82	-50.60	4.98	-2.26

Table 3.2 Intensity-based Parameters of Selected Ground Motion Records (Cont.)

Record ID (In this Study)	Low Cut Freq. / High Cut Freq. (Hz)	Arias Intensity Duration / Total duration (sec)	PGA (cm/s^2)			PGV (cm/s)			PGD (cm)		
			EW	NS	UD	EW	NS	UD	EW	NS	UD
B41	0.10 / 30.00	50.85 / 79.86	94.22	-6.76	3.13	-97.31	-15.02	5.34	-68.46	-6.66	5.65
C1	0.10 / 30.00	8.42 / 30.00	-638.31	43.76	-6.64	302.56	25.89	3.33	-468.28	12.20	-1.68
C2	0.15 / 30.00	5.75 / 30.00	-527.01	23.08	2.73	-373.13	-36.54	5.27	-389.22	-19.58	-3.01
C3	0.06 / 40.00	10.65 / 100.00	435.68	-23.58	-4.58	-495.19	21.12	5.70	253.33	6.06	-1.66
C4	0.05 / 40.00	8.65 / 150.00	411.37	31.33	-8.25	-373.01	52.38	21.07	-361.54	13.80	5.14
C5	0.05 / 40.00	11.20 / 150.00	392.11	-35.41	-7.75	-301.20	26.11	5.87	258.26	-5.72	2.21
C6	0.06 / 40.00	8.57 / 150.00	-361.21	-20.88	5.60	331.88	-24.86	5.77	171.15	-3.82	2.12
C7	0.07 / 40.00	9.10 / 100.00	-330.60	28.13	-5.32	-248.93	-19.23	-3.05	-313.85	4.88	0.72
C8	0.07 / 40.00	12.40 / 90.00	-204.10	-14.61	3.84	321.00	34.41	7.48	-398.29	6.89	2.62
C9	0.10 / 40.00	9.30 / 70.00	-258.80	17.36	6.29	290.71	-24.15	7.20	170.59	-4.97	1.62

Table 3.2 Intensity-based Parameters of Selected Ground Motion Records (Cont.)

Record ID (In this Study)	Low Cut Freq. / High Cut Freq. (Hz)	Arias Intensity Duration / Total duration (sec)	PGA (cm/s^2)			PGV (cm/s)			PGD (cm)		
			EW	NS	UD	EW	NS	UD	EW	NS	UD
C10	0.07 / 40.00	8.57 / 68.56	-218.58	28.49	-9.35	-288.63	57.53	-14.41	-840.74	-26.43	-5.64
C11	0.05 / 40.00	10.20 / 100.00	466.72	-38.24	-11.24	288.28	-23.21	-11.66	536.48	-24.93	-11.35
C12	0.06 / 50.00	8.75 / 80.00	611.83	-19.99	-1.33	367.61	-9.67	-1.76	166.38	-3.76	-0.90
C13	0.07 / 40.00	9.62 / 138.00	219.76	16.89	-3.36	-294.13	-13.82	3.02	-63.79	2.59	0.66
C14	0.07 / 40.00	12.42 / 150.00	173.87	-14.78	-3.46	269.31	-19.82	-7.31	-148.88	4.34	-1.66
C15	0.06 / 40.00	11.375/ 150.00	-243.18	13.26	-3.50	164.07	8.20	-2.37	69.24	-1.48	-0.73
C16	0.08 / 40.00	10.90 / 115.00	235.62	-26.61	-3.76	167.08	20.52	-6.31	124.18	-5.00	1.61
C17	0.05 / 30.00	11.52 / 119.00	207.74	-17.56	-2.99	-234.28	16.98	-2.86	189.07	2.96	0.90
C18	0.05 / 30.00	12.70 / 98.30	96.70	-9.16	1.07	206.41	-15.88	1.45	-45.21	4.08	1.01
C19	0.05 / 30.00	11.70 / 59.95	201.82	-6.42	1.56	-152.75	4.92	1.35	-66.67	-4.52	-2.01

Table 3.2 Intensity-based Parameters of Selected Ground Motion Records (Cont.)

Record ID (In this Study)	Low Cut Freq. / High Cut Freq. (Hz)	Arias Intensity Duration / Total duration (sec)	PGA (cm/s^2)			PGV (cm/s)			PGD (cm)		
			EW	NS	UD	EW	NS	UD	EW	NS	UD
C20	0.06 / 40.00	11.95 / 150.00	-138.73	-11.66	-4.08	-184.66	17.26	-7.02	-108.85	-2.95	1.37
C21	0.04 / 30.00	7.40 / 87.84	-1001.65	55.04	-8.68	747.74	-73.60	14.26	260.20	-31.04	-6.45
C22	0.04 / 70.00	7.32 / 92.15	-633.77	50.08	7.23	793.29	-85.39	-24.81	380.50	-39.43	-11.20
C23	0.04 / 60.00	10.62 / 70.00	273.69	-5.59	2.39	392.65	-10.04	6.68	249.12	-6.40	-2.76
C24	0.03 / 50.00	10.90 / 60.00	-372.18	-12.55	-3.79	335.60	6.88	-1.99	-219.23	5.06	-1.31
C25	0.03 / 50.00	9.62 / 65.00	-319.47	-15.67	-9.25	-209.17	13.03	-3.60	135.27	-9.43	2.90
C26	0.03 / 30.00	15.62 / 127.03	270.39	7.86	5.06	-237.81	-8.18	7.03	-82.70	-6.19	-4.44
C27	0.04 / 40.00	8.15 / 130.15	-257.24	-29.97	8.27	-258.80	46.33	10.38	297.30	-5.92	-1.87
C28	0.10 / 30.00	18.70 / 50.00	-114.86	7.50	1.55	122.40	-8.06	2.14	-66.79	4.40	1.64
C29	0.02 / 30.00	17.35 / 70.00	-109.78	-6.27	-3.10	95.81	5.67	-2.47	-51.30	3.19	-2.05

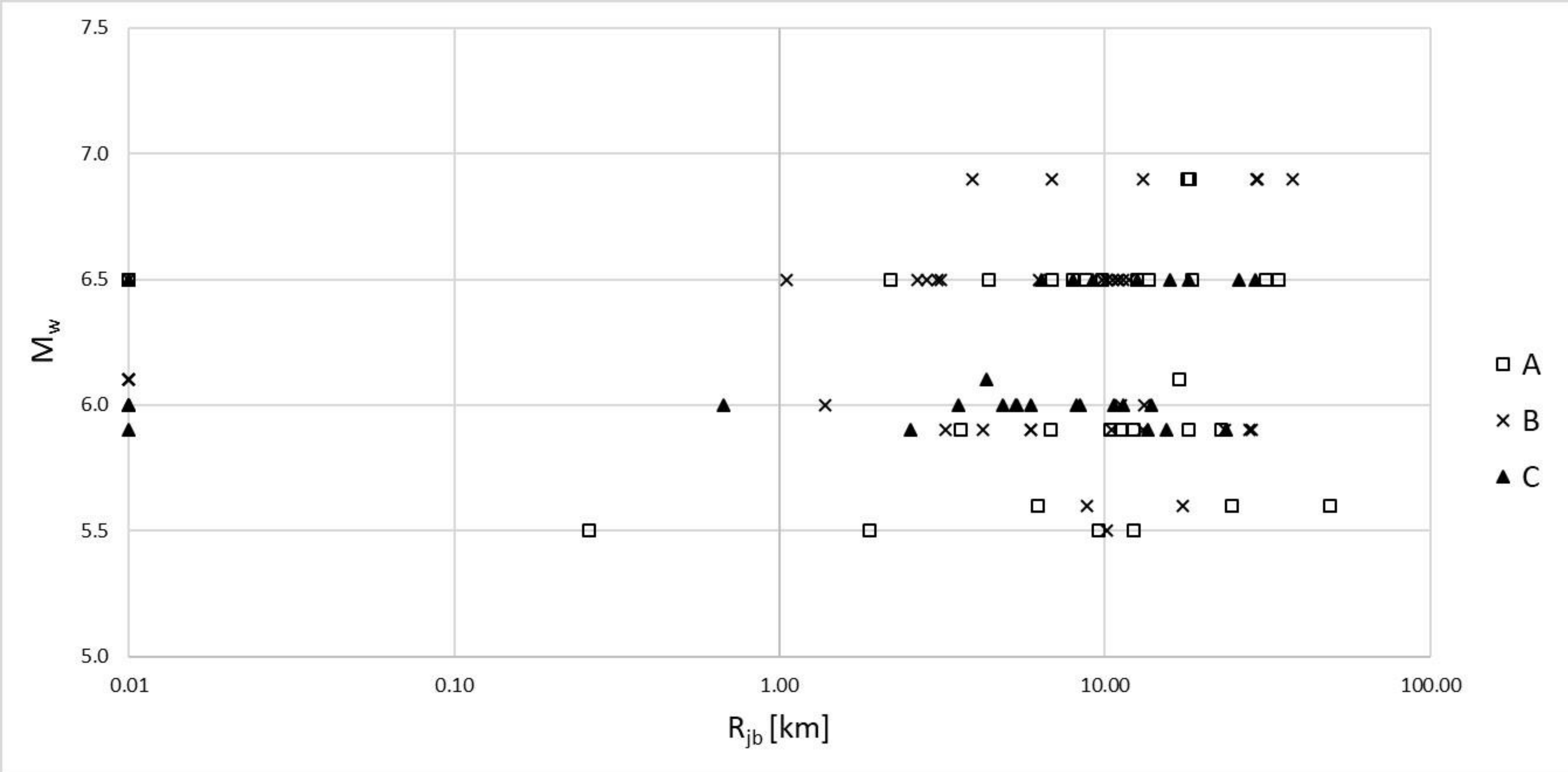

Figure 3.2. M_w – R_{jb} (R_{jb} in logarithmic scale) Distribution

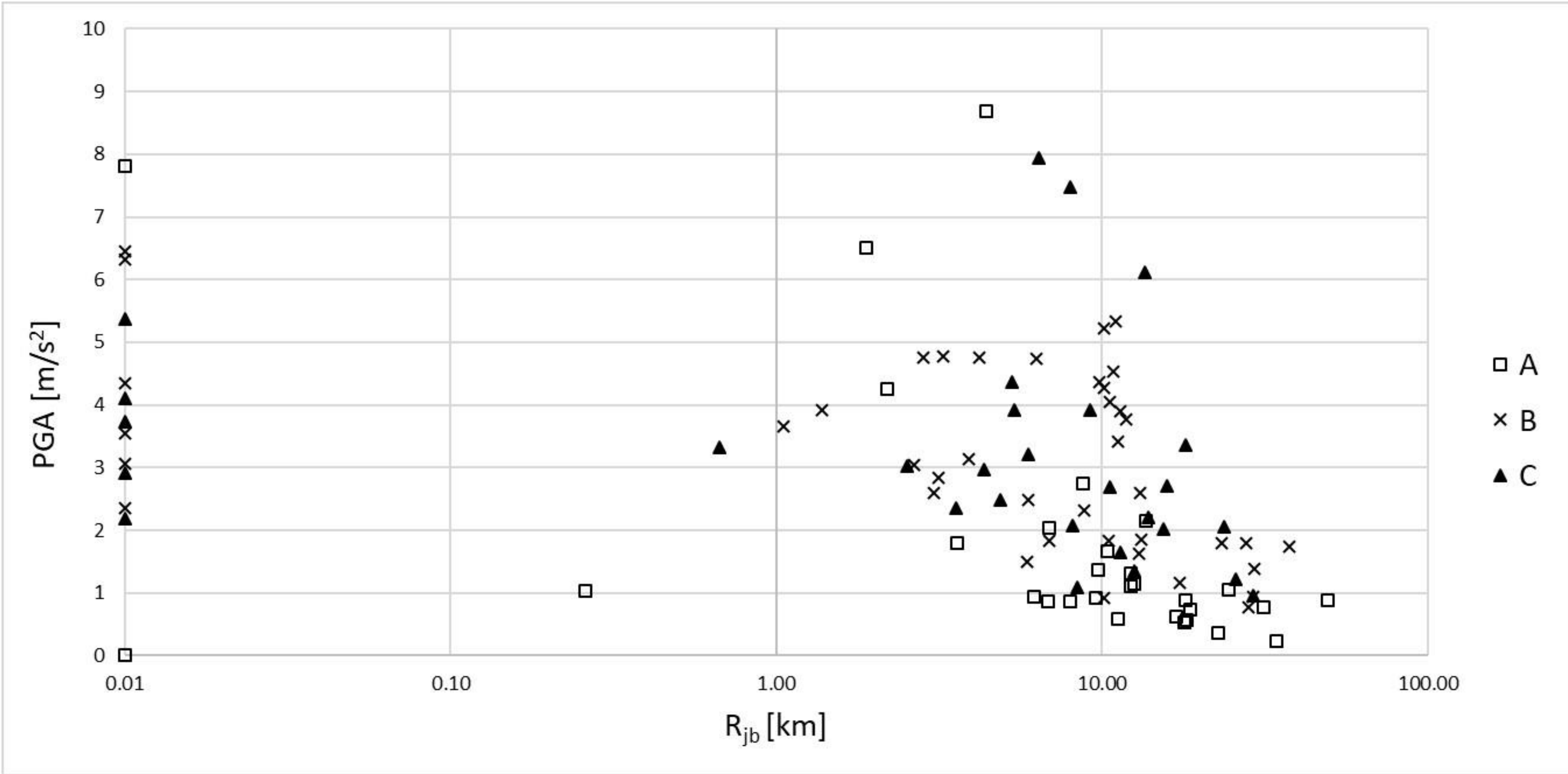

Figure 3.3. PGA – R_{jb} (R_{jb} in logarithmic scale) Distribution

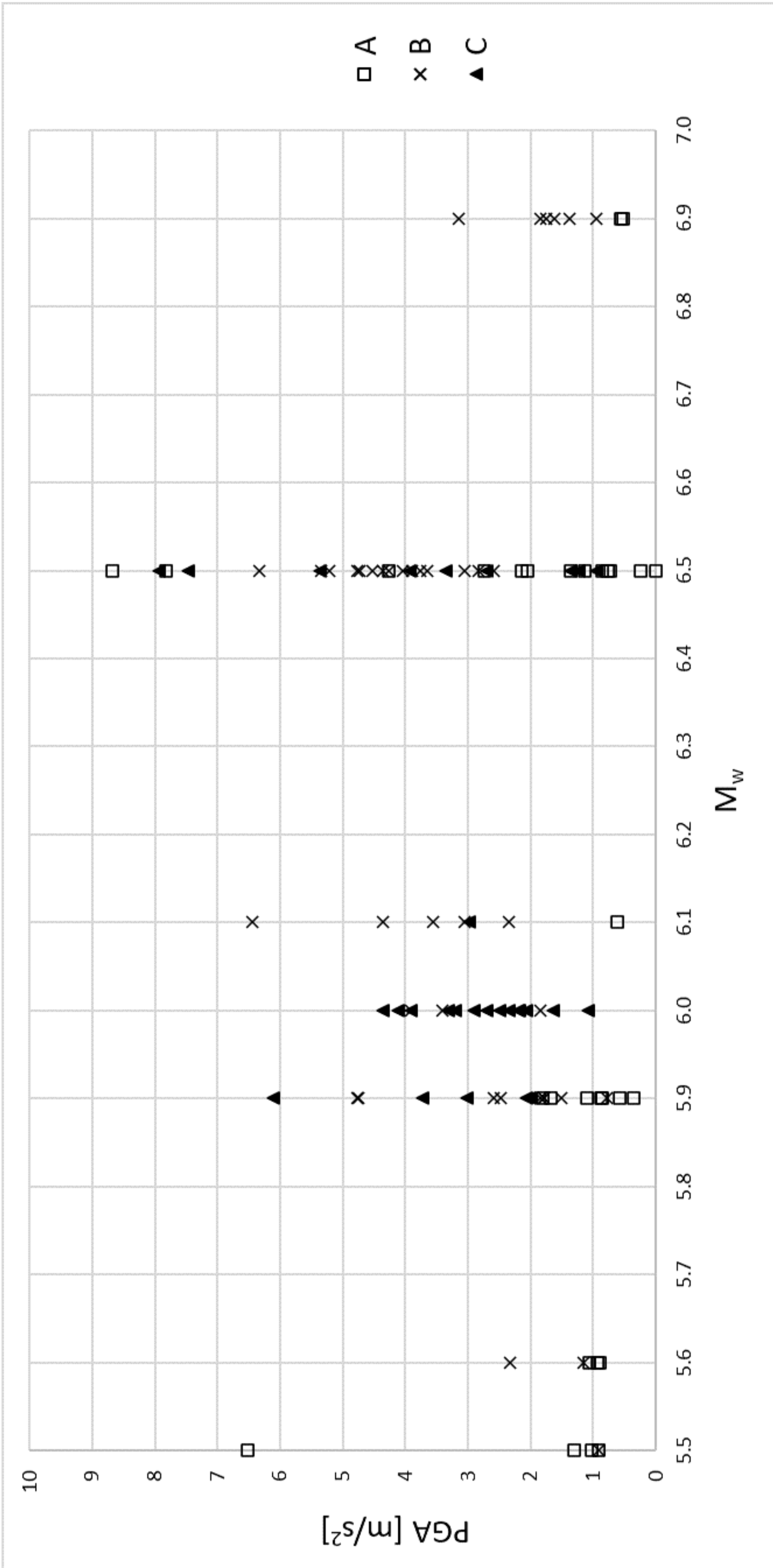

Figure 3.4. PGA – M_w Distribution

3.2 Data Processing

Raw ground motion data has to be filtered and baseline corrected to eliminate noise in the records. In this study, filtered data from *EPOS* website is employed. In *EPOS*, Second-order Butterworth filters are employed along with a linear baseline correction.

In order to take into account the effective duration, *Arias Intensity* definition is used. By considering an Arias Intensity plot, significant duration of ground motion records can be described as the timespan between 5% and 95% of the total intensity on a *Husid* plot (Wyllie, 2017). In this thesis, in order to get rid of ineffective data and shorten analysis process, the content corresponding to the significant duration of each ground motion data is extracted with the help of *Husid* plots. The dataset described herein is used in time history analyses presented in *Chapter 4*.

CHAPTER 4

MODELING AND ANALYSIS

4.1 Modeling of the Case Study Building

The case study building has been modeled as a 3D model in PERFORM 3D (COMPUTERS AND STRUCTURES, INC. version 7.0). The building is considered as fixed at the base and the foundation is not explicitly modeled. Beam and columns are modeled as frame element while walls are modeled as shell element. To shorten analysis time, slabs are not included in the model. Instead, rigid diaphragm constraint is applied at floor levels in order to simulate slab behavior. 3D view of case study model is presented in *Figure 4.1.* Detailed information regarding material and structural modeling is given in *Sections 4.1.1 – 4.1.4* of this chapter. Some important factors that may change analysis results significantly are explained in *Sections 4.1.5 – 4.1.6*.

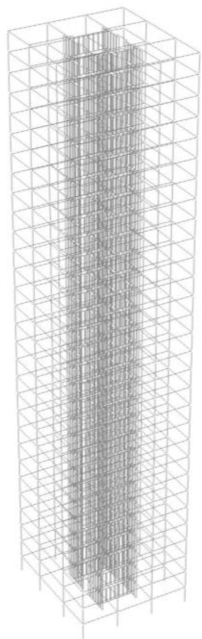

Figure 4.1. 3D view of Case Study Model

4.1.1 Materials

Concrete is modeled as an idealized uniaxial inelastic material according to *Figure 5A.1* of *TBSC18*. Stress – strain graph is given in *Figure 4.2*. Relationship between compressive stress of concrete (f_c) and concrete strain (ε_c) is given in *Equation 4.1* (*Equation 5A.1* of the Code).

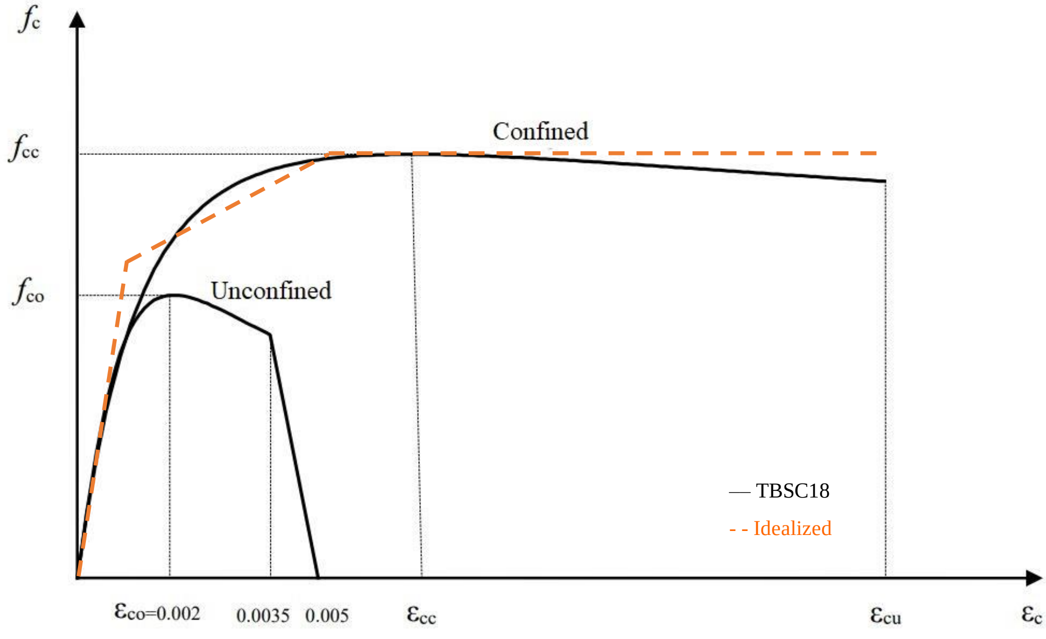

Figure 4.2. Stress – Strain Relationship of Concrete (TBSC18)

$$f_c = \frac{f_{cc}\, x\, r}{r - 1 + x^r} \quad \text{--------------------} (4.1)$$

In this equation, compressive strength of confined concrete (f_{cc}) is defined as in *Equation 4.2*. Parameters, x and r in *Equation 4.1*, are given in *Equation 4.3* and *Equation 4.4* respectively,

$$f_{cc} = \lambda_c\, f_{co} \quad \text{--------------------} (4.2)$$

$$x = \frac{\varepsilon_c}{\varepsilon_{cc}} \quad \text{-------------------- (4.3)}$$

$$r = \frac{E_c}{E_c - E_{sec}} \quad \text{-------------------- (4.4)}$$

where λ_c is defined as in *Equation 4.5*. f_{co} represents the compressive strength of unconfined concrete. Definition of strain on concrete corresponding to f_{cc} on *Figure 4.2* (ε_{cc}) is given in *Equation 4.6*. Elasticity modulus of concrete (E_c) and E_{sec} coefficient given in *Equation 4.4* are defined as in *Equations 4.7* and *4.8* respectively,

$$\lambda_c = 2.254\sqrt{1 + 7.94\frac{f_e}{f_{co}}} - 2\frac{f_e}{f_{co}} - 1.254 \quad \text{-------------------- (4.5)}$$

$$\varepsilon_{cc} = \varepsilon_{co}(1 + 5(\lambda_c - 1)) \quad \text{-------------------- (4.6)}$$

$$E_c \cong 5000\sqrt{f_{co}} \quad \text{-------------------- (4.7)}$$

$$E_{sec} = \frac{f_{cc}}{\varepsilon_{cc}} \quad \text{-------------------- (4.8)}$$

where effective confinement stress (f_e) is defined as mean of effective confinement stress in X and Y directions (f_{ex} and f_{ey}) as defined in *Equations 4.9 (a)* and *4.9 (b)* respectively. Concrete strain corresponding to f_{co} (ε_{co}) is defined in *Equation 4.10*.

$$f_{ex} = k_e\, \rho_x\, f_{yw} \quad \text{------------------ (4.9 a)}$$

$$f_{ey} = k_e\, \rho_y\, f_{yw} \quad \text{------------------ (4.9 b)}$$

$$\varepsilon_{co} \cong 0.002 \quad \text{------------------- (4.10)}$$

In *Equations 4.9 (a)* and *4.9 (b)*, f_{yw} is yield strength of transverse reinforcement, ρ_x and ρ_y are volumetric ratio of transverse reinforcement in corresponding direction and k_e is defined as

$$k_e = (1 - \frac{\sum a_i^2}{6b_0h_0})(1 - \frac{s}{2b_0})(1 - \frac{s}{2h_0})(1 - \frac{A_s}{b_0h_0})^{-1} \quad \text{-------------- (4.11)}$$

In *Equation 4.11*, a_i represents the distance between longitudinal reinforcements, b_0 and h_0 are the dimensions of confined area, s is the spacing of stirrups and A_s is the longitudinal reinforcement area.

Reinforcement is modeled as an idealized (bilinear without strain hardening) inelastic material according to *Figure 5A.2* of *TBSC18*. Stress – strain graph is given in *Figure 4.3*. Relationship between steel stress (f_s) and steel strain (ε_s) is given in *Equation 4.12* (*Equation 5A.7* of TBSC18).

$$f_s = E_s\varepsilon_s \qquad (\varepsilon_s \leq \varepsilon_{sy}) \quad \text{------------- (4.12 a)}$$

$$f_s = f_{sy} \qquad (\varepsilon_{sy} < \varepsilon_s \leq \varepsilon_{sh}) \quad \text{------------- (4.12 b)}$$

$$f_s = f_{su} - (f_{su} - f_{sy})\frac{(\varepsilon_{su} - \varepsilon_s)^2}{(\varepsilon_{su} - \varepsilon_{sh})^2} \qquad (\varepsilon_{sh} < \varepsilon_s \leq \varepsilon_{su}) \quad \text{------------- (4.12 c)}$$

The modulus of elasticity of steel (E_s) is taken as 2x10^5 MPa. Parameters in *Equation 4.12* are taken from *Table 5A.1* of *TBSC18*.

Table 4.1. Table 5A.1 of TBSC18

Grade	f_{sy} (MPa)	ε_{sy}	ε_{sh}	ε_{su}	f_{su} / f_{sy}
S220	220	0.0011	0.011	0.12	1.2
S420	420	0.0021	0.008	0.08	1.15 – 1.35
B420C	420	0.0021	0.008	0.08	1.15 – 1.35
B500C	500	0.0025	0.008	0.08	1.15 – 1.35

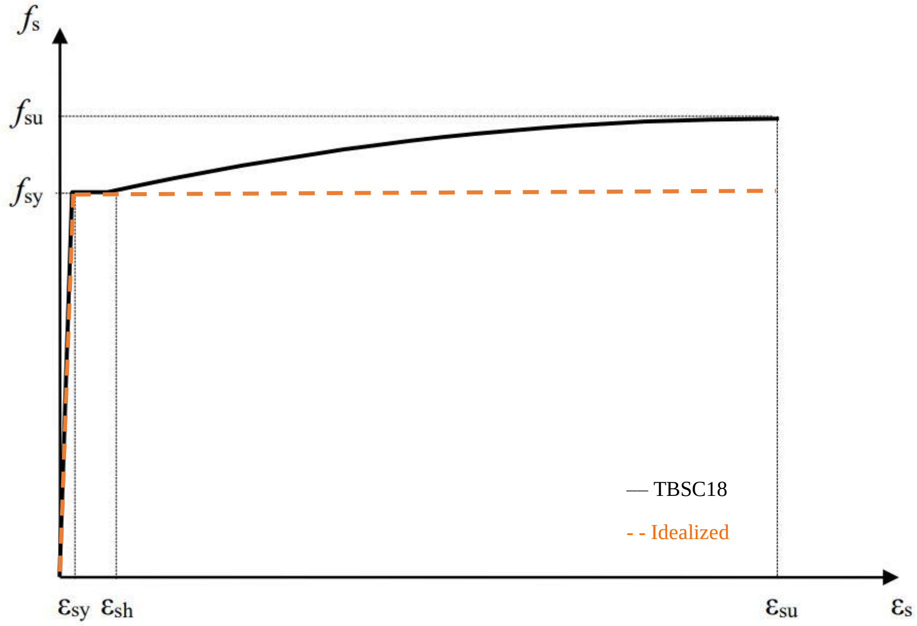

Figure 4.3. Stress – Strain Relationship of Steel (TBSC18)

4.1.2 Beam Elements

Expected behavior of beam members is flexure rather than axial load – moment interaction since these members are not expected to have more than $0.1A_cf_{ck}$ according to *TBSC18*, where A_c is gross cross-sectional area and f_{ck} is characteristic compressive strength of concrete. Therefore, beams are modeled with rotational moment hinge. This type of hinge has a rigid-plastic behavior, which is presented in *Figure 4.4*. Hinge does not have any plastic rotation until it reaches yield moment (Point Y). Between yield moment and ultimate moment (Point U) it exhibits inelastic action. Point U is the ultimate capacity, at which the hinge can no longer take additional moment with increasing rotation. After the capping point L, a descending portion exists which simulates the reduction in capacity up to the residual point R. From this point on, the residual moment capacity is constant as a percentage of the ultimate capacity. In this study, hysteretic model for the moment-rotation relationship is chosen as elastic perfectly plastic (E-P-P) (See *Section 4.1.6*).

Moreover, it is assumed that there is no cyclic degradation in strength. The beams are modeled in accordance with *Figure 4.5* without considering the rigid end zone and shear failure (According to capacity design requirements, the dominant failure mode of beams is expected to be flexural failure rather than shear failure).

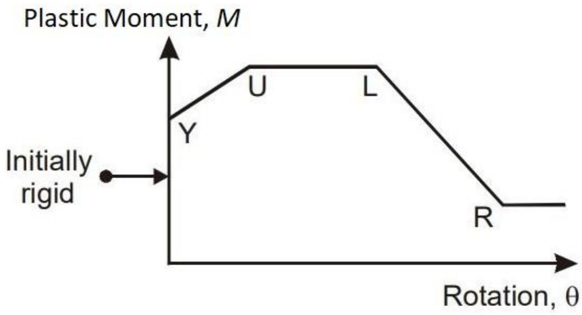

Figure 4.4. Plastic Hinge Moment – Rotation Relationship (Hill & Mallais, 2004)

Figure 4.5. Schematic Beam Model

4.1.3 Column Elements

Main difference between column and beam is that column is expected to take significant levels of axial force as well as bending moment. In order to include strength loss caused by the exceedance of the strain limit and to consider P-M-M (Axial force – moment interaction) effect, columns are modeled as inelastic fiber sections without considering shear failure. Schematic column model is presented in *Figure 4.6*.

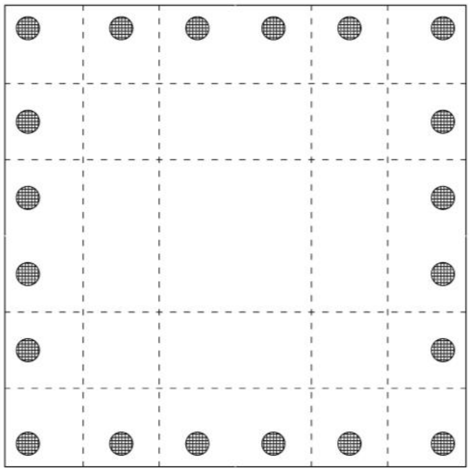

Figure 4.6. Schematic Column Model

4.1.4 Wall Elements

Like columns, structural walls are modeled as inelastic fiber sections since structural walls are also expected to take both axial force and bending moment. Both moment and shear capacity of structural walls are calculated. It is observed that shear capacity of structural walls is higher than the shear limit in moment capacity. Thus, shear behavior of structural walls is assumed to remain elastic under seismic loading. Each shell member of walls is modeled in accordance with *Figure 4.7.*

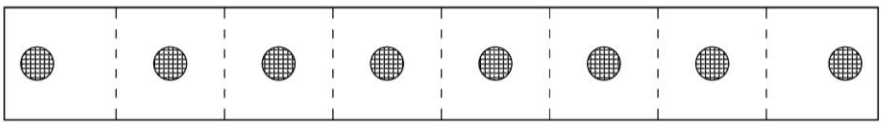

Figure 4.7. Schematic Wall Model

4.1.5 P – Δ Effect

P – Δ effect, also known as geometric nonlinearity effect, is considered if the secondary moment due to vertical forces cannot be neglected. Building deflects when horizontal loads act on it. This causes eccentricity of gravity loads resulting from laterally deflected vertical members on the building. This situation leads an increase in secondary moments on the members (Gaiotti & Smith, 1989). Then increase in secondary moment causes more lateral displacement. This lateral displacement also causes more moment on columns. This creates a loop that may repeatedly increase the moment on columns. Even small displacements on base columns may cause increase in moment drastically since axial force on base columns are expected to be high. For buildings that behave dominantly in the inelastic range P – Δ effect has a great importance (Montgomery, 1981). Therefore, in this study geometric nonlinearity is taken into account during the modeling phase. Schematic geometry of P – Δ effect is presented in *Figure 4.8.*

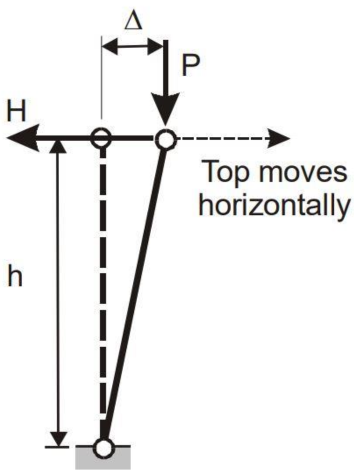

Figure 4.8. Schematic Representation of the P – Δ Effect (Hill & Mallais, 2004)

4.1.6 Simulation of Hysteretic Behavior

Reinforced concrete structures are expected to deform into inelastic range and dissipate energy through hysteretic behavior of materials under predefined ductility levels according to seismic code regulations. Development of realistic analytical models that can simulate this hysteretic behavior has an important effect on reliable prediction of the structure's dynamic behavior during earthquake excitations (Filippou, Popov, & Bertero, 1983). There are many different hysteresis models proposed in the literature. The simplest one is the hysteresis model with no stiffness degradation. In this study, *Non-Degrading Elastic Perfectly Plastic (E-P-P) hysteresis model is used* in order to keep analysis duration short. Schematic representation of *E-P-P Behavior* is presented in *Figure 4.9*.

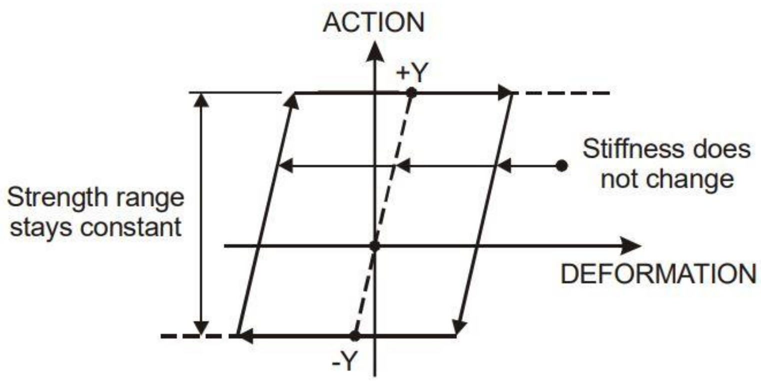

Figure 4.9. Schematic Geometry of E-P-P Behavior (Hill & Mallais, 2004)

4.2 Dynamic Characteristics of the Case Study Building Model

In this study, Eigenvalue analysis is carried out to see the modal behavior of the structure. During the modal analysis, minimum number of modes is determined according to *Equation 4.13*.

$$\sum_{n=1}^{YM} m_{txn}^{(X)} \geq 0.95\ m_t \quad \text{------------------} \quad (4.13\ \text{a})$$

$$\sum_{n=1}^{YM} m_{tyn}^{(Y)} \geq 0.95\ m_t \quad \text{------------------} \quad (4.13\ \text{b})$$

In *Equation 4.13*, $m_{txn}^{(X)}$ and $m_{tyn}^{(Y)}$ represent the nth mode effective modal base shear force obtained from earthquake load in (X) and (Y) directions, respectively and m_t is the total mass of the building.

To have a better understanding about dynamic behavior of the building, the modal participating mass ratios of important modes are presented in *Table 4.2* in tabular form and four mode shapes of the building are presented in *Figure 4.10 – Figure 4.13*.

Table 4.2 Modal Participating Mass Ratios of the Building

Mode Number	Period [sec]	UX	UY	UZ	RX	RY	RZ
1	2.825	0.633	0	0	0	0.366	0
2	2.514	0	0.668	0	0.334	0	0
3	1.846	0	0	0	0	0	0.757
4	0.690	0	0.169	0	0.239	0	0
5	0.613	0.190	0	0	0.292	0	0
6	0.589	0	0	0	0	0	0.104
7	0.329	0	0.052	0	0	0	0.043
8	0.319	0	0	0	0.093	0	0
9	0.256	0.07	0	0	0	0.098	0
10	0.243	0	0	0.505	0	0	0
Total Ratio		0.953	0.952	0.827	0.849	0.851	0.970

Modal Mass Participation Ratios

UX	UY	UZ	RX	RY	RZ
0.633	0	0	0	0.366	0

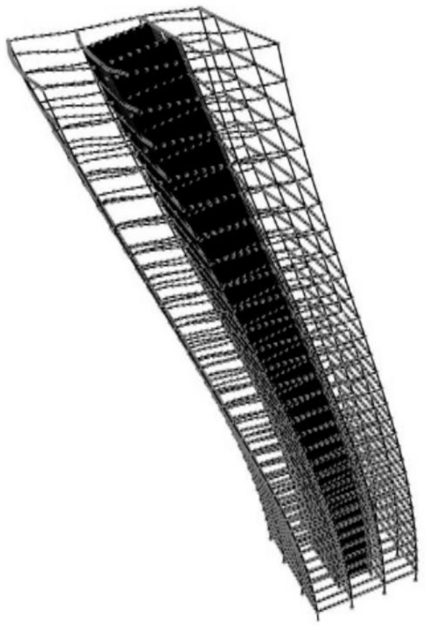

Figure 4.10. Mode 1 (T = 2.825 sec)

Modal Mass Participation Ratios

UX	UY	UZ	RX	RY	RZ
0	0.668	0	0.334	0	0

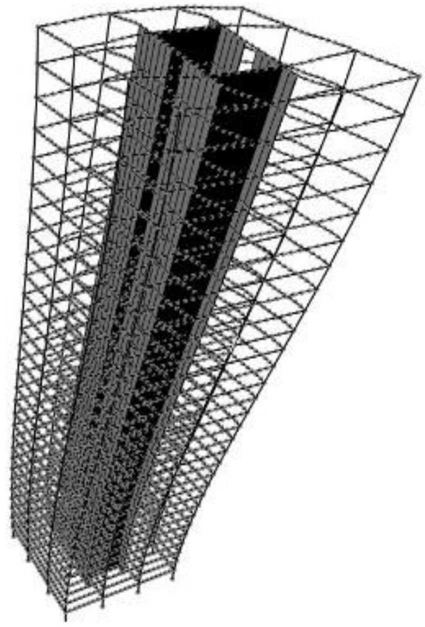

Figure 4.11. Mode 2 (T = 2.514 sec)

Modal Mass Participation Ratios

UX	UY	UZ	RX	RY	RZ
0	0	0	0	0	0.757

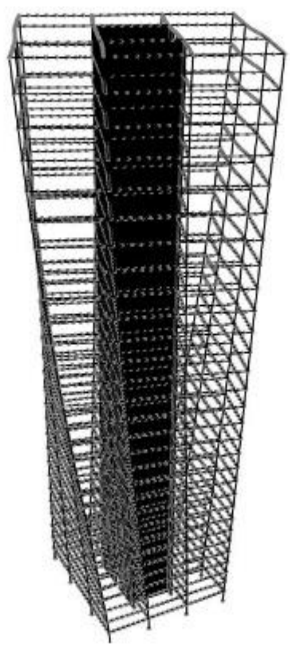

Figure 4.12. Mode 3 (T = 1.846 sec)

Modal Mass Participation Ratios

UX	UY	UZ	RX	RY	RZ
0	0	0.505	0	0	0

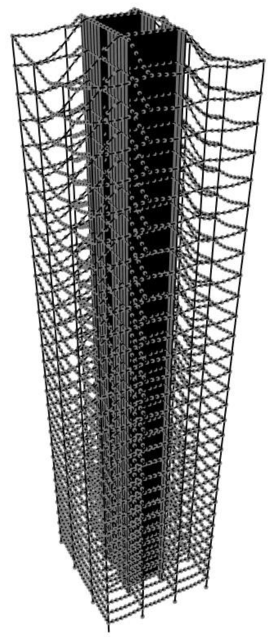

Figure 4.13. Mode 10 (T = 0.243 sec)

CHAPTER 5

TIME HISTORY ANALYSIS RESULTS

The building is analyzed based on the ground motion records given in *Chapter 3*. All records consist of horizontal (East – West and North – South) and vertical (Up – Down) components. 4 cases per each ground motion record is evaluated and summarized in *Table 5.1.* A total of 4 x 100 = 400 time history analyses are conducted.

Table 5.1. 4 Cases per Each Ground Motion Record

	Building X Direction	Building Y Direction	Building Z Direction
Case 1	East - West	North - South	-
Case 2	East - West	North - South	Up - Down
Case 3	North - South	East - West	-
Case 4	North - South	East - West	Up - Down

The effect of the vertical component of ground motion can be understood through the evaluation of the amplification factor (Amp. in *Equation 5.1*) which is defined as the ratio of maximum result obtained from the case with vertical component to the result obtained from the case without vertical component (See *Equation 5.1*).

$$\text{Amp.} = \frac{\text{Result(V+H)}_{max}}{\text{Result(H)}_{max}} \text{ ----------------- } (5.1)$$

It is observed that the axial forces on columns in some cases are close to zero. Therefore, to represent the amplification factor in axial force on column more realistically, *Equation 5.2* is used instead of *Equation 5.1*. In *Equation 5.2, Amp.* represents the ratio of the effect of vertical ground motion to column axial capacity.

$$\text{Amp.} = \frac{\text{Result(V+H)}_{max} - \text{Result(H)}_{max}}{Column\ Axial\ Capacity} \quad \text{-------------} \quad (5.2)$$

5.1 Results of Time History Analysis

In this section, all results are presented in tabular form in *Table 5.2*. The columns in the table contain time series ID (in this study), M_w, R_{jb} of the earthquakes, and site class of the records, and response parameters. Detailed results classified in terms of site class and M_w are presented in *Appendix – B.*

Table 5.2 Results in terms of Selected Response Parameters

ID (on this study)	M_w	R_{jb}	Site Class	Drift Ratio	Max. Drift Ratio on the Building	Overturning Moment	Axial Load on Column (T)	Axial Load on Column (C)	Story Shear Force
A1	5.5	1.89	A	0.99	0.0016	1.21	0.15	0.15	1.00
A2	5.9	3.60	A	1.16	0.0021	1.05	0.17	0.15	1.01
A3	5.6	6.20	A	1.11	0.0006	1.00	0.04	0.05	1.00
A4	5.9	12.28	A	1.03	0.0005	1.03	0.08	0.08	1.00
A5	5.5	9.58	A	1.14	0.0004	1.00	0.08	0.07	1.00
A6	5.5	0.26	A	1.02	0.0005	1.00	0.03	0.03	1.00
A7	5.9	11.20	A	1.15	0.0009	1.00	0.05	0.03	1.00
A8	6.5	0.00	A	0.99	0.0095	1.23	0.46	0.76	1.02
A9	6.5	4.41	A	1.06	0.0068	1.20	0.33	0.45	1.07
A10	6.5	0.00	A	1.11	0.0139	1.50	0.47	1.05	1.00

Table 5.2 Results in terms of Selected Response Parameters (Cont.)

ID (on this study)	M_w	R_{jb}	Site Class	Drift Ratio	Max. Drift Ratio on the Building	Overturning Moment	Axial Load on Column (T)	Axial Load on Column (C)	Story Shear Force
A11	6.5	8.77	A	1.07	0.0042	1.04	0.16	0.12	1.01
A12	5.9	10.40	A	1.02	0.0017	1.01	0.13	0.13	1.02
A13	5.5	12.29	A	0.97	0.0005	1.00	0.02	0.02	1.00
A14	5.9	6.84	A	0.89	0.0016	1.00	0.09	0.09	1.01
A15	5.6	24.58	A	1.03	0.0012	1.00	0.05	0.05	1.00
A16	5.9	22.82	A	1.03	0.0004	1.00	0.04	0.04	1.00
A17	5.6	49.35	A	1.09	0.0007	1.00	0.04	0.03	1.00
A18	5.9	18.05	A	1.00	0.0006	1.00	0.02	0.02	1.00
A19	6.5	2.19	A	1.05	0.0084	1.24	0.41	0.50	1.04
A20	6.5	6.88	A	1.03	0.0061	1.08	0.19	0.20	1.05
A21	6.5	13.61	A	1.03	0.0016	1.01	0.26	0.26	1.00
A22	6.5	8.00	A	0.96	0.0089	1.02	0.12	0.12	1.01
A23	6.5	9.78	A	1.08	0.0023	1.06	0.23	0.25	1.02
A24	6.5	12.55	A	1.22	0.0011	1.01	0.12	0.11	1.03
A25	6.5	31.26	A	1.02	0.0018	1.00	0.03	0.05	1.00
A26	6.5	18.61	A	0.98	0.0014	1.00	0.06	0.06	1.00
A27	6.5	34.29	A	1.02	0.0014	1.00	0.05	0.05	1.00
A28	6.1	16.95	A	1.05	0.0007	1.00	0.02	0.03	1.00
A29	6.9	17.98	A	1.02	0.0048	1.01	0.04	0.03	1.00
A30	6.9	18.27	A	1.04	0.0011	1.00	0.04	0.04	1.00
B1	5.5	10.15	B	1.16	0.0011	1.06	0.09	0.07	1.02
B2	5.6	8.82	B	0.92	0.0033	1.10	0.14	0.09	1.05
B3	5.9	4.21	B	0.95	0.0013	1.13	0.25	0.27	1.02
B4	5.9	5.92	B	1.17	0.0022	1.08	0.16	0.10	1.06
B5	5.9	5.91	B	1.07	0.0011	1.05	0.12	0.15	1.02
B6	5.9	3.25	B	1.03	0.0086	1.08	0.22	0.30	1.10
B7	6.0	1.38	B	1.06	0.0064	1.12	0.25	0.34	0.99
B8	6.1	0.00	B	0.97	0.0052	1.04	0.10	0.08	0.98
B9	6.1	0.00	B	0.92	0.0046	1.05	0.20	0.18	1.00
B10	6.1	0.00	B	1.04	0.0059	1.07	0.37	0.36	1.01

Table 5.2 Results in terms of Selected Response Parameters (Cont.)

ID (on this study)	M_w	R_{jb}	Site Class	Drift Ratio	Max. Drift Ratio on the Building	Overturning Moment	Axial Load on Column (T)	Axial Load on Column (C)	Story Shear Force
B11	6.1	0.00	B	1.00	0.0056	1.10	0.22	0.29	1.02
B12	6.1	0.00	B	1.04	0.0045	1.05	0.15	0.16	1.00
B13	6.5	3.14	B	0.95	0.0101	1.11	0.32	0.28	1.07
B14	6.5	2.84	B	1.16	0.0086	1.11	0.33	0.57	0.99
B15	6.5	2.65	B	1.04	0.0021	1.07	0.11	0.10	1.01
B16	6.5	0.00	B	1.09	0.0069	1.07	0.33	0.44	1.00
B17	6.5	3.06	B	1.11	0.0020	1.05	0.13	0.14	1.03
B18	6.0	11.22	B	0.95	0.0033	1.07	0.34	0.39	1.00
B19	5.9	13.06	B	1.03	0.0012	1.04	0.16	0.15	1.00
B20	5.9	28.18	B	1.20	0.0015	1.02	0.06	0.06	1.01
B21	5.6	17.36	B	1.13	0.0009	1.12	0.25	0.23	1.01
B22	6.0	13.21	B	1.15	0.0008	1.10	0.07	0.09	1.00
B23	5.9	10.48	B	0.99	0.0008	1.00	0.04	0.03	1.00
B24	5.9	23.40	B	0.92	0.0017	1.00	0.04	0.05	1.00
B25	5.9	27.71	B	1.02	0.0012	1.01	0.07	0.10	0.99
B26	6.5	10.57	B	1.05	0.0047	1.05	0.12	0.13	1.03
B27	6.5	11.05	B	1.02	0.0044	1.06	0.52	0.46	0.96
B28	6.5	10.12	B	1.09	0.0045	1.21	0.43	0.43	1.04
B29	6.5	10.12	B	1.16	0.0039	1.13	0.40	0.44	1.03
B30	6.5	10.88	B	1.14	0.0051	1.21	0.18	0.24	1.03
B31	6.5	6.30	B	1.06	0.0116	1.09	0.32	0.20	1.02
B32	6.5	9.79	B	0.98	0.0033	1.12	0.21	0.20	1.00
B33	6.5	1.05	B	1.11	0.0066	1.09	0.14	0.24	1.08
B34	6.5	11.37	B	1.01	0.0047	1.07	0.26	0.21	1.01
B35	6.5	11.85	B	0.98	0.0046	1.03	0.08	0.05	1.02
B36	6.9	3.91	B	1.01	0.0097	1.06	0.11	0.13	1.03
B37	6.9	37.70	B	0.99	0.0019	1.03	0.10	0.11	1.01
B38	6.9	6.87	B	1.01	0.0052	1.03	0.11	0.14	1.02
B39	6.9	13.05	B	1.01	0.0070	1.06	0.13	0.13	1.00
B40	6.9	29.37	B	1.02	0.0016	1.02	0.05	0.05	1.00

Table 5.2 Results in terms of Selected Response Parameters (Cont.)

ID (on this study)	M_w	R_{jb}	Site Class	Drift Ratio	Max. Drift Ratio on the Building	Overturning Moment	Axial Load on Column (T)	Axial Load on Column (C)	Story Shear Force
B41	6.9	29.22	B	1.04	0.0031	1.02	0.08	0.09	1.00
C1	5.9	2.53	C	1.10	0.0064	1.09	0.27	0.24	1.08
C2	5.9	0.00	C	1.16	0.0046	1.18	0.38	0.26	0.99
C3	6.0	5.30	C	1.00	0.0036	1.03	0.17	0.15	0.99
C4	6.0	0.00	C	1.04	0.0083	1.06	0.16	0.13	0.98
C5	6.0	5.37	C	1.01	0.0039	1.02	0.03	0.04	1.01
C6	6.0	0.67	C	1.07	0.0033	1.03	0.06	0.08	1.02
C7	6.0	4.86	C	0.97	0.0042	1.05	0.05	0.05	1.00
C8	6.0	5.92	C	0.99	0.0034	1.02	0.10	0.09	1.00
C9	6.0	0.00	C	1.01	0.0037	1.02	0.06	0.05	1.01
C10	6.0	0.00	C	0.98	0.0088	1.11	0.35	0.42	1.02
C11	6.5	0.00	C	1.09	0.0048	1.11	0.28	0.36	0.96
C12	5.9	13.55	C	1.04	0.0010	1.06	0.22	0.22	1.04
C13	6.0	13.92	C	1.00	0.0026	1.04	0.11	0.10	1.00
C14	6.0	10.62	C	0.99	0.0036	1.04	0.11	0.12	1.00
C15	6.0	11.37	C	1.01	0.0013	1.00	0.04	0.04	1.00
C16	6.0	3.56	C	1.17	0.0032	1.05	0.13	0.13	1.00
C17	6.0	8.15	C	0.96	0.0022	1.02	0.05	0.07	1.01
C18	5.9	23.63	C	0.97	0.0014	1.05	0.06	0.06	1.02
C19	5.9	15.49	C	1.07	0.0012	1.07	0.06	0.05	1.00
C20	6.0	8.40	C	1.00	0.0030	1.05	0.04	0.03	1.01
C21	6.5	7.99	C	1.13	0.0112	1.07	0.11	0.11	0.99
C22	6.5	6.39	C	1.00	0.0133	1.28	0.43	0.68	1.09
C23	6.5	9.16	C	1.05	0.0022	1.04	0.15	0.14	1.00
C24	6.5	18.13	C	1.09	0.0013	1.14	0.08	0.13	1.00
C25	6.5	12.54	C	1.07	0.0027	1.00	0.22	0.21	0.99
C26	6.5	15.85	C	0.97	0.0021	1.01	0.10	0.09	1.00
C27	6.1	4.34	C	0.96	0.0067	1.03	0.12	0.14	1.03
C28	6.5	25.81	C	0.98	0.0015	1.00	0.19	0.18	1.01
C29	6.5	29.06	C	1.03	0.0013	1.00	0.05	0.05	1.00

Each response parameter is evaluated separately. Results presented in *Table 5.2* and *Appendix – B* are examined in detail and summarized in *Table 5.3 – Table* 5.7. In these tables, numbers given in brackets represent related record number.

1. Inter-story Drift Ratio

Inter-story drift ratio results are summarized in *Table 5.3* and can be interpreted as follows:

- Maximum amplification factor in inter-story drift ratio is 1.222 for site class A, 1.195 for site class B, and 1.71 for site class C.
- Average amplification factor in inter-story drift ratio is around 1 for all site classes. This indicates that there is no significant increase in inter-story drift ratio.

Table 5.3 Maximum and Average Amplification Factor in Inter-story Drift Ratio

	Site Class [A]							
	M_w [5.5 – 6.0]		M_w [6.1 – 6.5]		M_w [>6.5]		M_w [All]	
	R_{jb}[<15] (10)	R_{jb}[>15] (4)	R_{jb}[<15] (10)	R_{jb}[>15] (4)	R_{jb}[<15] (0)	R_{jb}[>15] (2)	R_{jb}[<15] (20)	R_{jb}[>15] (10)
Max.	1.157	1.086	1.222	1.050	-	1.038	1.222	1.086
Ave.	1.012	1.008	1.038	1.004	-	1.006	1.025	1.006
	Site Class [B]							
	M_w [5.5 – 6.0]		M_w [6.1 – 6.5]		M_w [>6.5]		M_w [All]	
	R_{jb}[<15] (11)	R_{jb}[>15] (4)	R_{jb}[<15] (20)	R_{jb}[>15] (0)	R_{jb}[<15] (3)	R_{jb}[>15] (3)	R_{jb}[<15] (34)	R_{jb}[>15] (7)
Max.	1.172	1.195	1.159	-	1.013	1.041	1.172	1.195
Ave.	1.016	1.021	1.009	-	1.005	0.988	1.011	1.007
	Site Class [C]							
	M_w [5.5 – 6.0]		M_w [6.1 – 6.5]		M_w [>6.5]		M_w [All]	
	R_{jb}[<15] (17)	R_{jb}[>15] (2)	R_{jb}[<15] (6)	R_{jb}[>15] (4)	R_{jb}[<15] (0)	R_{jb}[>15] (0)	R_{jb}[<15] (23)	R_{jb}[>15] (6)
Max.	1.171	1.067	1.134	1.093	-	-	1.171	1.093
Ave.	1.010	1.002	1.009	0.992	-	-	1.010	0.995

2. Overturning Moment

Results of the overturning moment are summarized in *Table 5.4* and can be interpreted as follows:

- Average amplification factor in overturning moment is 1.040 for site class A, 1.058 for site class B, and 1.044 for site class C. This indicates that there is no significant increase in overturning moment. It should, however, be noted that decrease in compressive force, which could even lead to the occurrence of tension force when excessive, on vertical structural members may lead to flexural failure.

Table 5.4 Maximum and Average Amplification Factor in Overturning Moment

	Site Class [A]							
	M_w [5.5 – 6.0]		M_w [6.1 – 6.5]		M_w [>6.5]		M_w [All]	
	R_{jb}[<15] (10)	R_{jb}[>15] (4)	R_{jb}[<15] (10)	R_{jb}[>15] (4)	R_{jb}[<15] (0)	R_{jb}[>15] (2)	R_{jb}[<15] (20)	R_{jb}[>15] (10)
Max.	1.211	1.002	1.498	1.002	-	1.007	1.498	1.007
Ave.	1.019	1.001	1.099	1.001	-	1.002	1.059	1.001
	Site Class [B]							
	M_w [5.5 – 6.0]		M_w [6.1 – 6.5]		M_w [>6.5]		M_w [All]	
	R_{jb}[<15] (11)	R_{jb}[>15] (4)	R_{jb}[<15] (20)	R_{jb}[>15] (0)	R_{jb}[<15] (3)	R_{jb}[>15] (3)	R_{jb}[<15] (34)	R_{jb}[>15] (7)
Max.	1.134	1.119	1.215	-	1.060	1.033	1.215	1.119
Ave.	1.060	1.024	1.072	-	1.039	1.016	1.065	1.020
	Site Class [C]							
	M_w [5.5 – 6.0]		M_w [6.1 – 6.5]		M_w [>6.5]		M_w [All]	
	R_{jb}[<15] (17)	R_{jb}[>15] (2)	R_{jb}[<15] (6)	R_{jb}[>15] (4)	R_{jb}[<15] (0)	R_{jb}[>15] (0)	R_{jb}[<15] (23)	R_{jb}[>15] (6)
Max.	1.179	1.068	1.282	1.137	-	-	1.282	1.137
Ave.	1.034	1.042	1.079	1.031	-	-	1.046	1.034

3. Axial Load on Columns

Results of the axial force on columns are summarized in *Table 5.5 and Table* 5.6 and can be interpreted as follows:

- According to results of this study R_{jb} *[< 15]* has more effect than R_{jb} *[> 15]* on the columns in terms of compressive and tension force. Results comply with the statement suggested by Ambraseys & Douglas (2003) stating that ratio of vertical peak ground acceleration to horizontal peak ground acceleration is distance dependent and decreases with distance.
- It is observed that site class doesn't have significant effect on axial force on columns. The reason could be attributed to the fact that only sites A, B, and C are studied herein. In case of softer soils, the behavior could have been different.
- The maximum increase in compressive force on the columns is 105%, 57%, and 68% for site classes A, B, and C, respectively. Results are in line with the statement made by Mwafy & Elnashai (2006) indicating that the axial compressive forces on columns increased by 45%.
- The maximum increase in tension force on columns is 47%, 52%, and 43% for site classes A, B, and C, respectively.
- It is observed that the amplification factor for tension and compression is similar for R_{jb} *[> 15]* whilst the amplification factor for compression is relatively higher than the amplification factor for tension for R_{jb} *[< 15]*.

Table 5.5 Maximum and Average Amplification Factor in Tension Force on Column

	Site Class [A]							
	M_w [5.5 – 6.0]		M_w [6.1 – 6.5]		M_w [>6.5]		M_w [All]	
	R_{jb}[<15] (10)	R_{jb}[>15] (4)	R_{jb}[<15] (10)	R_{jb}[>15] (4)	R_{jb}[<15] (0)	R_{jb}[>15] (2)	R_{jb}[<15] (20)	R_{jb}[>15] (10)
Max.	0.172	0.047	0.467	0.056	-	0.042	0.467	0.056
Ave.	0.084	0.035	0.276	0.042	-	0.041	0.180	0.039
	Site Class [B]							
	M_w [5.5 – 6.0]		M_w [6.1 – 6.5]		M_w [>6.5]		M_w [All]	
	R_{jb}[<15] (11)	R_{jb}[>15] (4)	R_{jb}[<15] (20)	R_{jb}[>15] (0)	R_{jb}[<15] (3)	R_{jb}[>15] (3)	R_{jb}[<15] (34)	R_{jb}[>15] (7)
Max.	0.340	0.255	0.515	-	0.127	0.100	0.515	0.255
Ave.	0.168	0.108	0.246	-	0.115	0.076	0.209	0.095
	Site Class [C]							
	M_w [5.5 – 6.0]		M_w [6.1 – 6.5]		M_w [>6.5]		M_w [All]	
	R_{jb}[<15] (17)	R_{jb}[>15] (2)	R_{jb}[<15] (6)	R_{jb}[>15] (4)	R_{jb}[<15] (0)	R_{jb}[>15] (0)	R_{jb}[<15] (23)	R_{jb}[>15] (6)
Max.	0.379	0.061	0.428	0.190	-	-	0.428	0.190
Ave.	0.137	0.060	0.219	0.106	-	-	0.158	0.091

Table 5.6 Maximum and Average Amplification Factor in Compression Force on Column

	Site Class [A]							
	M_w [5.5 – 6.0]		M_w [6.1 – 6.5]		M_w [>6.5]		M_w [All]	
	R_{jb}[<15] (10)	R_{jb}[>15] (4)	R_{jb}[<15] (10)	R_{jb}[>15] (4)	R_{jb}[<15] (0)	R_{jb}[>15] (2)	R_{jb}[<15] (20)	R_{jb}[>15] (10)
Max.	0.151	0.047	1.053	0.057	-	0.038	1.053	0.057
Ave.	0.080	0.033	0.381	0.046	-	0.032	0.231	0.038
	Site Class [B]							
	M_w [5.5 – 6.0]		M_w [6.1 – 6.5]		M_w [>6.5]		M_w [All]	
	R_{jb}[<15] (11)	R_{jb}[>15] (4)	R_{jb}[<15] (20)	R_{jb}[>15] (0)	R_{jb}[<15] (3)	R_{jb}[>15] (3)	R_{jb}[<15] (34)	R_{jb}[>15] (7)
Max.	0.393	0.232	0.568	-	0.142	0.107	0.568	0.232
Ave.	0.181	0.110	0.260	-	0.134	0.084	0.223	0.099
	Site Class [C]							
	M_w [5.5 – 6.0]		M_w [6.1 – 6.5]		M_w [>6.5]		M_w [All]	
	R_{jb}[<15] (17)	R_{jb}[>15] (2)	R_{jb}[<15] (6)	R_{jb}[>15] (4)	R_{jb}[<15] (0)	R_{jb}[>15] (0)	R_{jb}[<15] (23)	R_{jb}[>15] (6)
Max.	0.416	0.058	0.676	0.176	-	-	0.676	0.176
Ave.	0.130	0.055	0.272	0.110	-	-	0.167	0.091

4. Story Shear Force

Analysis results for the story shear force are summarized in *Table 5.7* and can be interpreted as follows:

- All site classes have similar effect on story shear forces. Almost no amplification factor is observed for story shear force.
- Maximum amplification factor in base shear force is 1.067 for site class A, 1.097 for site class B, and 1.094 for site class C. This shows that base shear force is not affected by vertical ground motion.

Table 5.7 Maximum and Average Amplification Factor in Story Shear Force

	Site Class [A]							
	M_w [5.5 – 6.0]		M_w [6.1 – 6.5]		M_w [>6.5]		M_w [All]	
	R_{jb}[<15] (10)	R_{jb}[>15] (4)	R_{jb}[<15] (10)	R_{jb}[>15] (4)	R_{jb}[<15] (0)	R_{jb}[>15] (2)	R_{jb}[<15] (20)	R_{jb}[>15] (10)
Max.	1.015	1.001	1.067	1.001	-	0.999	1.067	1.001
Ave.	1.002	1.000	0.999	1.000	-	0.998	1.000	1.000
	Site Class [B]							
	M_w [5.5 – 6.0]		M_w [6.1 – 6.5]		M_w [>6.5]		M_w [All]	
	R_{jb}[<15] (11)	R_{jb}[>15] (4)	R_{jb}[<15] (20)	R_{jb}[>15] (0)	R_{jb}[<15] (3)	R_{jb}[>15] (3)	R_{jb}[<15] (34)	R_{jb}[>15] (7)
Max.	1.097	1.013	1.083	-	1.029	1.007	1.097	1.013
Ave.	0.996	0.998	0.994	-	1.011	1.002	0.996	1.000
	Site Class [C]							
	M_w [5.5 – 6.0]		M_w [6.1 – 6.5]		M_w [>6.5]		M_w [All]	
	R_{jb}[<15] (17)	R_{jb}[>15] (2)	R_{jb}[<15] (6)	R_{jb}[>15] (4)	R_{jb}[<15] (0)	R_{jb}[>15] (0)	R_{jb}[<15] (23)	R_{jb}[>15] (6)
Max.	1.080	1.024	1.094	1.013	-	-	1.094	1.024
Ave.	0.998	1.005	0.987	1.001	-	-	0.995	1.003

5.2 Comparison of Time History Analysis Results with TBSC18

A new analysis series have been run in order to improve the study by looking into the analysis prescribed in *TBSC18* and to get to a comparative baseline for the study. During the analysis process, vertical earthquake load is considered as in *Equation 5.3* which is prescribed in *TBSC18* as an approximate method for the effect of vertical earthquake load. In this equation $E_d^{(z)}$ denotes vertical earthquake load.

$$E_d^{(z)} = (2/3)S_{DS}G \quad \text{-------------------} \quad (5.3)$$

Comparison has been made between the case with the vertical component and the case prescribed in *TBSC18* by introducing the amplification factor which is the ratio of the result obtained from the case with a vertical component to result obtained from the case prescribed according to *TBSC18* (see *Equation 5.4*). The comparison of the two shows no significant difference in the result obtained in terms of the overturning moment, column axial force, and story shear force. The amplification factor for these response parameters has remained within the range of 1±0.15. What is of significant difference is the inter-story drift ratio values. Analysis results for the inter-story drift ratio is summarized in *Table 5.8.* According to the table, the amplification factor is quite bigger than 1 in all cases.

$$\text{Amp.} = \frac{\text{Result(V+H)}_{max}}{\text{Result(TBSC18)}_{max}} \quad \text{---------------} \quad (5.4)$$

Table 5.8 Maximum and Average Amplification Factor in Inter-Story Drift Ratio

	Site Class [A]							
	M_w [5.5 – 6.0]		M_w [6.1 – 6.5]		M_w [>6.5]		M_w [All]	
	R_{jb}[<15] (10)	R_{jb}[>15] (4)	R_{jb}[<15] (10)	R_{jb}[>15] (4)	R_{jb}[<15] (0)	R_{jb}[>15] (2)	R_{jb}[<15] (20)	R_{jb}[>15] (10)
Max.	1.264	1.239	2.188	2.716	-	1.418	2.188	2.716
Ave.	1.043	1.049	1.369	1.974	-	1.354	1.206	1.480
	Site Class [B]							
	M_w [5.5 – 6.0]		M_w [6.1 – 6.5]		M_w [>6.5]		M_w [All]	
	R_{jb}[<15] (11)	R_{jb}[>15] (4)	R_{jb}[<15] (20)	R_{jb}[>15] (0)	R_{jb}[<15] (3)	R_{jb}[>15] (3)	R_{jb}[<15] (34)	R_{jb}[>15] (7)
Max.	1.590	1.686	1.654	-	1.574	1.411	1.654	1.686
Ave.	1.060	1.249	1.176	-	1.312	1.148	1.151	1.205
	Site Class [C]							
	M_w [5.5 – 6.0]		M_w [6.1 – 6.5]		M_w [>6.5]		M_w [All]	
	R_{jb}[<15] (17)	R_{jb}[>15] (2)	R_{jb}[<15] (6)	R_{jb}[>15] (4)	R_{jb}[<15] (0)	R_{jb}[>15] (0)	R_{jb}[<15] (23)	R_{jb}[>15] (6)
Max.	1.738	1.754	2.160	2.311	-	-	2.160	2.311
Ave.	1.114	1.410	1.280	1.505	-	-	1.157	1.473

CHAPTER 6

SUMMARY AND CONCLUSIONS

It should be noted that conclusions to be made in this chapter have been interpreted in the light of the ground motion records specified in *Chapter 3*. Therefore, in the case of different ground motion records, conclusions may change. Also, it should be noted that this study is carried out without considering soil – structure interaction. Thus, this should be taken into account when interpreting the conclusions.

6.1 Summary

The vertical and horizontal components of ground motion can be analyzed in terms of local site conditions, source-to-site distance, and earthquake magnitude. These factors are utilized in this study to outline the effect of the vertical component of ground motion on high-rise buildings.

In this study, it is aimed to bring attention to the fact that there are no generalized specifications that help explain the effects of vertical ground motion on high-rise buildings. Therefore, an examination is carried out to see the effect of the vertical component of ground motion on high-rise buildings specifically to understand if better descriptions of design specifications can be introduced. A model reinforced concrete structure building which has 30 floors with a typical floor height of 4 m. designed with a symmetric plan layout in accordance with *Turkish Building Seismic Code 2018 (TBSC18)*. A total of 100 ground motion records are selected for non-linear time history analysis. Earthquake magnitude (M_w), soil type and source-to-site distance are considered in the selection of these records. In the selection of records, earthquake magnitude, M_w, is aimed to be between 5.5 and 7.5. Epicentral distance is limited to be less than or equal to 50 km by dividing into two classes to observe near-field and intermediate-field effects: 0 – 15 km and 15 km – 50 km, respectively.

Non-linear time history analysis is carried out to observe the behavior of the structure under time series. The results of non-linear time-history analyses are interpreted in terms of inter-story drift ratio, overturning moment, axial force on columns, and story shear force. Based on the specific case study involving a certain model and a selected dataset, the numerical results can be summarized as follows.

- Maximum amplification factor in inter-story drift ratio is 1.222 for site class A, 1.195 for site class B, and 1.71 for site class C.
- Average amplification factor in inter-story drift ratio is around 1 for all site classes.
- Average amplification factor in overturning moment is 1.040 for site class A, 1.058 for site class B, and 1.044 for site class C.
- It is observed that site class does not have significant effect on axial force on columns.
- Maximum increase in axial tension forces (compared to their axial compressive capacity) on columns increased by 0.467, 0.515, and 0.428 of their capacity for site classes (near-field) A, B, and C, respectively.
- Maximum increase in axial compressive forces (compared to their axial compressive capacity) on columns increased by 1.053, 0.568, and 0.676 of their capacity for site classes (near-field) A, B, and C, respectively.
- All site classes have similar effect on story shear forces. Almost no amplification factor is observed for story shear force.
- Maximum amplification factor in base shear force is 1.067 for site class A, 1.097 for site class B, and 1.094 for site class C. This shows that base shear force is not affected by vertical ground motion.
- No plastic hinges on columns are observed.

6.2 Conclusions

From the numerical analyses presented in this thesis, the following conclusions can be made.

- The vertical ground motion has a relatively more significant effect on axial force on columns than inter-story drift ratio, the story shear forces and overturning moment. The columns are affected more since vertical ground motion is in the same direction as the columns, and it changes the axial load on columns in both compression and tension.
- Near-field ground motion records affect the structure more clearly than the intermediate-field ground motion records. In this study, generally, near-field distance ground motion records have a relatively bigger vertical component than the intermediate-field distance ground motion records around the first period of the building (The first period of the building is around 2.85 sec). Therefore, it is acceptable to have bigger amplification factors under near-field ground motion records. For example, one of the near-file ground motion records, *A8*, has an *PGA* of *0.10g (EW), 0.11g (NS), and 0.17g (UD)* at the period of around 2.85 seconds. This is an important finding which requires analysis of special structures such as tall buildings, tower and bridges which could be affected by variations in demand in terms of the axial forces.
- The building shows similar behavior in all site classes studied herein which involves sites A, B and C. Thus, in this study, no correlation between effects of vertical motion and site class can be made. This conclusion might vary when data from other site classes are considered in dynamics analyses. Since the periods of softer sites are closer to the fundamental periods of flexible structures, the behavior might vary.
- Similarly, a direct correlation between M_w and vertical behavior is not observed. However, it is observed that vertical ground motions with high *PGA* values affects the response parameters more significantly.

- According to *TBSC18,* for some specific structural systems (see Clause 4.4.3.1 of the Code), effect of vertical ground motion should be contributed as 0.2S_{DS} of the dead load. It can be stated that the results of this study are in accordance with the new rules in *TBSC18*. According to results presented in *Table 5.8*, it may seem that the inclusion of vertical ground motion effect to the analysis as 0.2S_{DS} of the dead load may not be conservative enough in terms of inter-story drift ratio since in most cases, the inter-story drift ratio has been amplified more than a 20% compared to the ones that have been conducted according to the approximate method prescribed in *TBSC18.* However, inter-story drift ratio results are within the limitations prescribed in the Code.
- According to the results of this study, the amplification factors obtained from the case with vertical ground motion are similar to the amplification factors obtained from the case prescribed according to TBSC18 in terms of the overturning moment, and story shear force. It is also stated that the amplification factors obtained from the case with vertical ground motion are similar to the amplification factors obtained from the case without vertical ground motion. In this case, it can be said that the inclusion of vertical ground motion to the new seismic code may be unnecessary in terms of overturning moment and story shear force.
- According to the results of this study, the amplification factors obtained from the case with vertical ground motion are similar to the amplification factors obtained from the case prescribed according to TBSC18 in terms of the column axial force. It is also stated that the amplification factors obtained from the case with vertical ground motion are quite bigger than the amplification factors obtained from the case without vertical ground motion. In this case, it can be said that the inclusion of vertical ground motion to the new seismic code is the right decision in terms of column axial force.

6.3 Future Recommendations

Following recommendations can be made for future studies:

- In the future studies, soil – structure interaction can be considered.
- Although this study is conducted with 100 ground motion records, the records do not have a uniform distribution in terms of M_w, site class, and source-to-site distance. A more uniform and larger dataset would lead improved conclusions regarding the effect of vertical ground motions on seismic response.
- The fault mechanism is not taken as a variable in this study. Such a parameter can further classify the behavior of flexible structures under vertical ground motions.
- In the future studies, other response parameters can be employed to assess the results in terms of other structural aspects.
- This study is conducted for one building only. In the future studies, different types of high-rise buildings and other types of structures which could be affected variations in axial forces can be investigated.
- In this study, the model building is symmetric in plan and does not have any irregularities. Irregularity in plan and elevation which has potential to affect the behavior can be accommodated in further studies involving vertical ground motions.
- D, E, and F site classes can be included in the future studies.

REFERENCES

Ambraseys, N. N., & Douglas, J. (2003). Near-field horizontal and vertical earthquake ground motions. Soil Dynamics and Earthquake Engineering, 23(1), 1–18. https://doi.org/10.1016/S0267-7261(02)00153-7

Ambraseys, N. N., Simpson, K. A., & Bommer, J. J. (1996). Prediction of horizontal response spectra in Europe. *Earthquake Engineering and Structural Dynamics*, *25*(4), 371–400. https://doi.org/10.1002/(SICI)1096-9845(199604)25:4<371::AID-EQE550>3.0.CO;2-A

Bhanu, V., Ozcebe, A. G., & Smerzini, C. (2008). *a Study on Vertical Component of Earthquake Ground Motion and Its Effects on a Bridge*. 1–12.

Bozorgnia, Y., & Campbell, K. W. (2004). the Vertical-To-Horizontal Response Spectral Ratio and Tentative Procedures for Developing Simplified V/H and Vertical Design Spectra. *Journal of Earthquake Engineering*, *8*(2), 175–207. https://doi.org/10.1080/13632460409350486

Chopra, A. (2011). *Dynamic of Structures Chopra*.

Collier, C. J., & Elnashai, A. S. (2001). A procedure for combining vertical and horizontal seismic action effects. Journal of Earthquake Engineering, 5(4), 521–539. https://doi.org/10.1080/13632460109350404

Elnashai, A. S., & Papazoglou, A. J. (1997). Procedure and spectra for analysis of rc structures subjected to strong vertical earthquake loads. In *Journal of Earthquake Engineering* (Vol. 1). https://doi.org/10.1080/13632469708962364

Filippou, F. C., Popov, E. P., & Bertero, V. V. (1983). Effects of Bond Deterioration on Hysteretic Behaviour of Reinforced Concrete Joints. Report to the National Science Foundation. *Earthquake Engineering Research Center*.

Gaiotti, R., & Smith, B. S. (1989). P-delta analysis of building structures. *Journal of Structural Engineering (United States)*. https://doi.org/10.1061/(ASCE)0733-9445(1989)115:4(755)

Gülerce, Z., & Abrahamson, N. A. (2011). Site-specific design spectra for vertical ground motion. *Earthquake Spectra*, *27*(4), 1023–1047. https://doi.org/10.1193/1.3651317

Hill, C., Mallais, S., Hill, C., & Mallais, S. (2004). Components and Elements. *Practical WebObjects*, 187–219. https://doi.org/10.1007/978-1-4302-0751-1_7

Kawashima, K. Aizawa, K. & Takahashi, K. "Attenuation of peak ground motion and absolute acceleration response spectra of vertical ground motion". Proceedings of Japan Society of Civil Engineers. 1985: 2(2), 169-176.

Kim, S., Kim, S. J., & Chang, C. (2018). Analytical Assessment of the Effect of Vertical Ground Motion on RC Frames Designed for Gravity Loads with Various Geometric Configurations. *Advances in Civil Engineering*, *2018*. https://doi.org/10.1155/2018/4029142

Montgomery, C. J. (1981). Influence of P-Delta Effects on Seismic Design. *Canadian Journal of Civil Engineering*, *8*(1), 31–43. https://doi.org/10.1139/l81-005

Mwafy, A., & Elnashai, A. S. (2006). Vulnerability of code-compliant RC buildings under multi-axial earthquake loading. *Proceedings of the 4th International Conference on Earthquake Engineering*, (January 2006).

Nasser, F., Li, Z., Gueguen, P., & Martin, N. (2016). Frequency and damping ratio assessment of high-rise buildings using an Automatic Model-Based Approach applied to real-world ambient vibration recordings. *Mechanical Systems and Signal Processing*, *75*, 196–208. https://doi.org/10.1016/j.ymssp.2015.12.022

Newmark, N. M. “A Study of Vertical and Horizontal Spectra”. Report WASH-1255. Washington, D.C.: U.S. Atomic Energy Commission, Directorate of Licensing. 1973.

Papazoglou, A. J., & Elnashai, A. S. (1996). Analytical and field evidence of the damaging effect of vertical earthquake ground motion. *Earthquake Engineering and Structural Dynamics*, *25*(10), 1109–1137. https://doi.org/10.1002/(SICI)1096-9845(199610)25:10<1109::AID-EQE604>3.0.CO;2-0

Reitherman, R. (2008). Elementary Seismology 50 Years Later. *Seismological Research Letters*, *79*(2), 239–242. https://doi.org/10.1785/gssrl.79.2.239

Şafak, E. (1998). Propagation of seismic waves in tall buildings. *Structural Design of Tall Buildings*, *7*(4), 295–306. https://doi.org/10.1002/(SICI)1099-1794(199812)7:4<295::AID-TAL117>3.0.CO;2-5

Sev, A., & Özgen, A. (2009). Space Efficiency In High-Rise Office Buildings. *METU Journal of the Faculty of Architecture*. https://doi.org/10.4305/metu.jfa.2009.2.4

Shearer, P. M. (2009). Introduction to Seismology. In *Introduction to Seismology*. https://doi.org/10.1017/cbo9780511841552

Sokolov, V. Y., Loh, C. H., & Jean, W. Y. (2007). Application of horizontal-to-vertical (H/V) Fourier spectral ratio for analysis of site effect on rock (NEHRP-class B) sites in Taiwan. *Soil Dynamics and Earthquake Engineering*, *27*(4), 314–323. https://doi.org/10.1016/j.soildyn.2006.09.001

Stein, S., & Wysession, M. (2009). *An Introduction to Seismology, Earthquakes, and Earth Structure (Google eBook)*. Retrieved from http://books.google.com/books?hl=en&lr=&id=-z80yrwFsqoC&pgis=1

Sucuoğlu, H., & Akkar, S. (2014). Basic Earthquake Engineering. In *Basic Earthquake Engineering*. https://doi.org/10.1007/978-3-319-01026-7

TBSC-2018. (2018). Deprem Etkisi Altında Binaların Tasarımı için Esaslar.

TDY-2007. (2007). Deprem Bölgelerinde Yapılacak Binalar Hakkında Esaslar.

TS-498. (1997). Design Loads for Buildings.

TS-500. (2000). Requirements for Design and Construction of Reinforced Concrete Structures

Wyllie, D. C. (2017). Rock slope engineering: Civil applications, fifth edition. In *Rock Slope Engineering: Civil Applications, Fifth Edition*. https://doi.org/10.4324/9781315154039

Xu, S. Y., & Zhang, J. (2012). Axial-shear-flexure interaction hysteretic model for RC columns under combined actions. *Engineering Structures*, *34*, 548–563. https://doi.org/10.1016/j.engstruct.2011.10.023

Yamazaki, F., & Ansary, M. A. (1997). Horizontal-to-vertical spectrum ratio of earthquake ground motion for site characterization. *Earthquake Engineering and Structural Dynamics*, *26*(7), 671–689. https://doi.org/10.1002/(SICI)1096-9845(199707)26:7<671::AID-EQE669>3.0.CO;2-S

APPENDICES

A. Time Series, Fourier Spectra, and Response Spectra

This part contains time histories of selected ground motion records, their Fourier Spectra and Response Spectra with 5% damping. The first row of plots are time series. Whilst X axis of plot represents time (sec), Y axis of plot represents acceleration (m/s^2). In time series plot, there are three records. From top to bottom respectively plots are of East – West (EW), North – South (NS), and Up – Down (UD) component of corresponding ground motion record. Peak ground acceleration (PGA) of each component is presented on related plot. The second row of plots are Fourier spectra. X and Y axes of plot represents frequency (Hz) and Fourier amplitude respectively. Similar to time series plots, plots are of East – West (EW), North – South (NS), and Up – Down (UD) component of corresponding ground motion record from top to bottom respectively. The third row of plots are response spectra. X and Y axes of plot represents period (sec) and response acceleration (m/s^2) respectively. Like time series plots and Fourier spectra, plots are given in same order. In response spectra plots, there are design spectra of Turkish Building Seismic Code (*TBSC18*). Horizontal design spectrum (TSC-H in plot legend) is given with horizontal components of ground motion record which are EW and NS components of the record. Vertical design spectrum (TSC-V in plot legend) is given with vertical component of ground motion record which is UD component of the record.

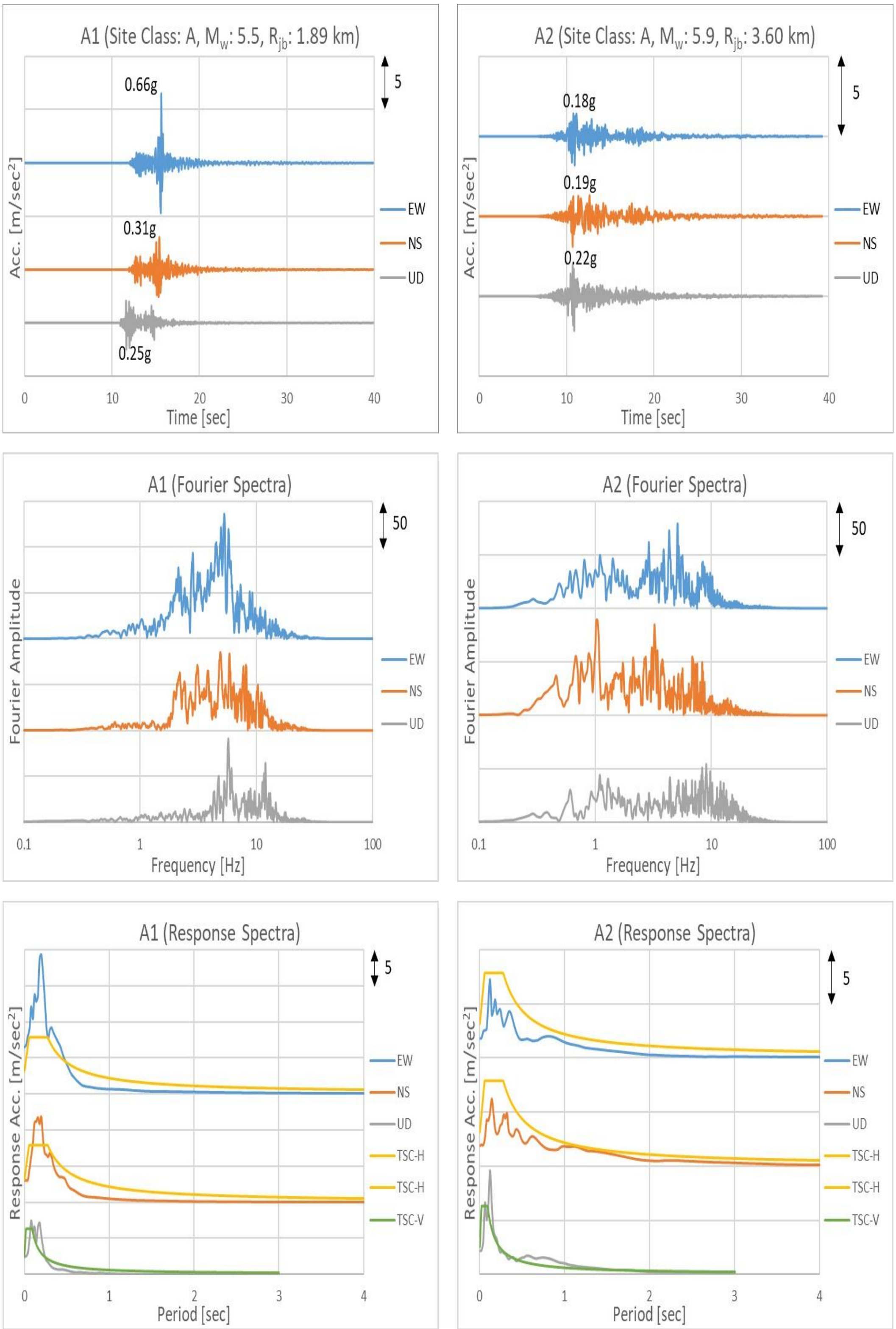

Figure A1. Acceleration Time Histories, Fourier Amplitude Spectra, and Response Spectra of the Selected Data

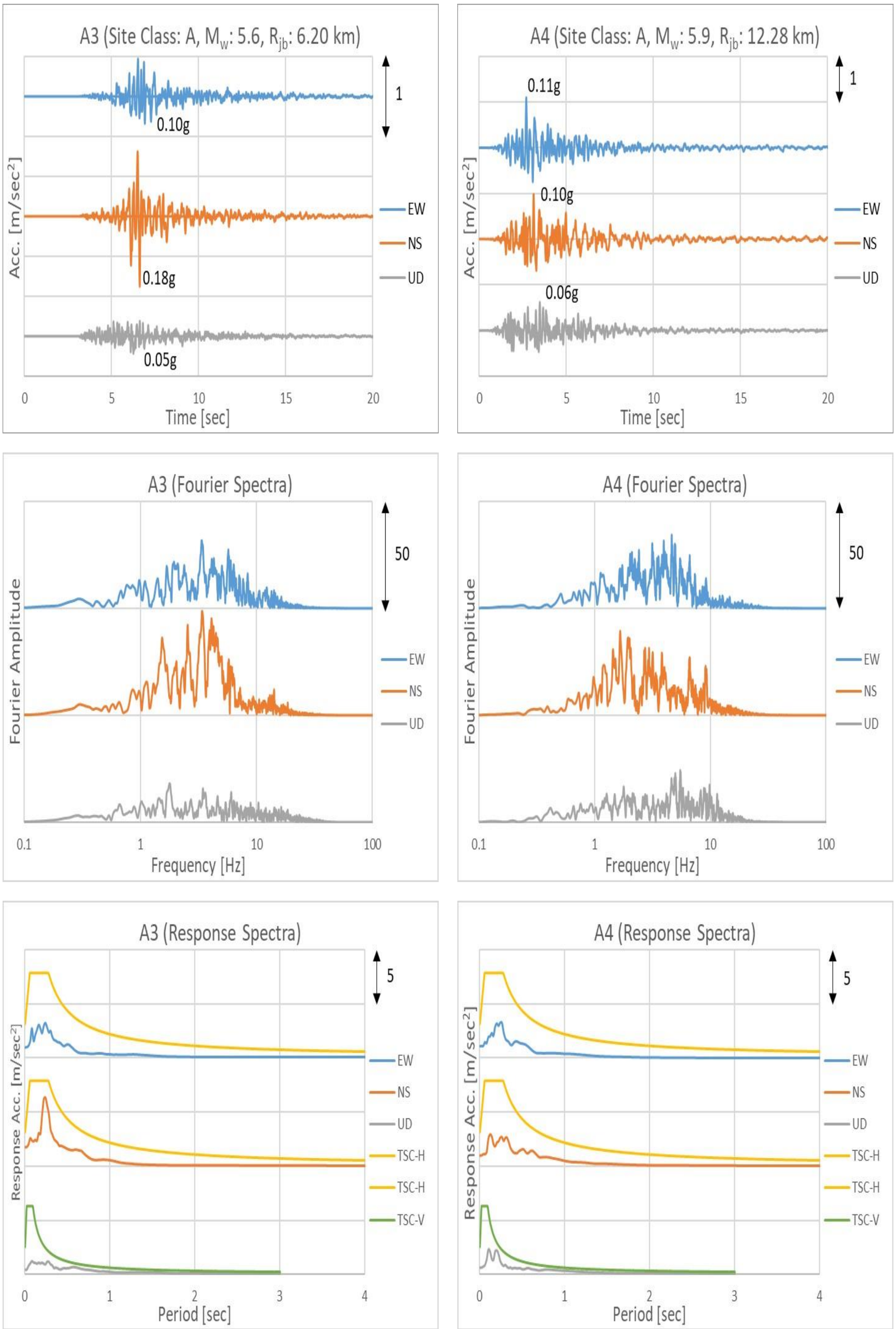

Figure A1. Acceleration Time Histories, Fourier Amplitude Spectra, and Response Spectra of the Selected Data (Cont.)

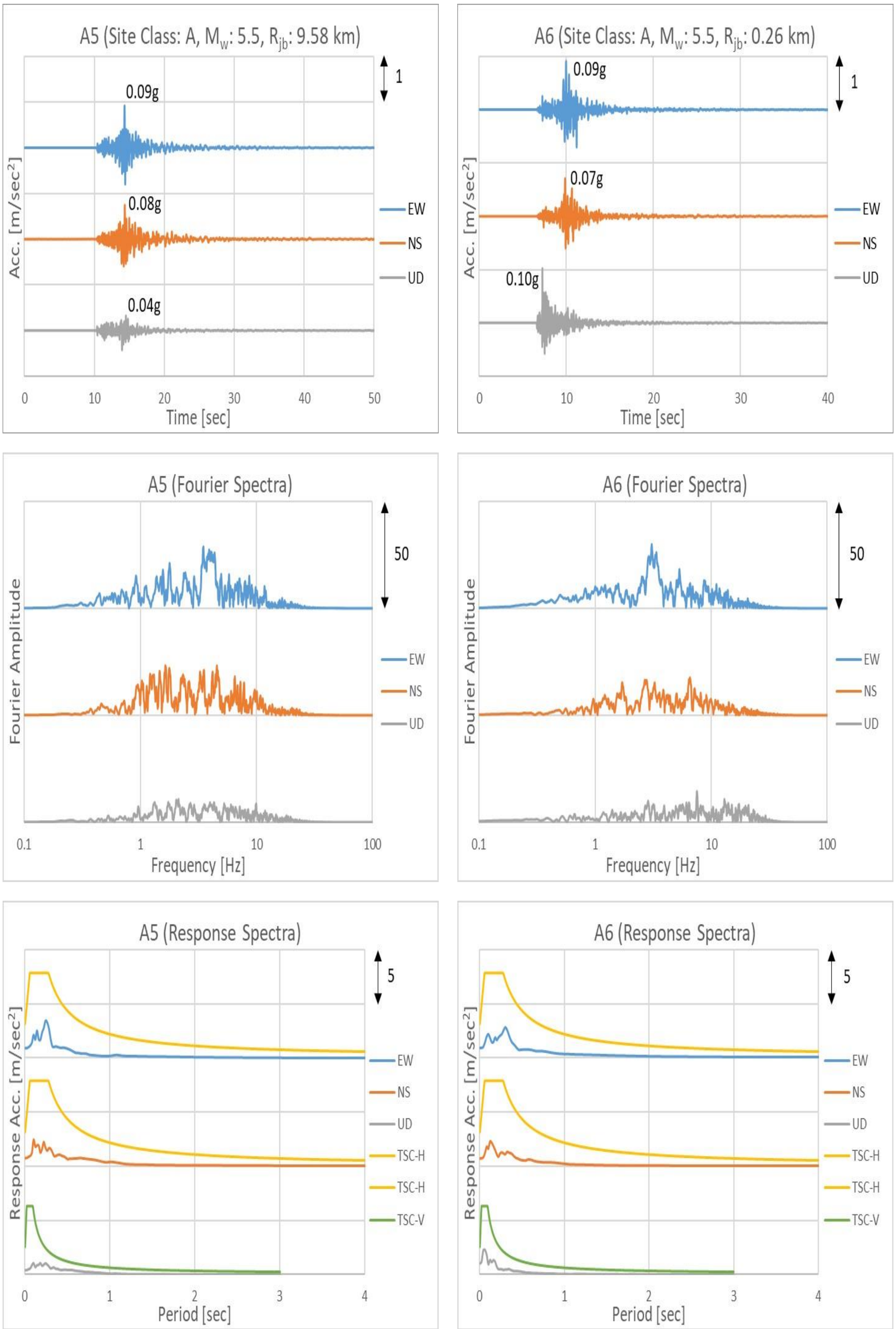

Figure A1. Acceleration Time Histories, Fourier Amplitude Spectra, and Response Spectra of the Selected Data (Cont.)

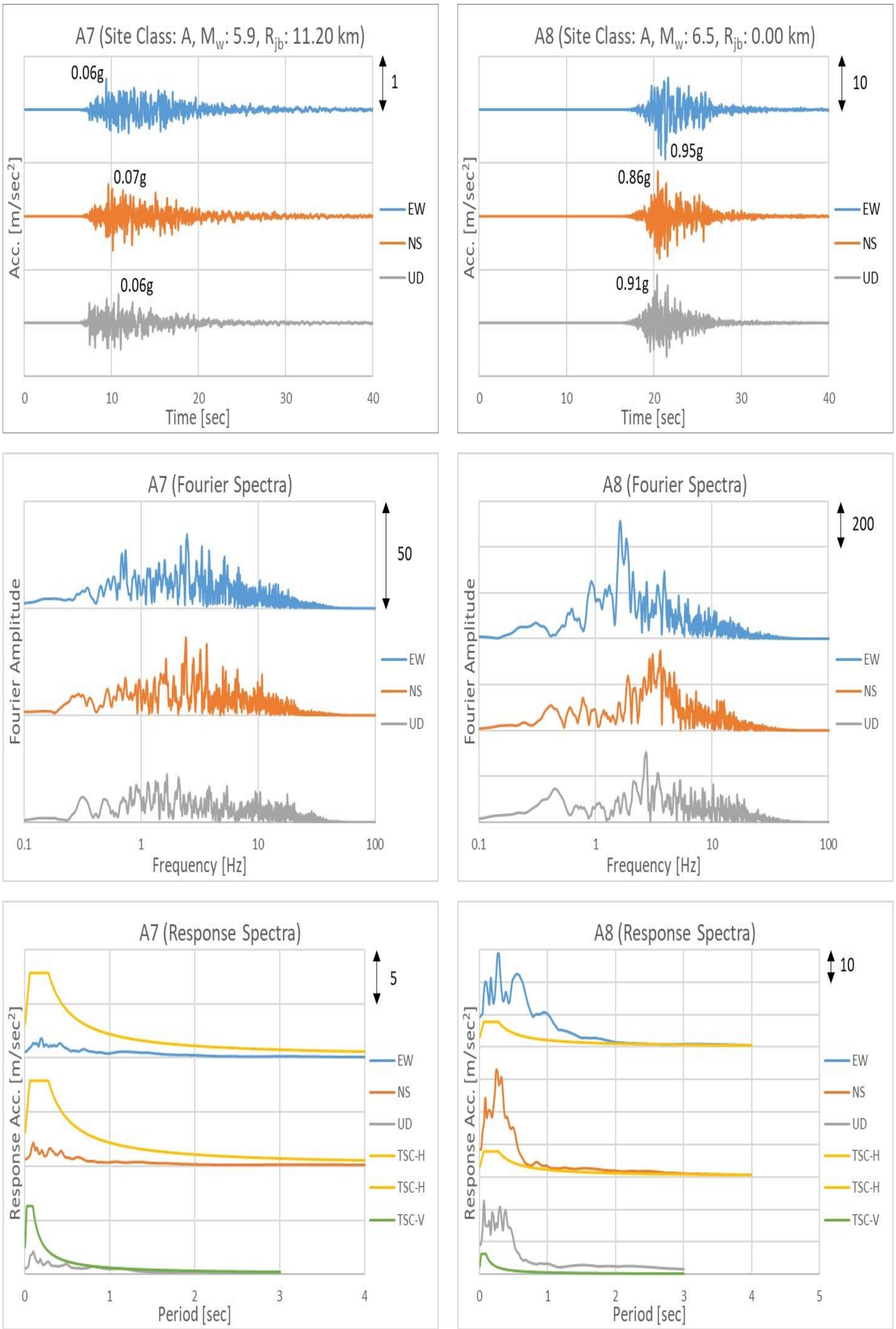

Figure A1. Acceleration Time Histories, Fourier Amplitude Spectra, and Response Spectra of the Selected Data (Cont.)

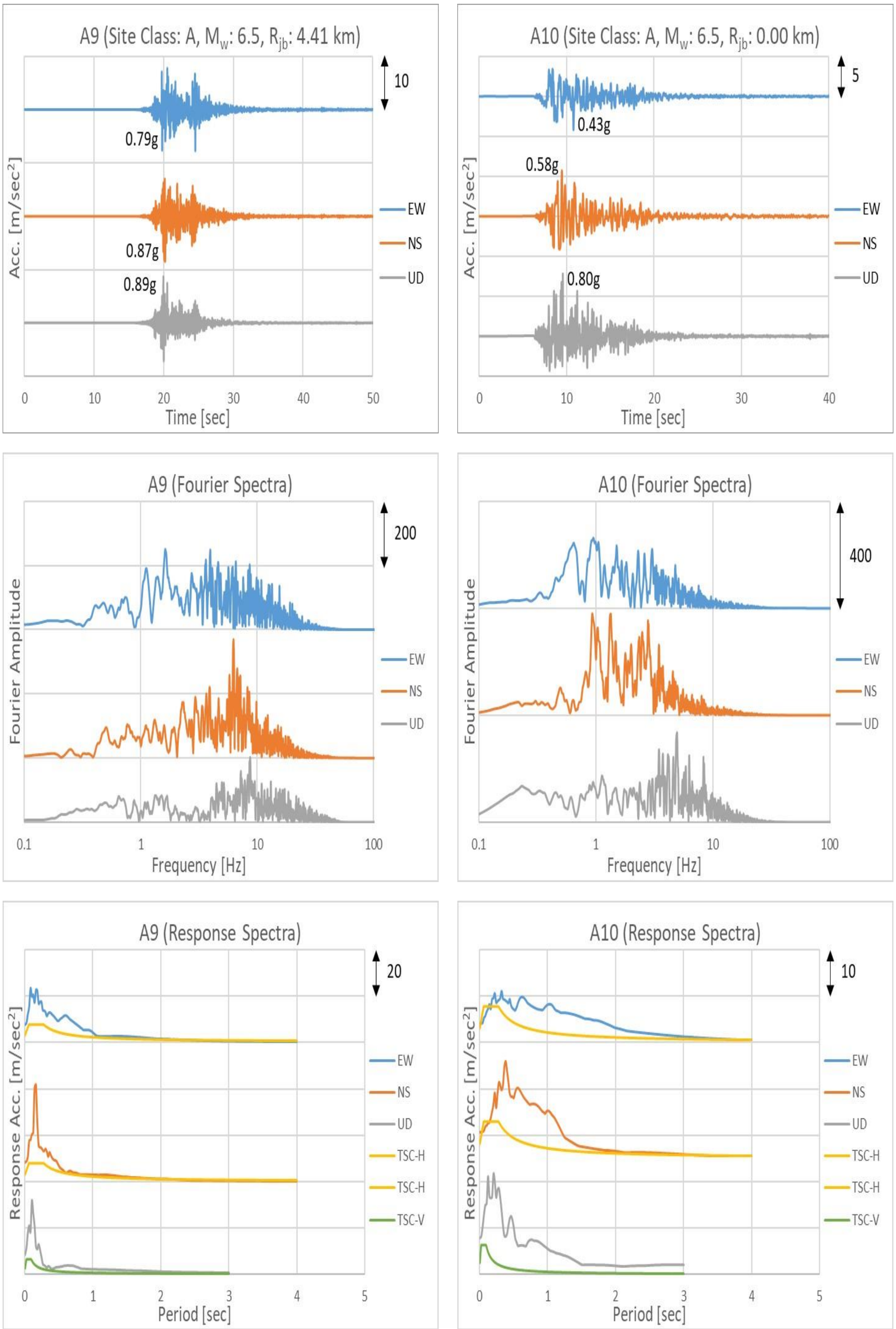

Figure A1. Acceleration Time Histories, Fourier Amplitude Spectra, and Response Spectra of the Selected Data (Cont.)

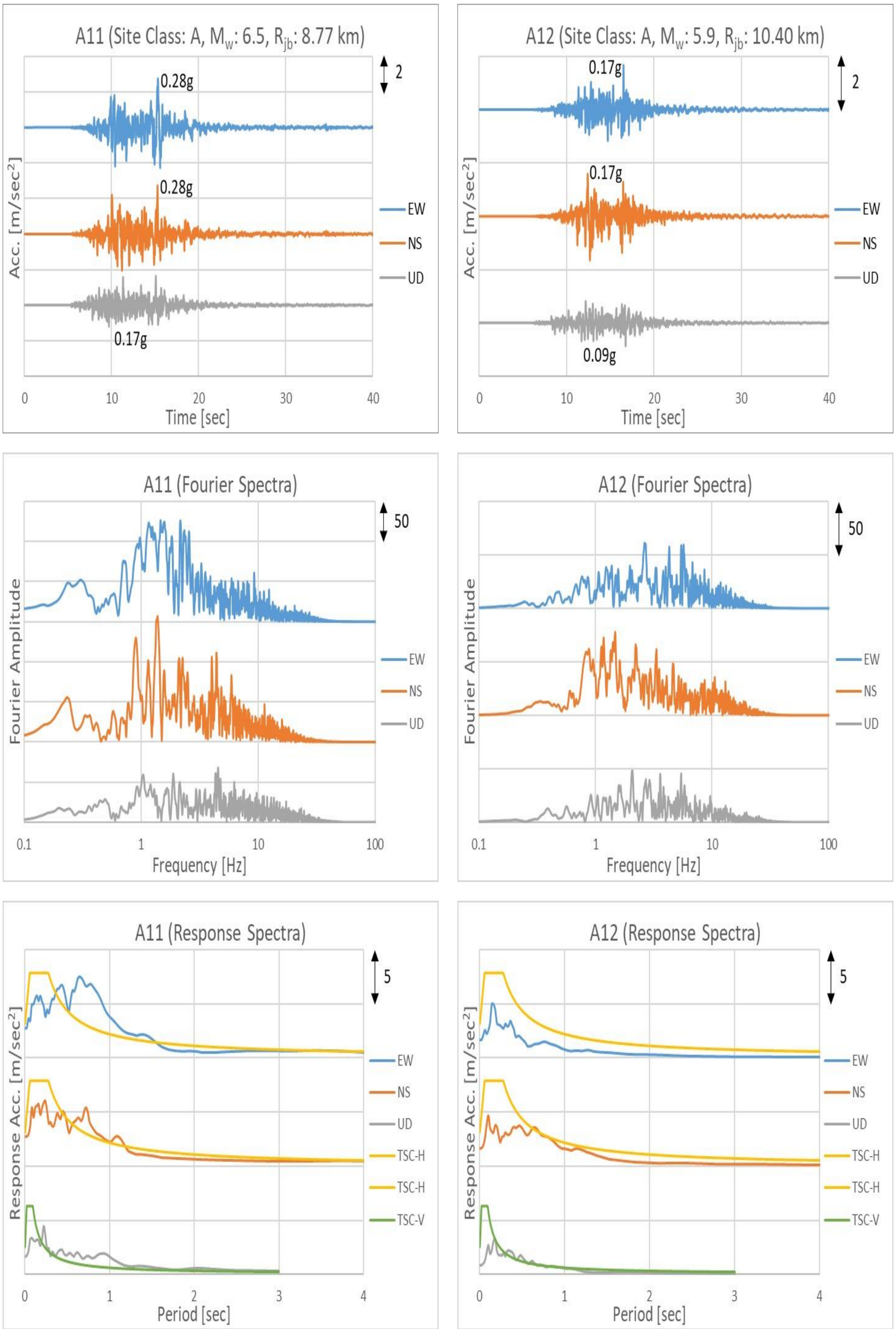

Figure A1. Acceleration Time Histories, Fourier Amplitude Spectra, and Response Spectra of the Selected Data (Cont.)

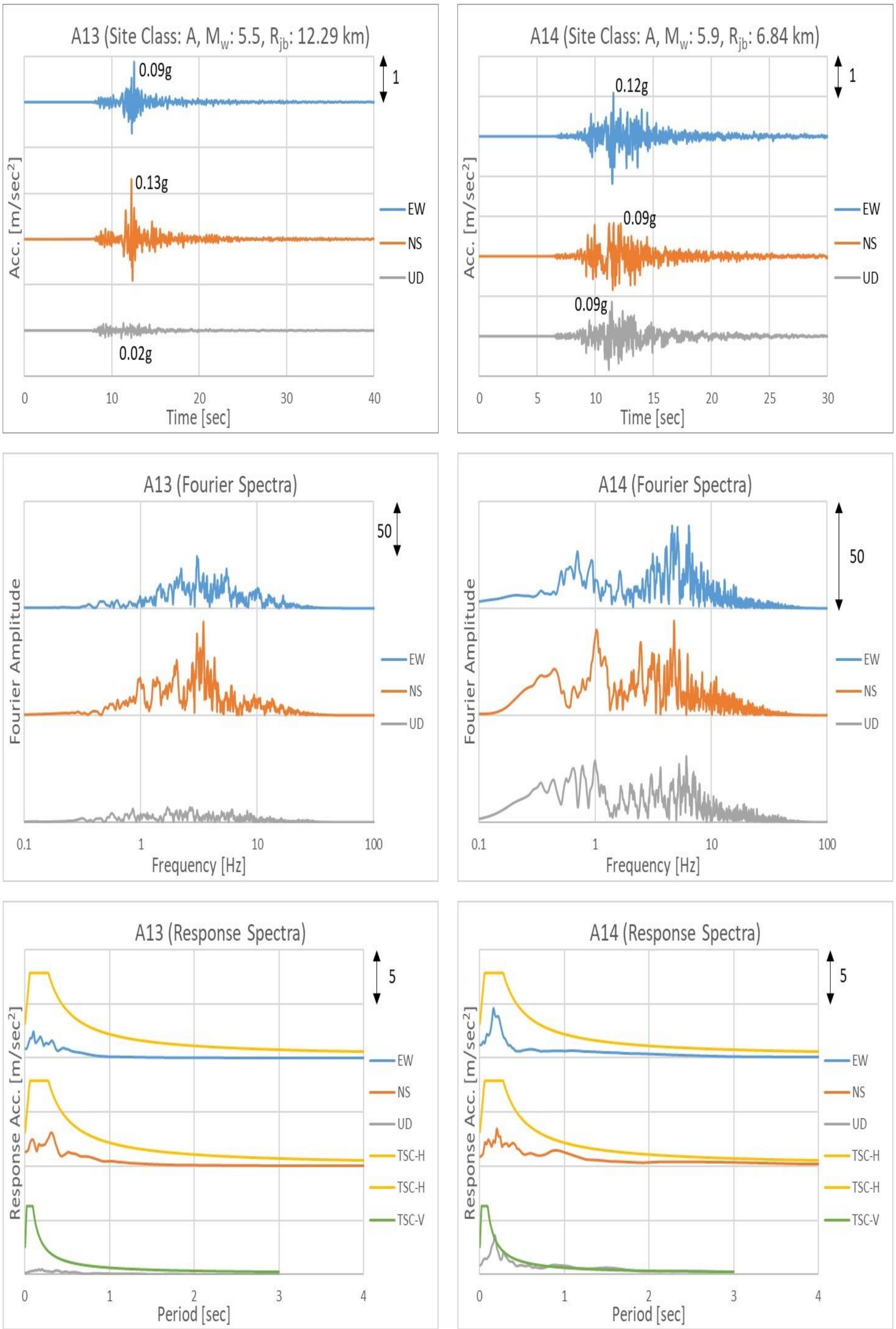

Figure A1. Acceleration Time Histories, Fourier Amplitude Spectra, and Response Spectra of the Selected Data (Cont.)

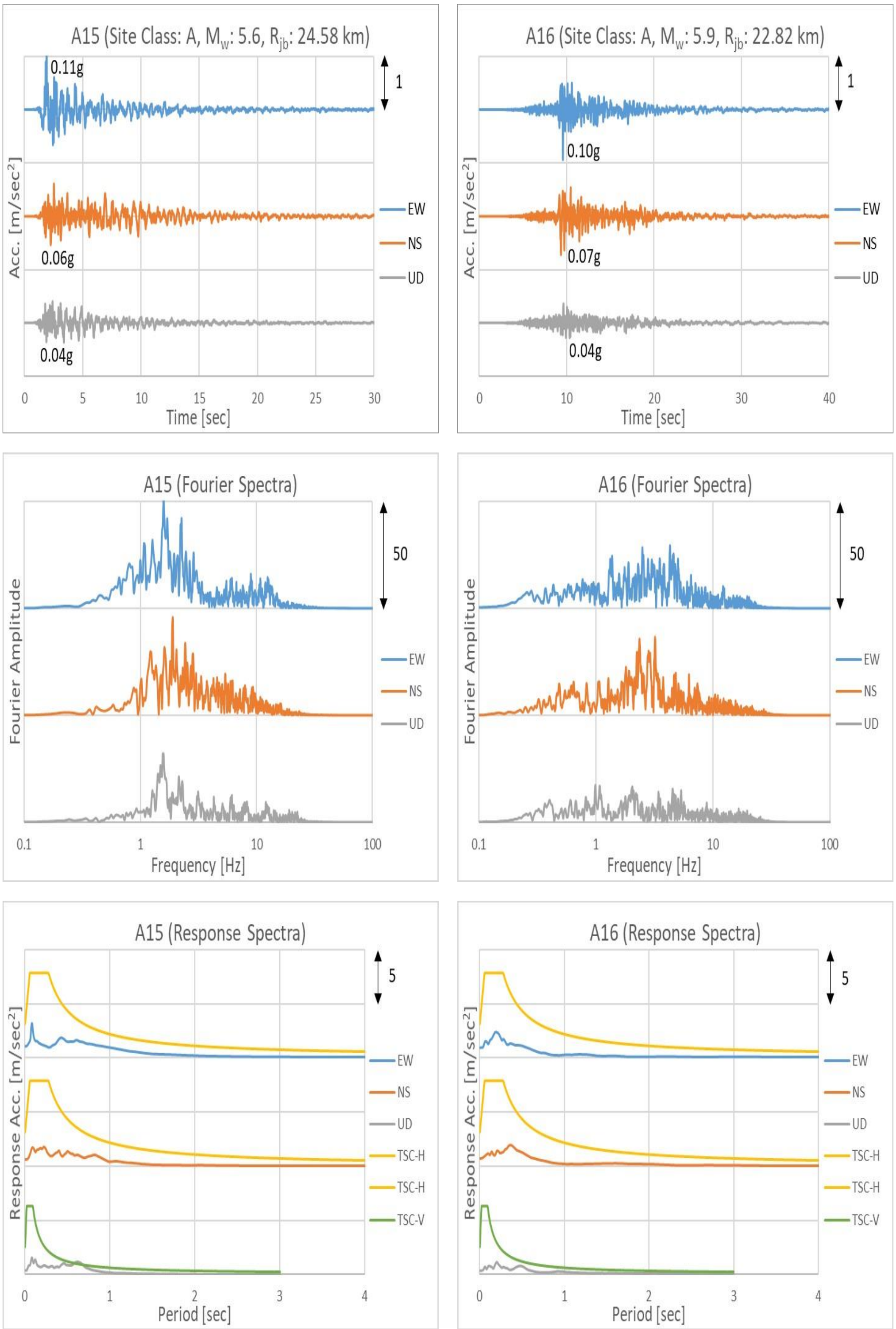

Figure A1. Acceleration Time Histories, Fourier Amplitude Spectra, and Response Spectra of the Selected Data (Cont.)

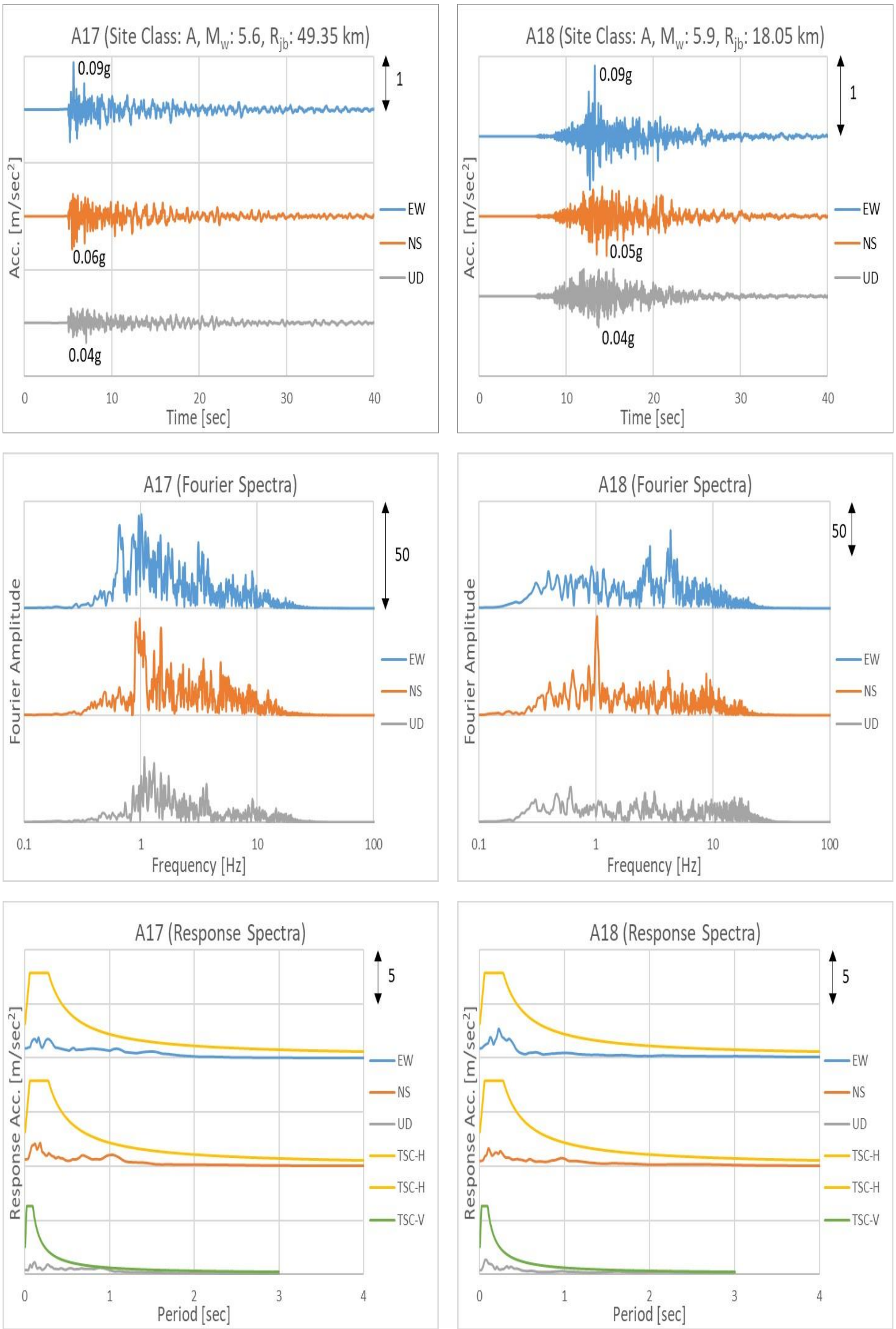

Figure A1. Acceleration Time Histories, Fourier Amplitude Spectra, and Response Spectra of the Selected Data (Cont.)

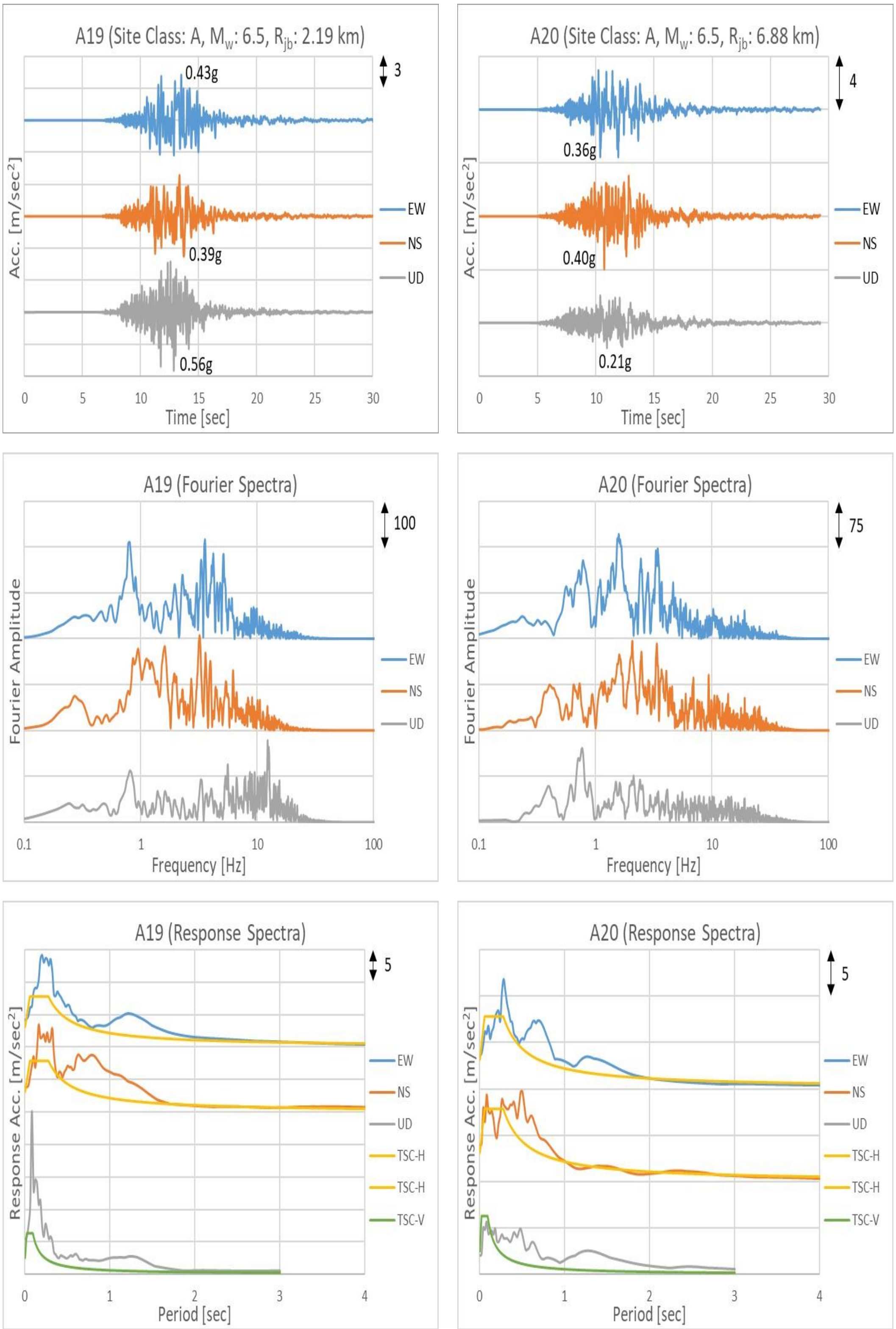

Figure A1. Acceleration Time Histories, Fourier Amplitude Spectra, and Response Spectra of the Selected Data (Cont.)

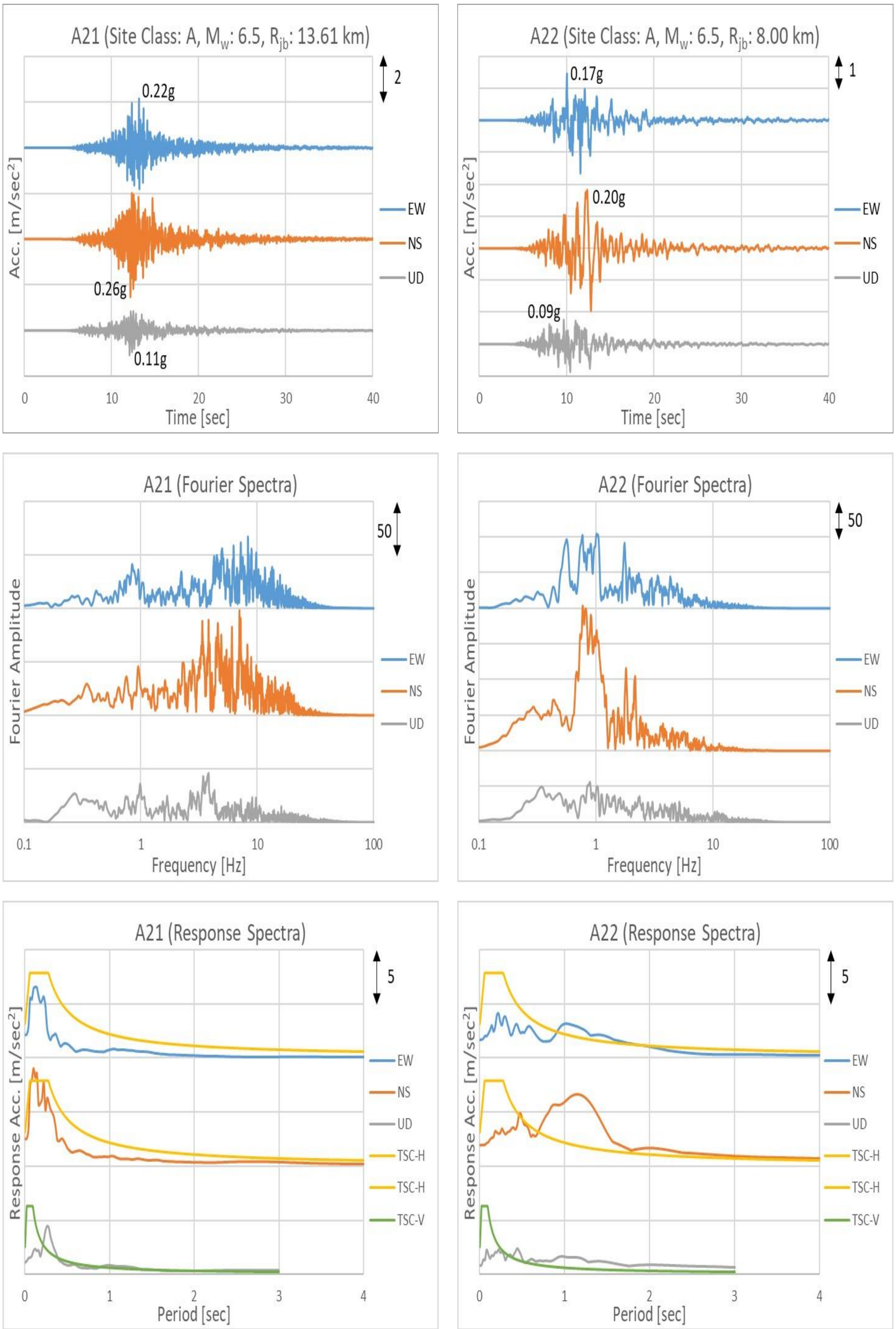

Figure A1. Acceleration Time Histories, Fourier Amplitude Spectra, and Response Spectra of the Selected Data (Cont.)

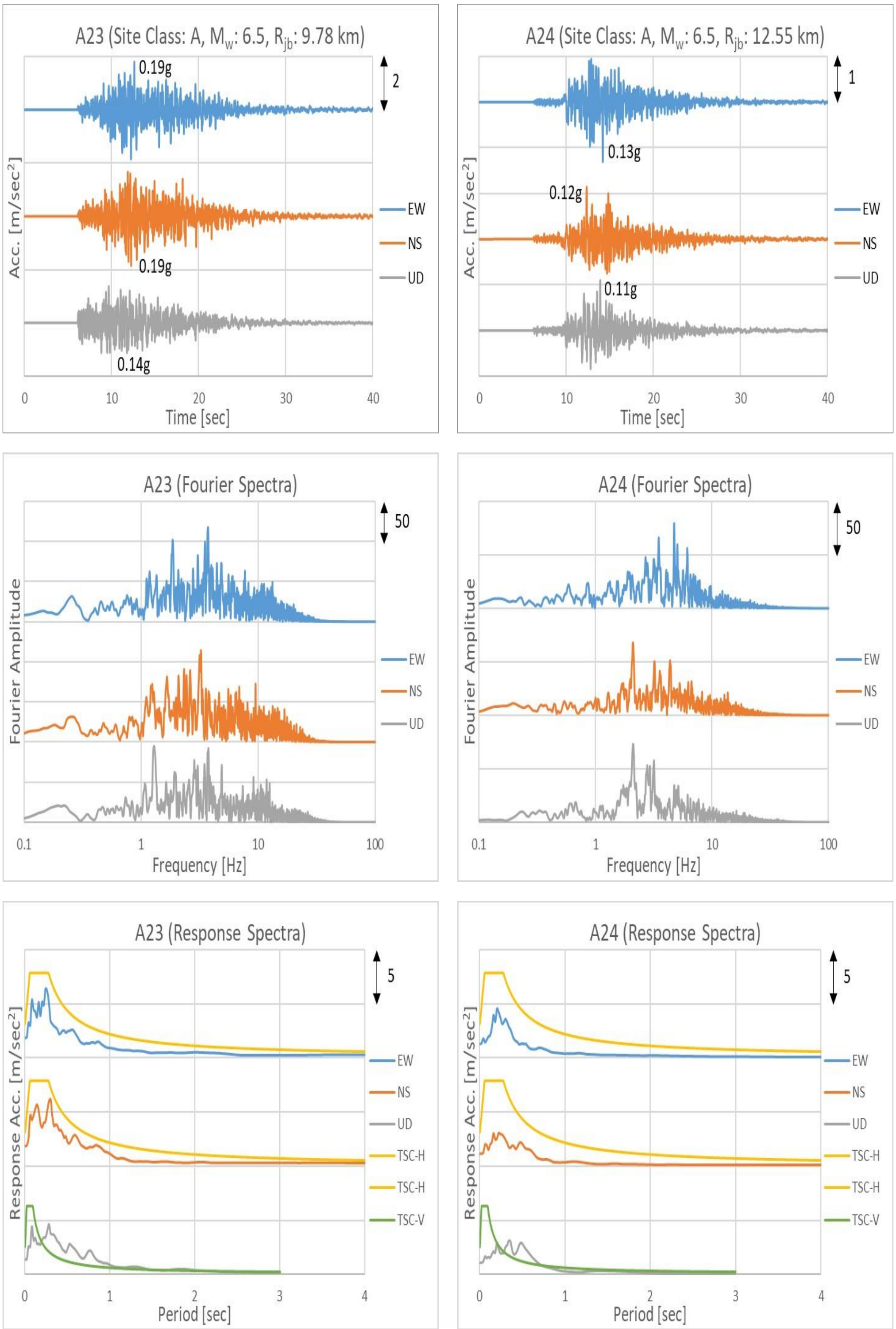

Figure A1. Acceleration Time Histories, Fourier Amplitude Spectra, and Response Spectra of the Selected Data (Cont.)

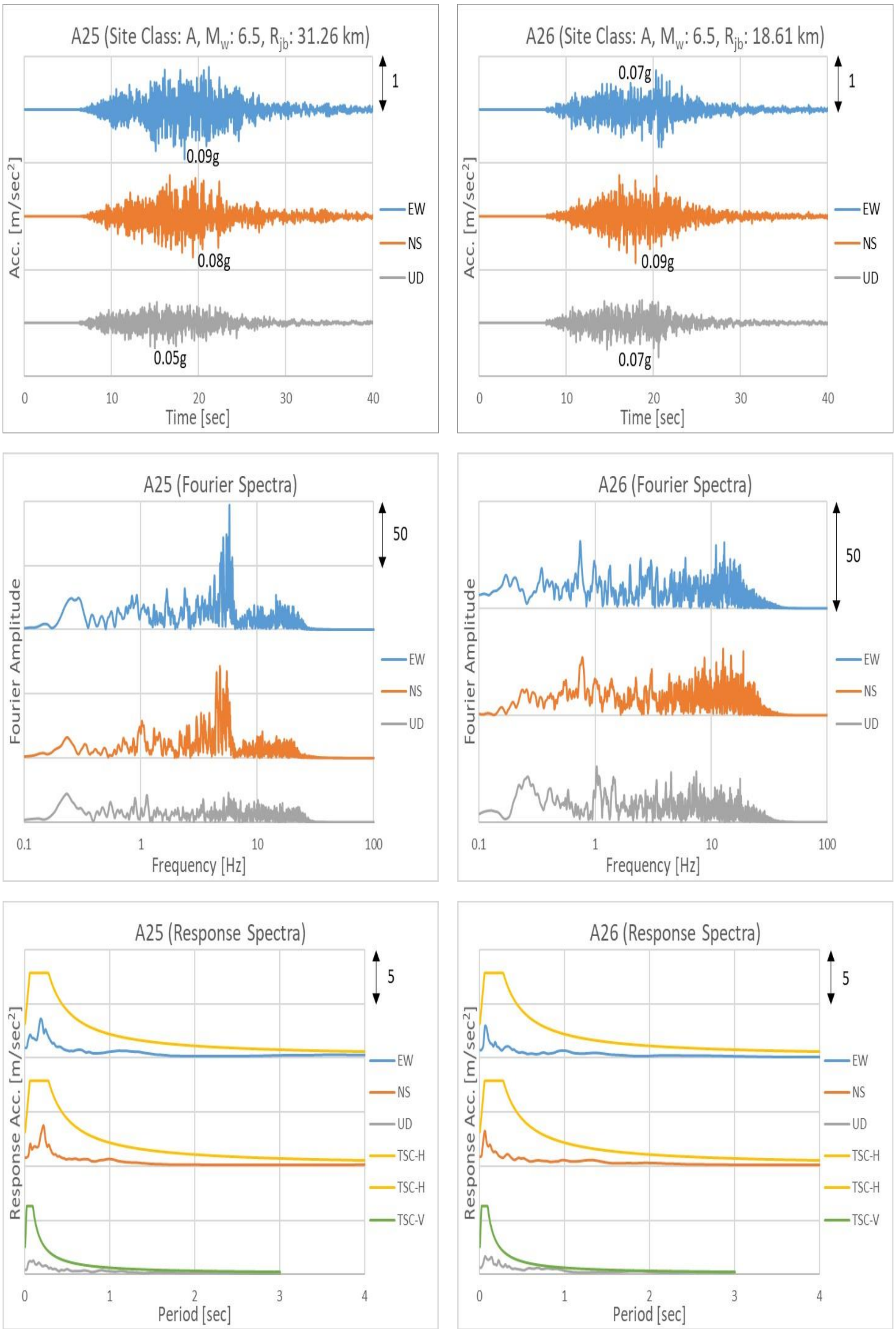

Figure A1. Acceleration Time Histories, Fourier Amplitude Spectra, and Response Spectra of the Selected Data (Cont.)

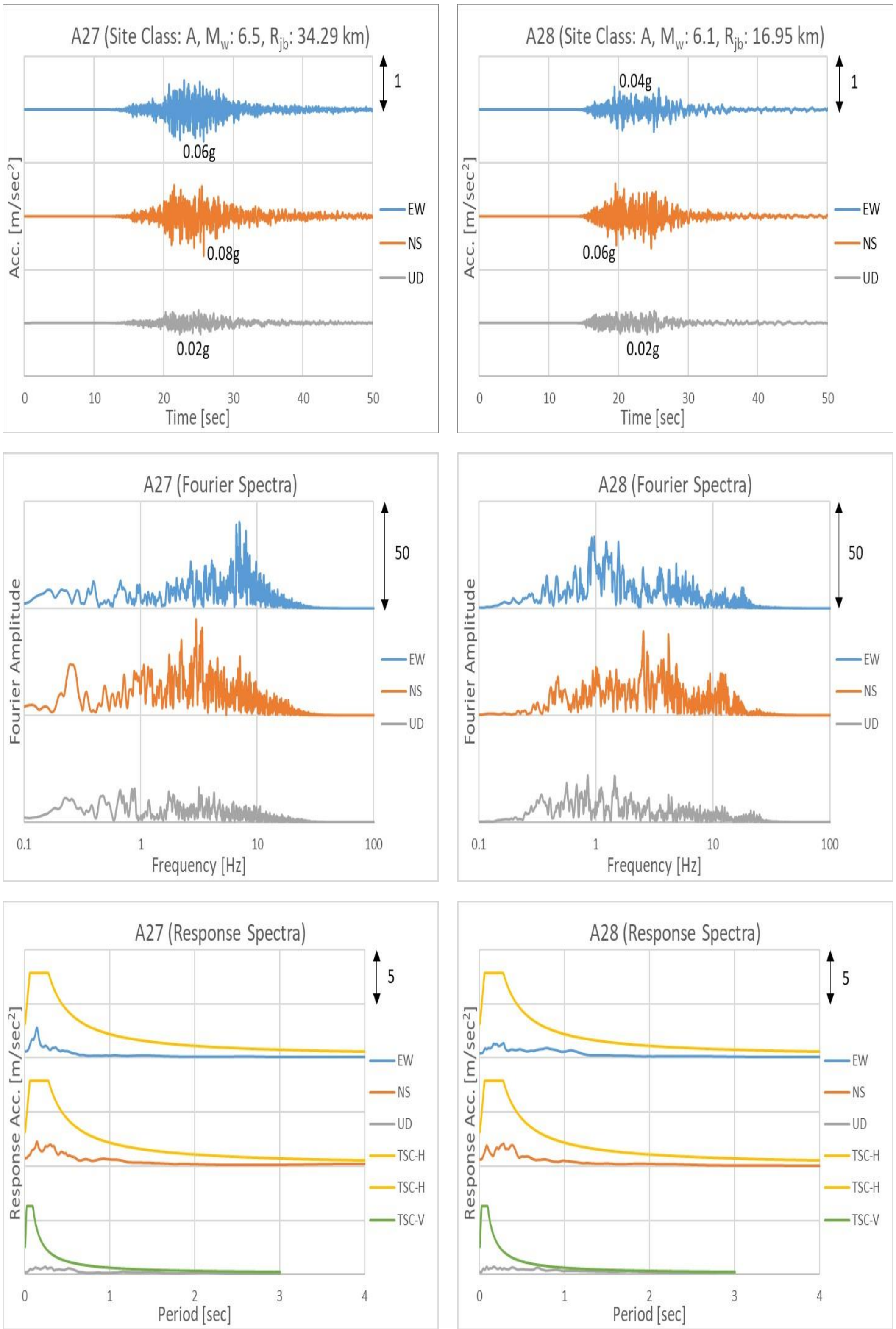

Figure A1. Acceleration Time Histories, Fourier Amplitude Spectra, and Response Spectra of the Selected Data (Cont.)

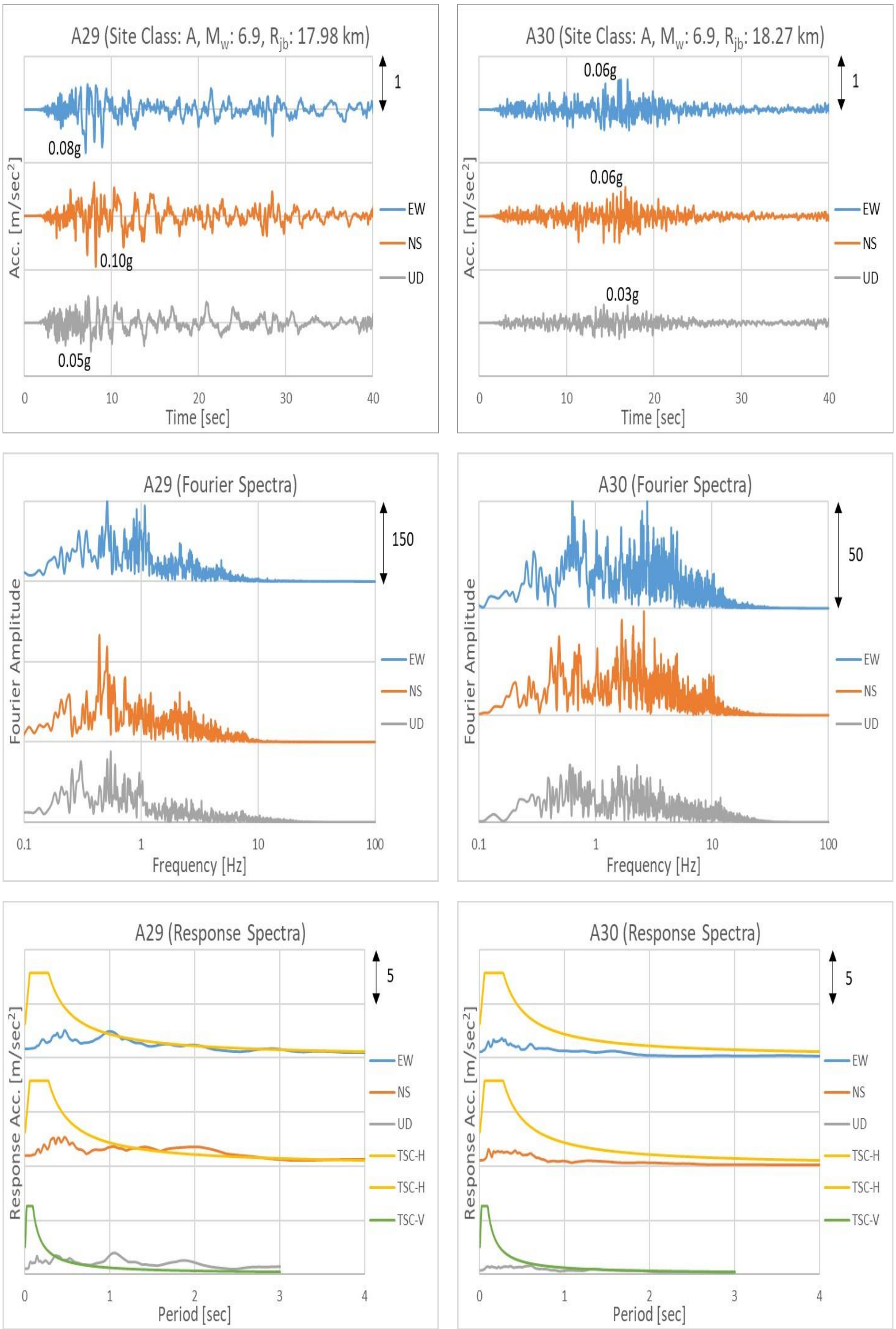

Figure A1. Acceleration Time Histories, Fourier Amplitude Spectra, and Response Spectra of the Selected Data (Cont.)

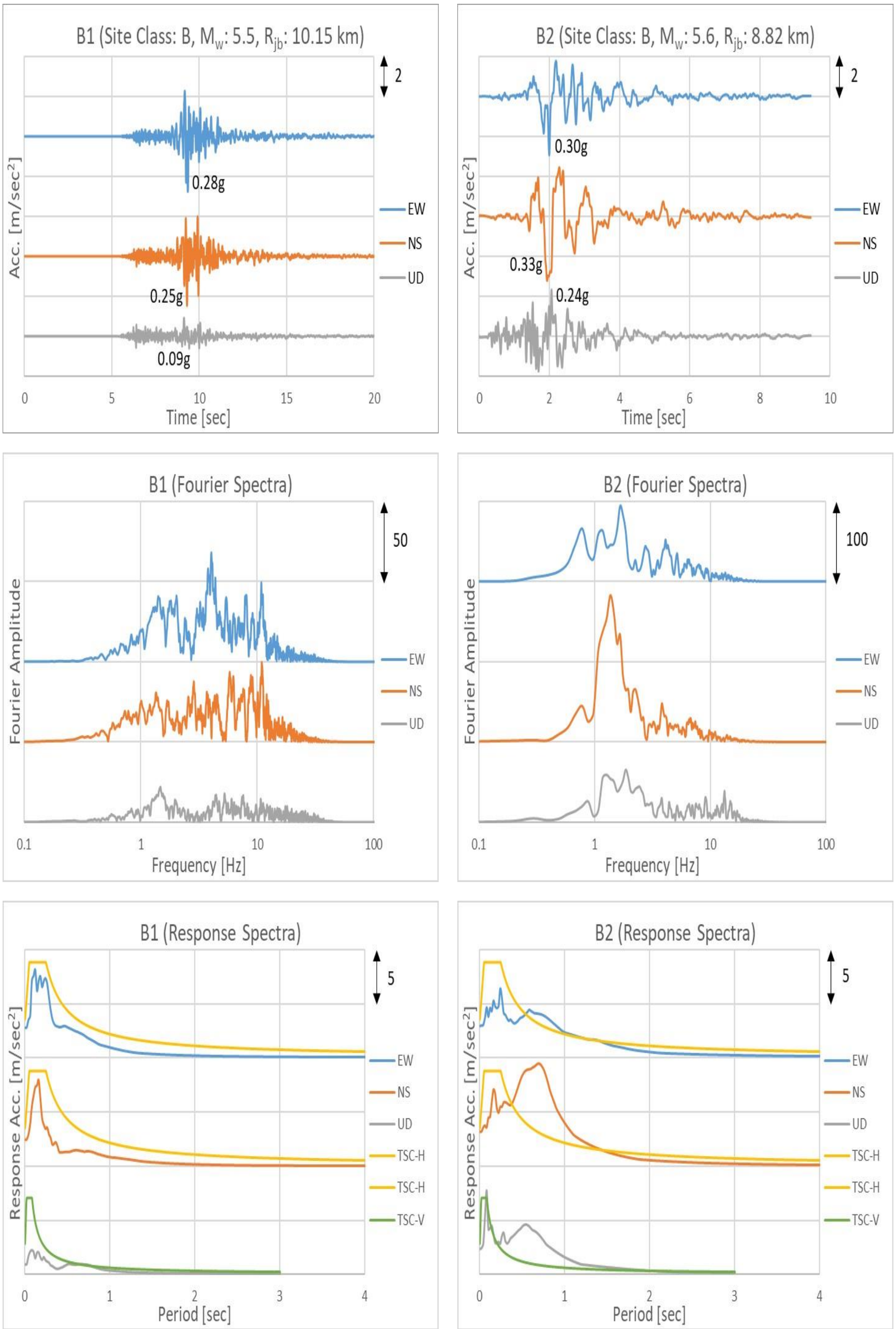

Figure A1. Acceleration Time Histories, Fourier Amplitude Spectra, and Response Spectra of the Selected Data (Cont.)

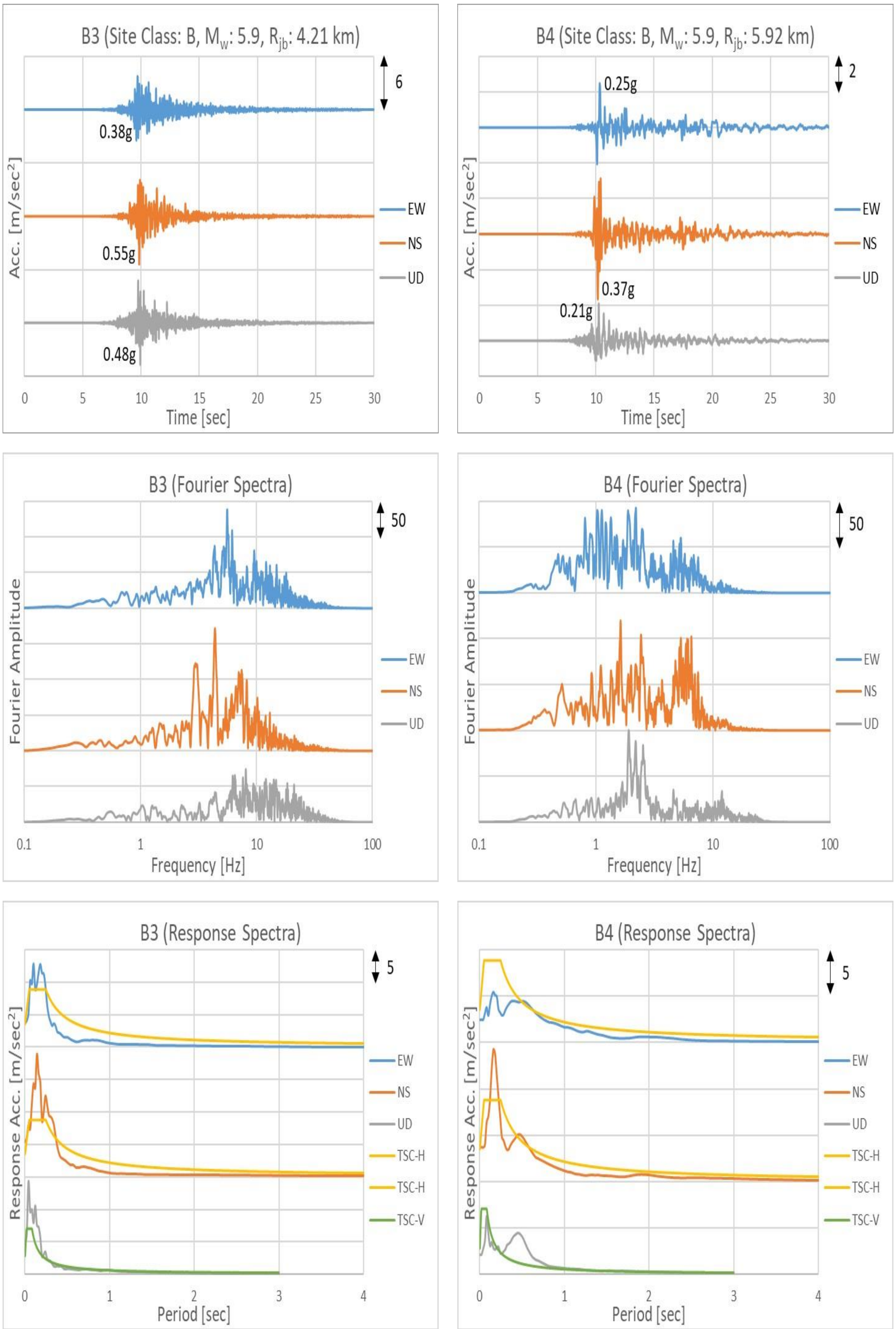

Figure A1. Acceleration Time Histories, Fourier Amplitude Spectra, and Response Spectra of the Selected Data (Cont.)

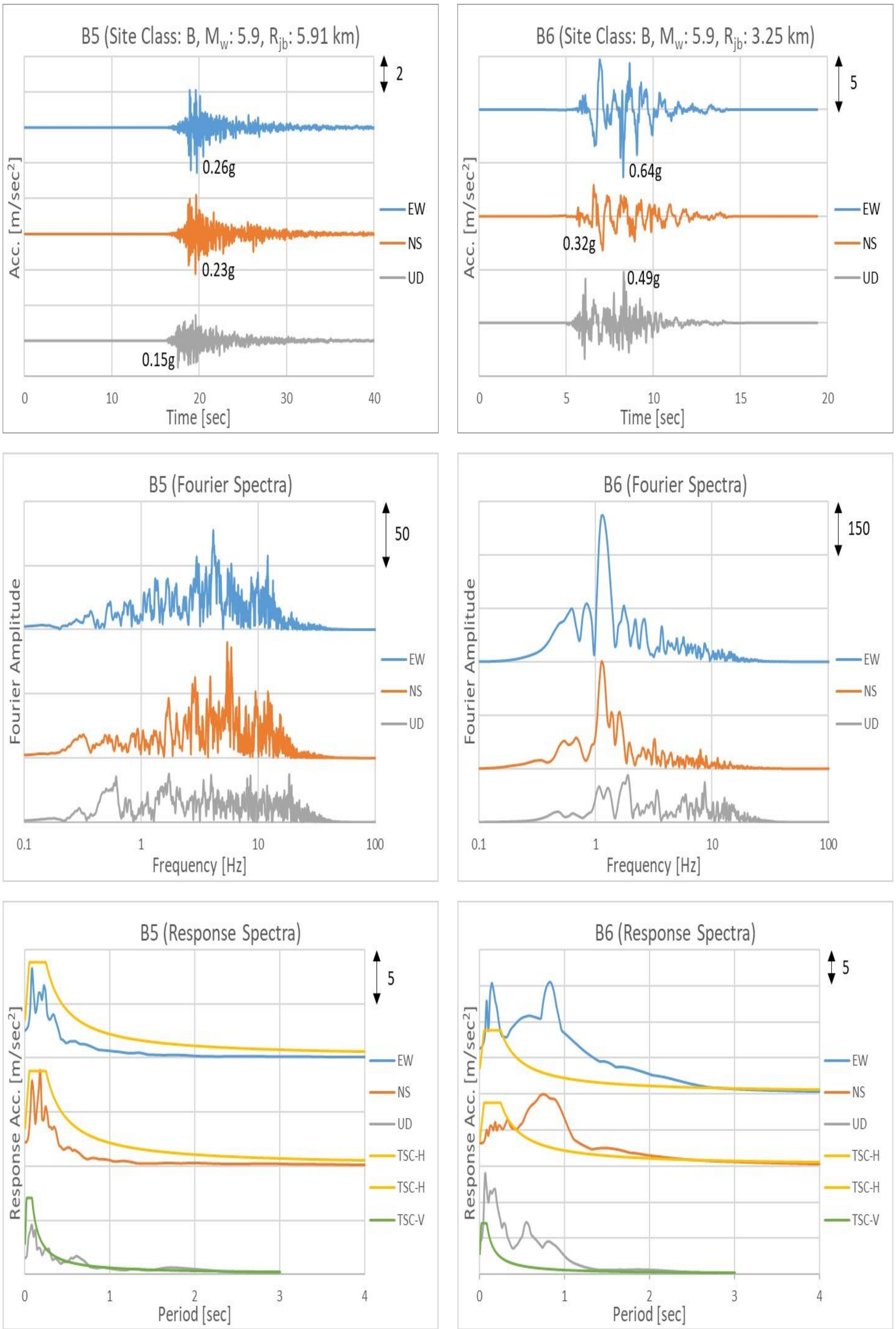

Figure A1. Acceleration Time Histories, Fourier Amplitude Spectra, and Response Spectra of the Selected Data (Cont.)

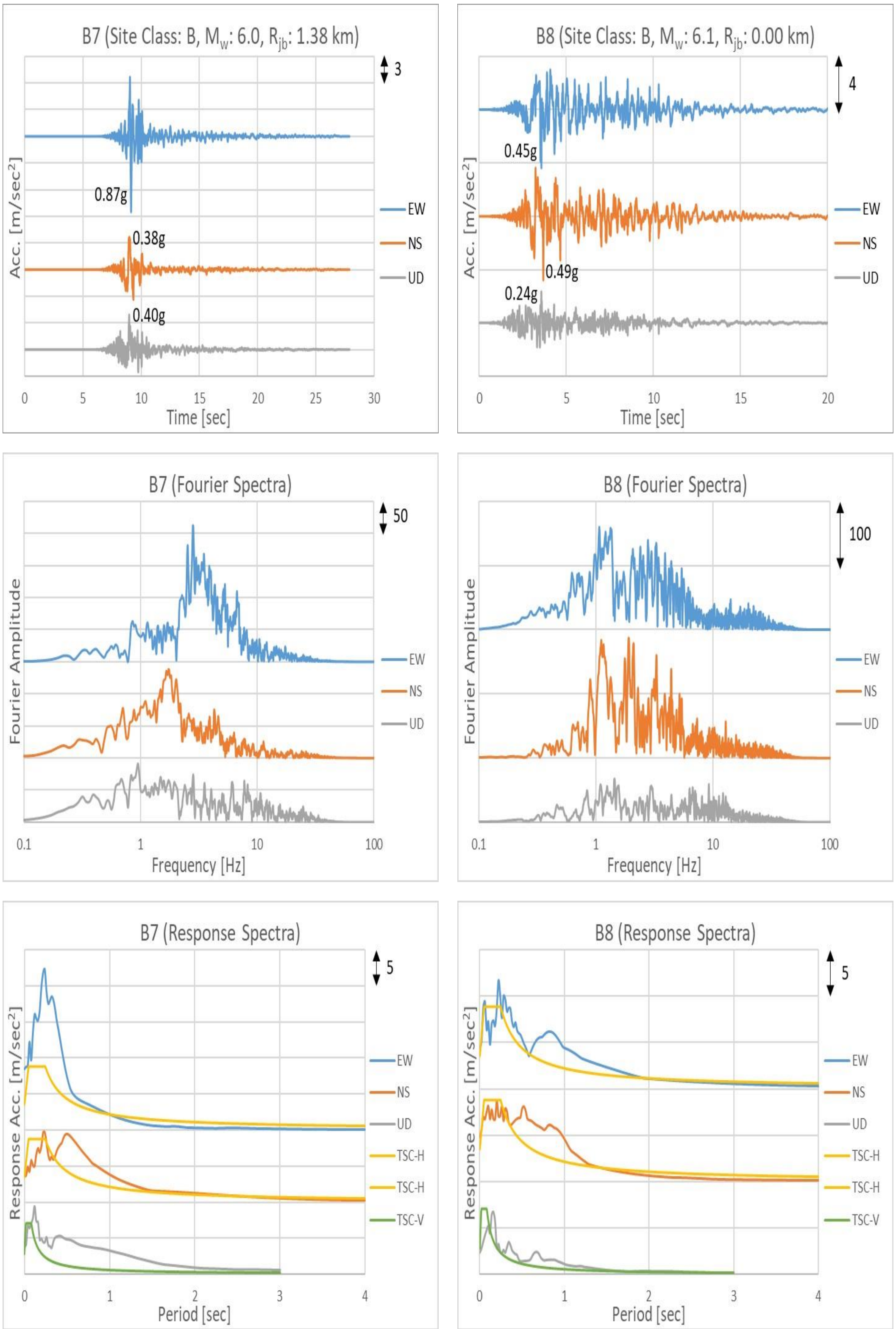

Figure A1. Acceleration Time Histories, Fourier Amplitude Spectra, and Response Spectra of the Selected Data (Cont.)

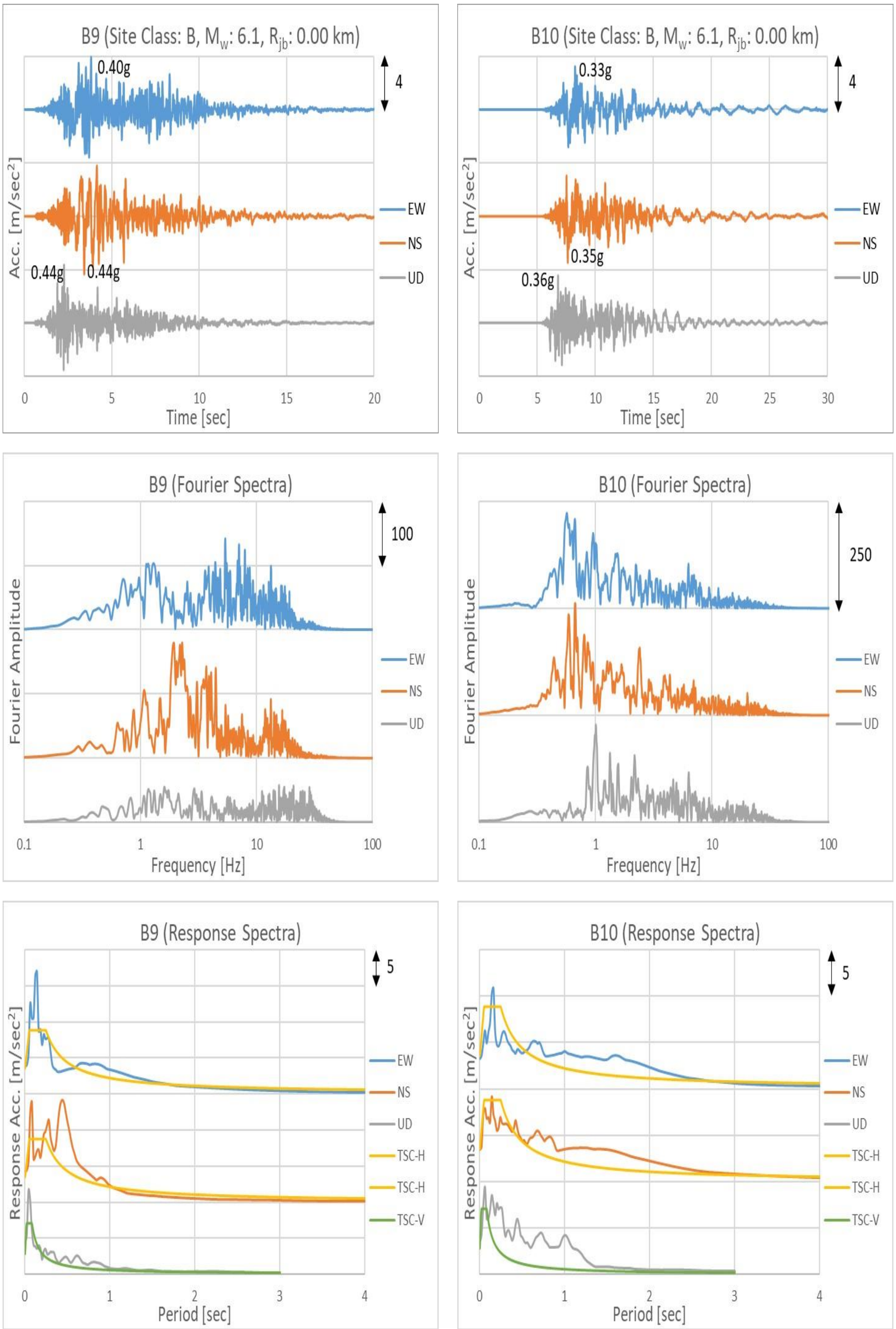

Figure A1. Acceleration Time Histories, Fourier Amplitude Spectra, and Response Spectra of the Selected Data (Cont.)

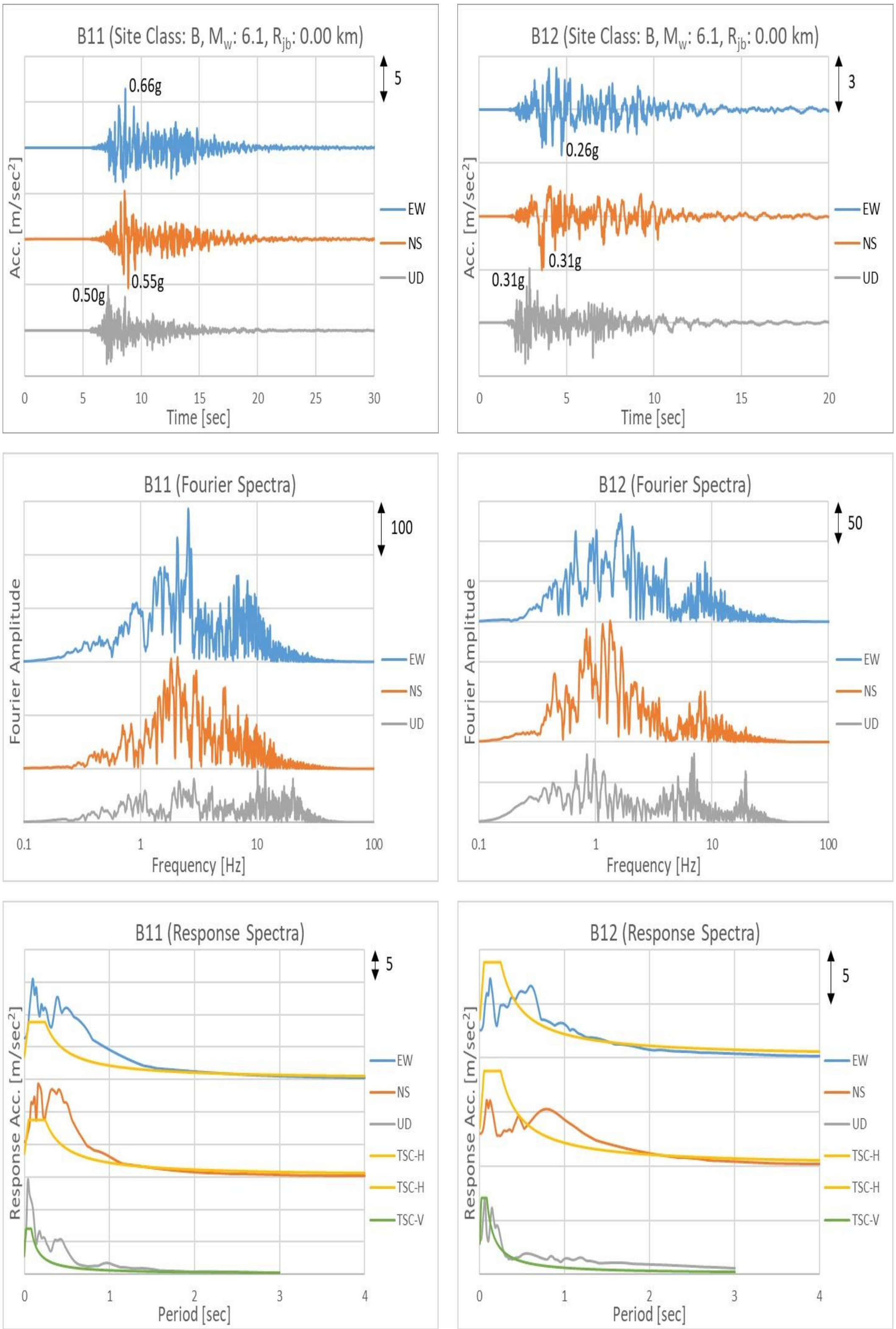

Figure A1. Acceleration Time Histories, Fourier Amplitude Spectra, and Response Spectra of the Selected Data (Cont.)

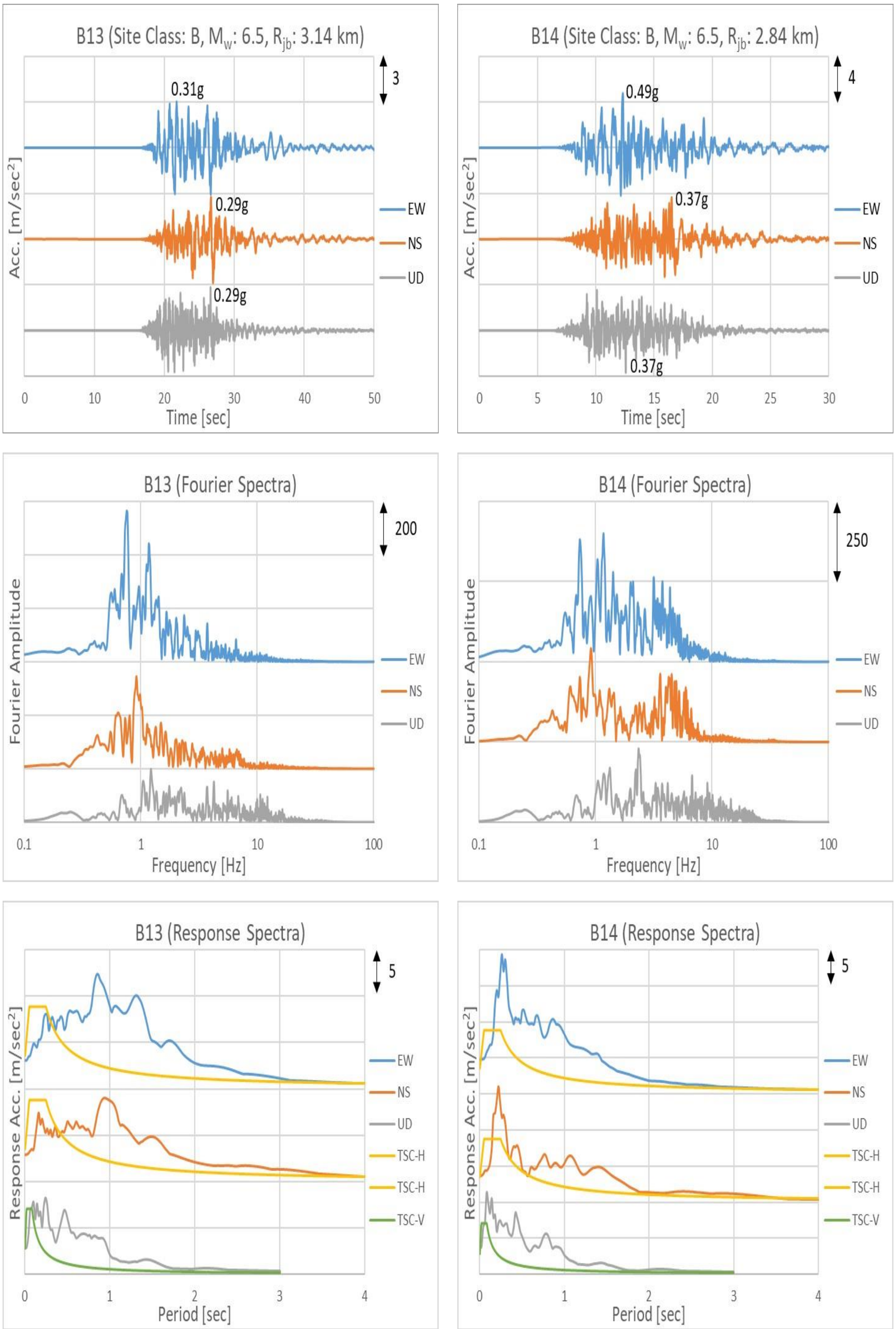

Figure A1. Acceleration Time Histories, Fourier Amplitude Spectra, and Response Spectra of the Selected Data (Cont.)

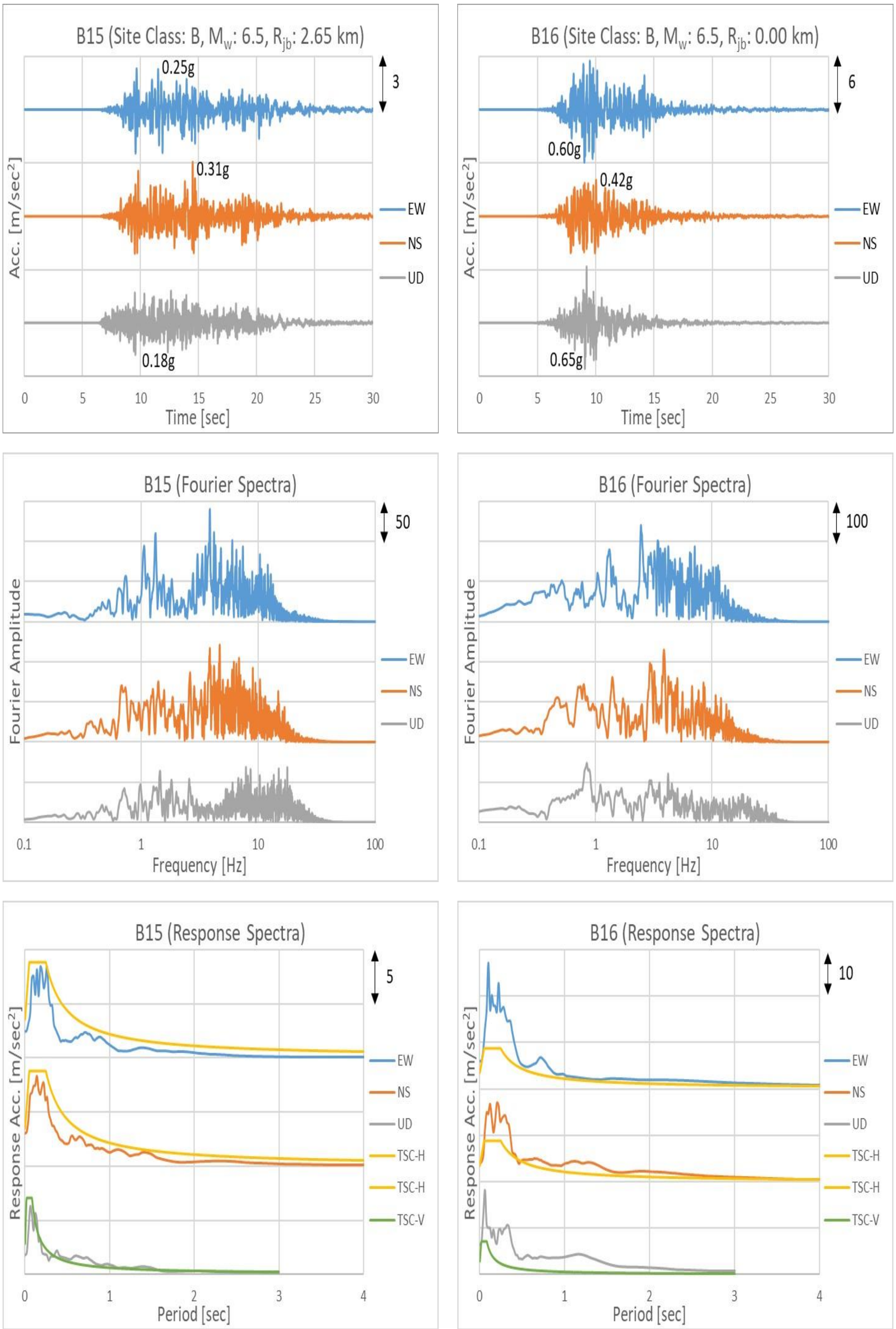

Figure A1. Acceleration Time Histories, Fourier Amplitude Spectra, and Response Spectra of the Selected Data (Cont.)

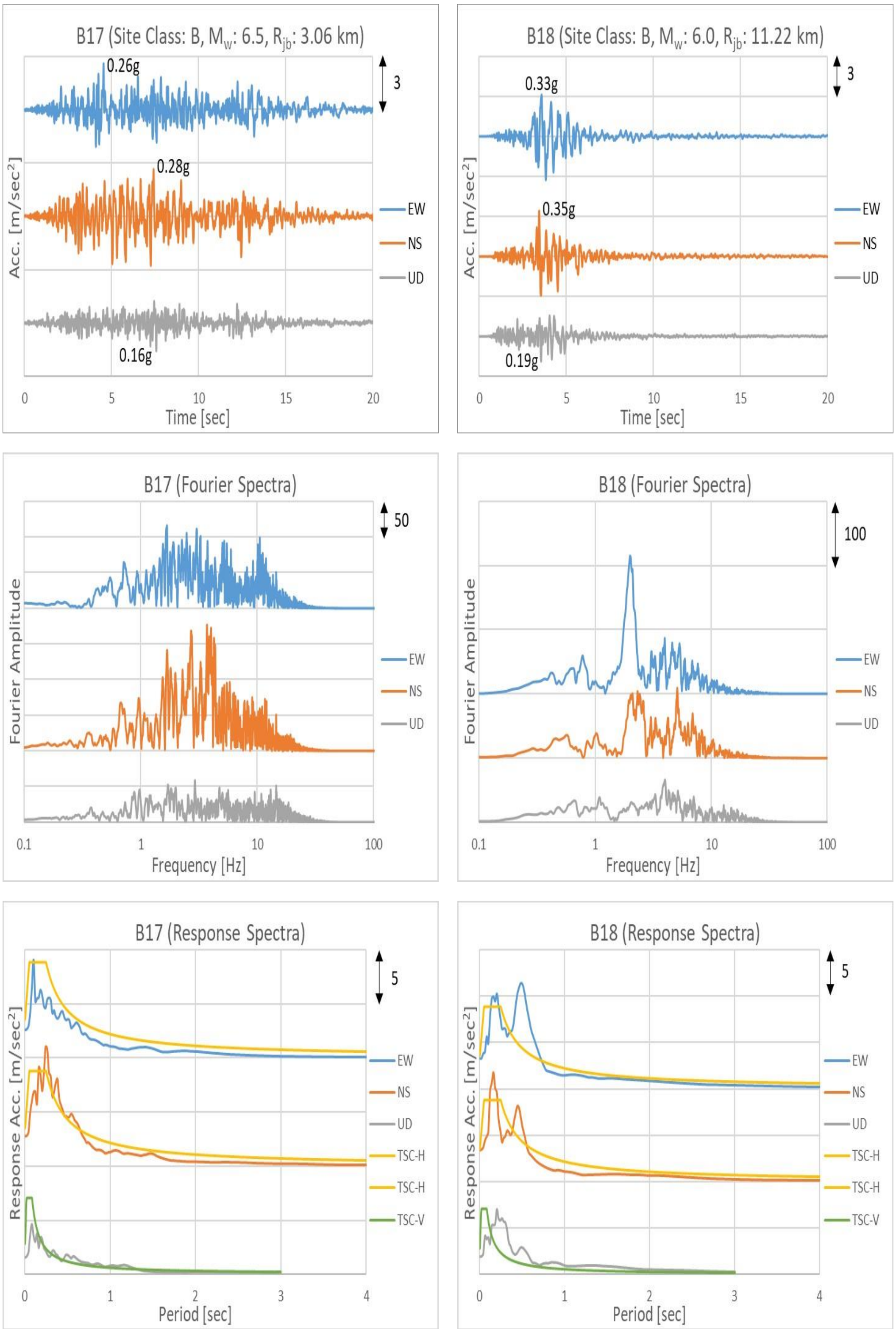

Figure A1. Acceleration Time Histories, Fourier Amplitude Spectra, and Response Spectra of the Selected Data (Cont.)

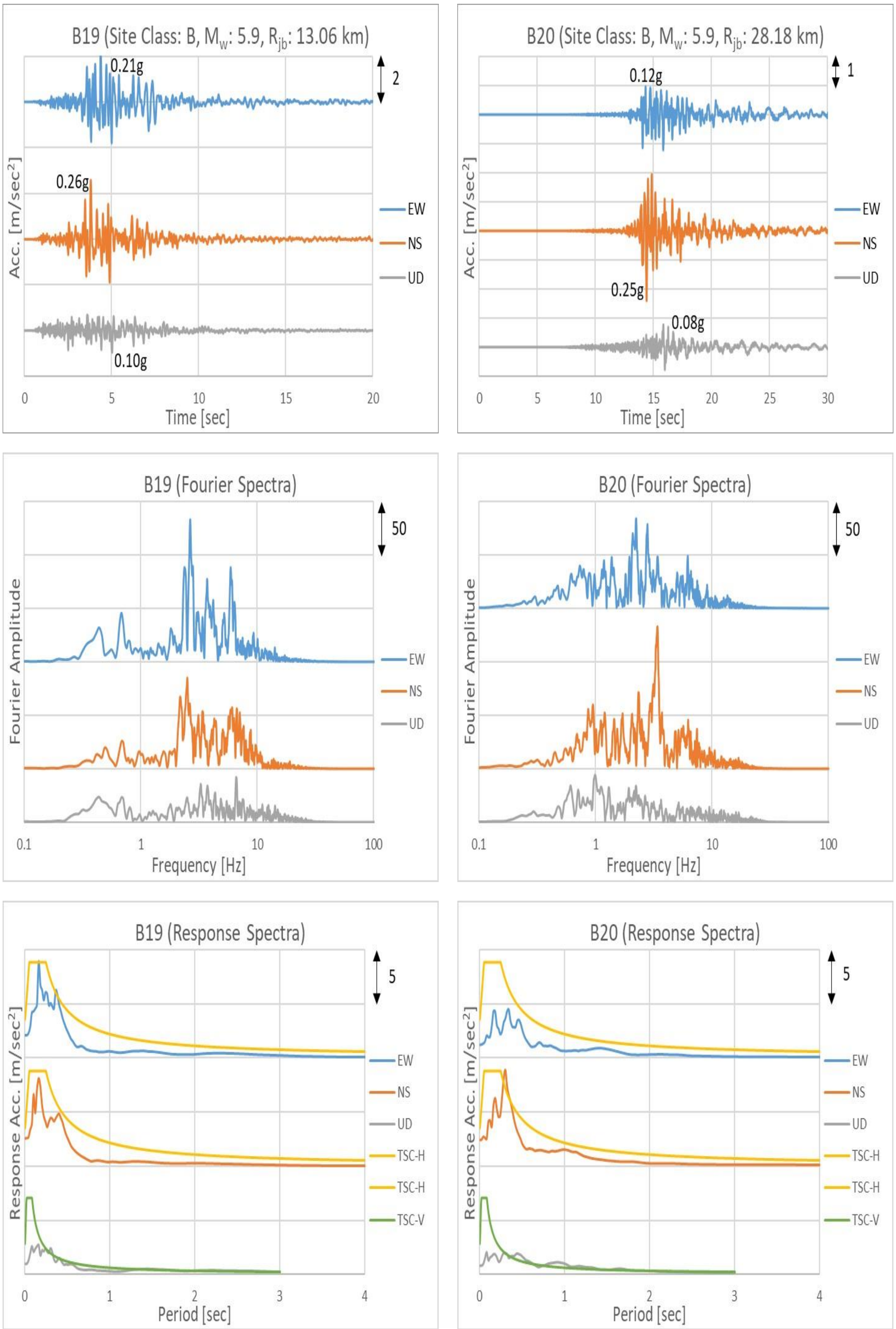

Figure A1. Acceleration Time Histories, Fourier Amplitude Spectra, and Response Spectra of the Selected Data (Cont.)

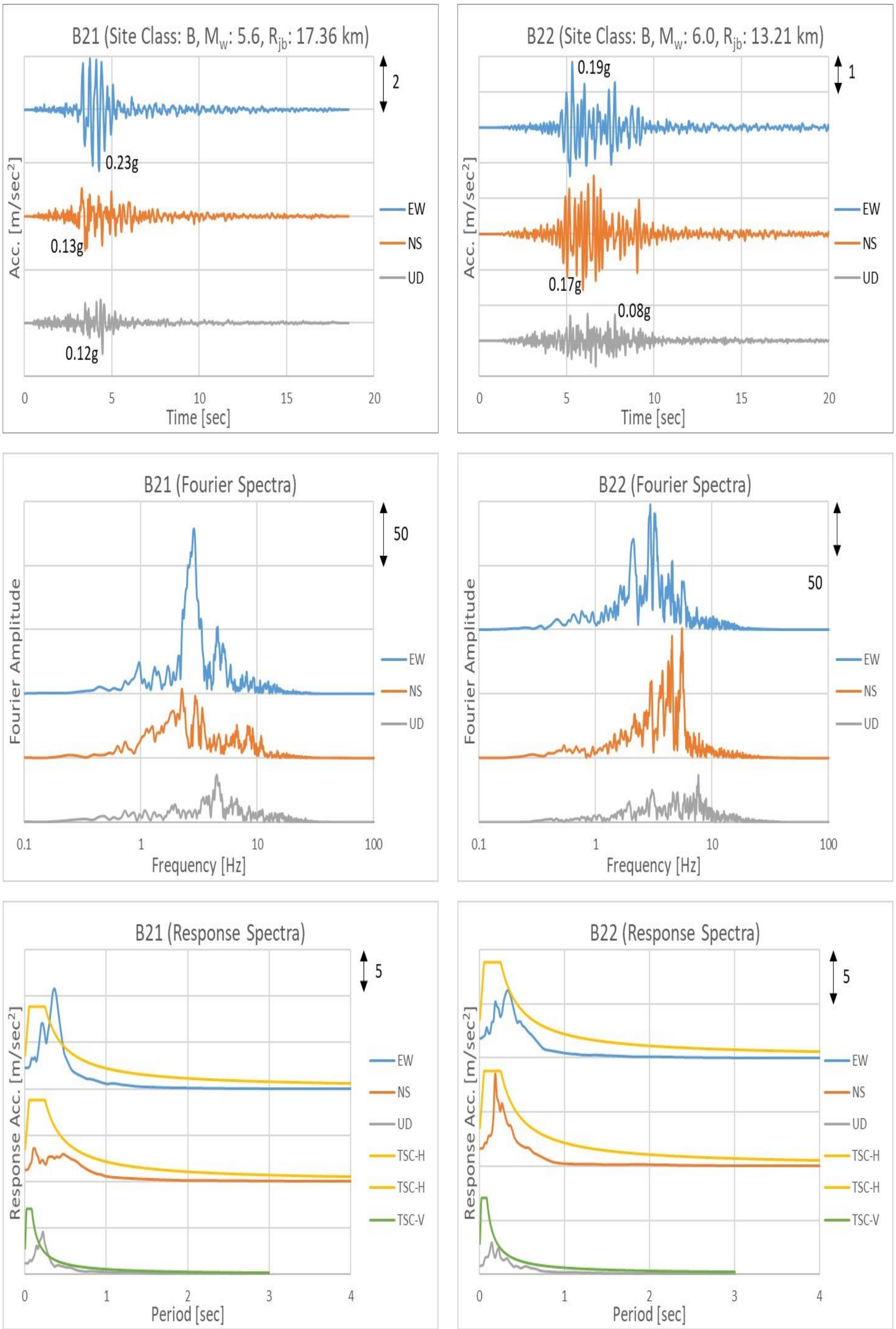

Figure A1. Acceleration Time Histories, Fourier Amplitude Spectra, and Response Spectra of the Selected Data (Cont.)

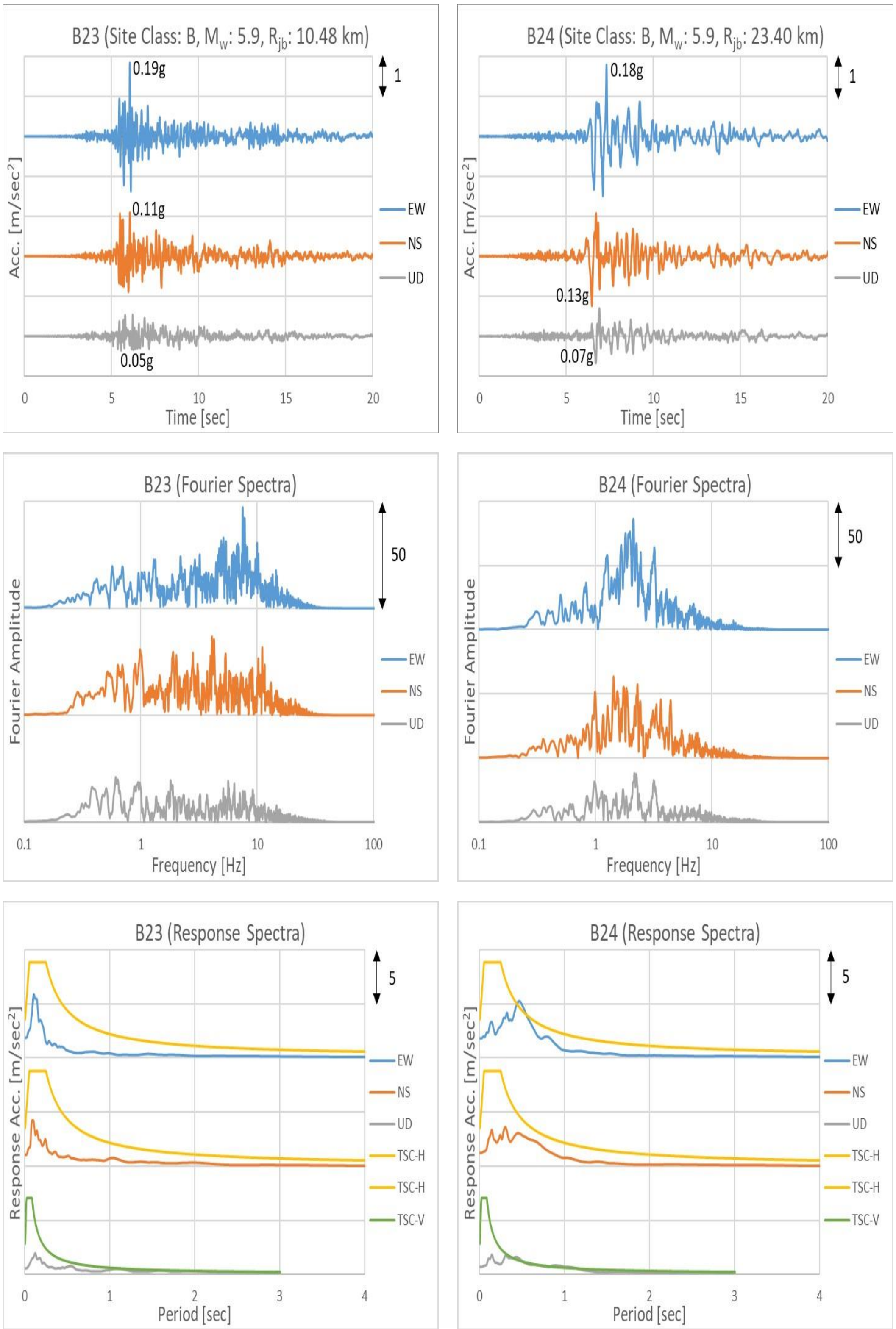

Figure A1. Acceleration Time Histories, Fourier Amplitude Spectra, and Response Spectra of the Selected Data (Cont.)

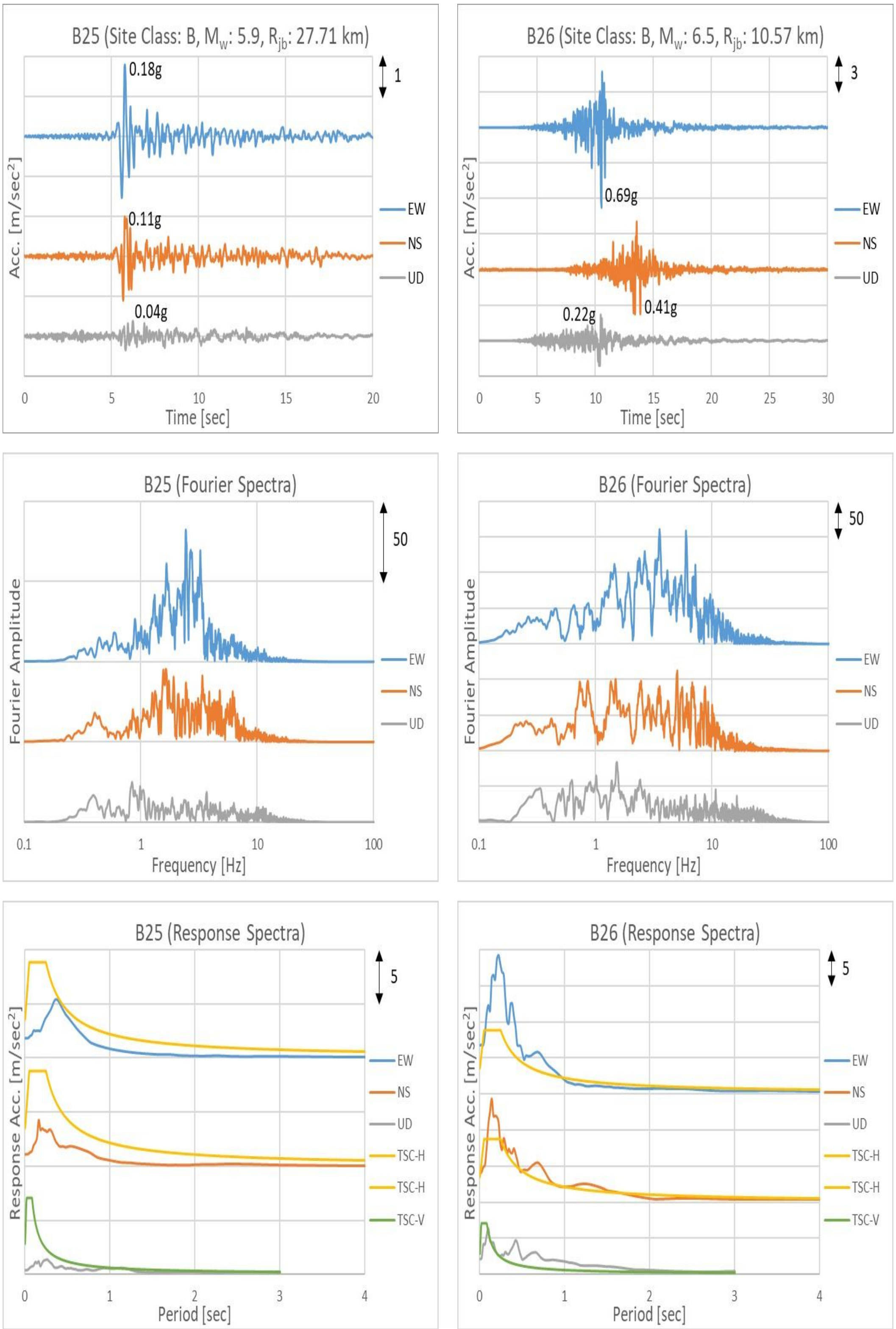

Figure A1. Acceleration Time Histories, Fourier Amplitude Spectra, and Response Spectra of the Selected Data (Cont.)

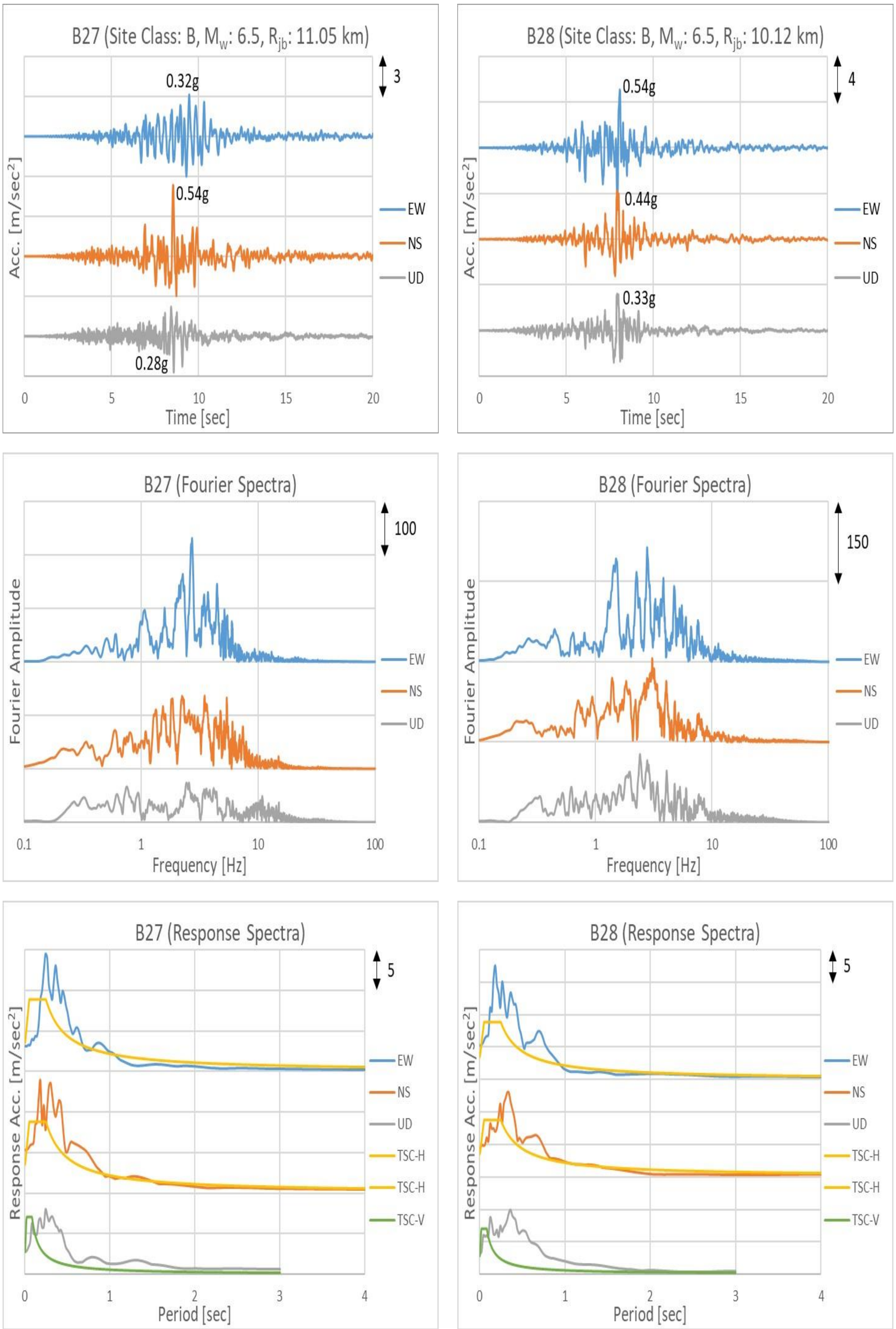

Figure A1. Acceleration Time Histories, Fourier Amplitude Spectra, and Response Spectra of the Selected Data (Cont.)

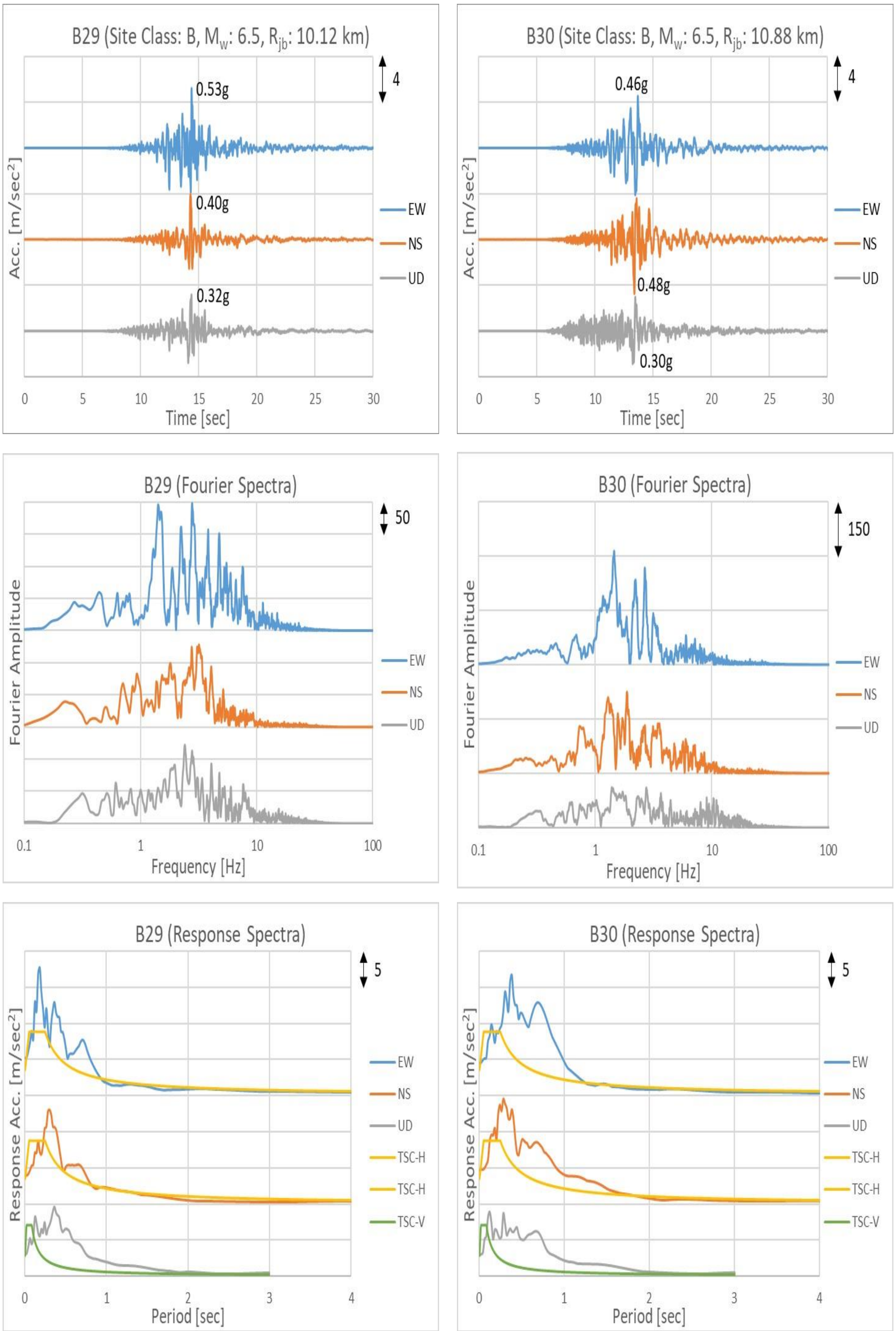

Figure A1. Acceleration Time Histories, Fourier Amplitude Spectra, and Response Spectra of the Selected Data (Cont.)

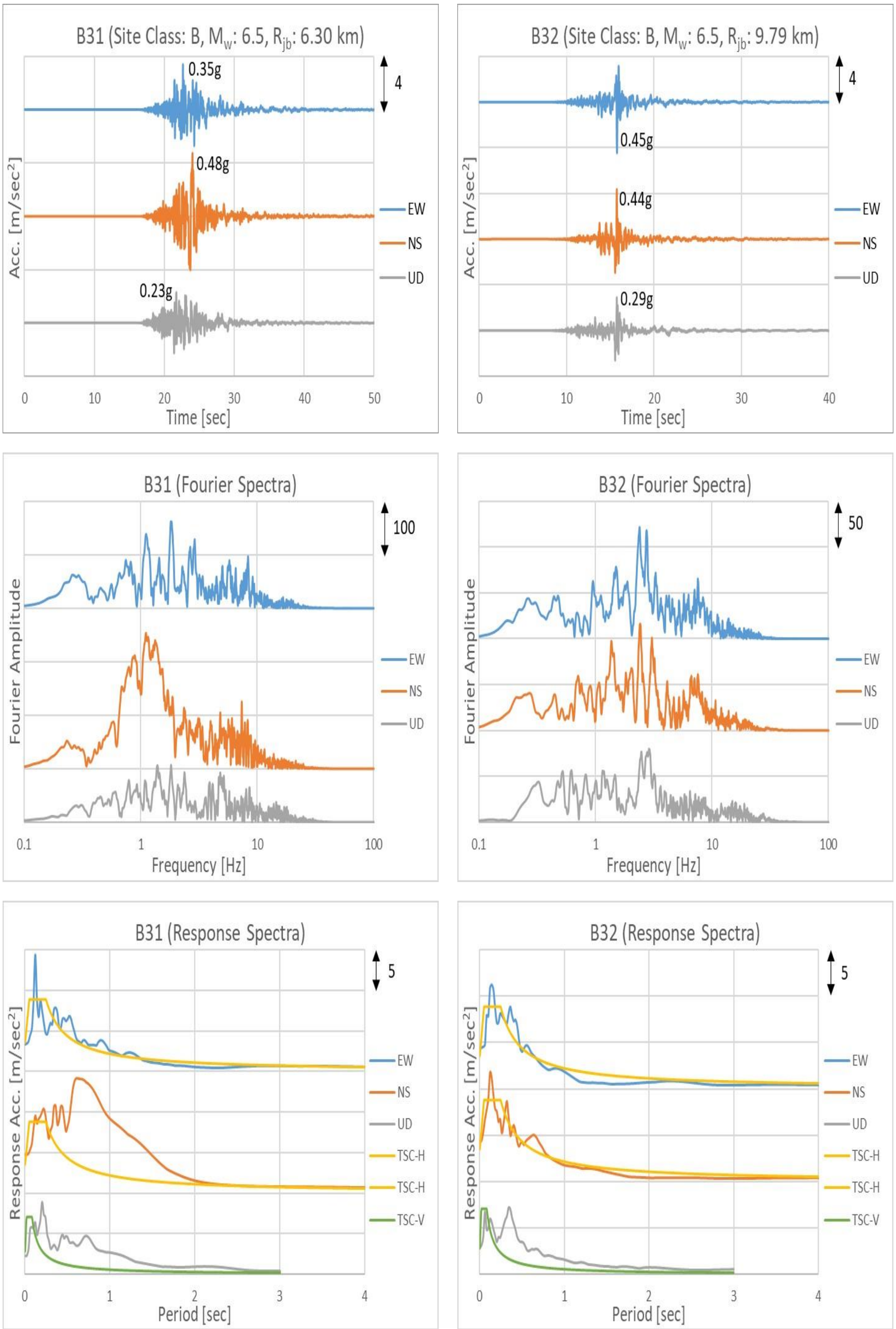

Figure A1. Acceleration Time Histories, Fourier Amplitude Spectra, and Response Spectra of the Selected Data (Cont.)

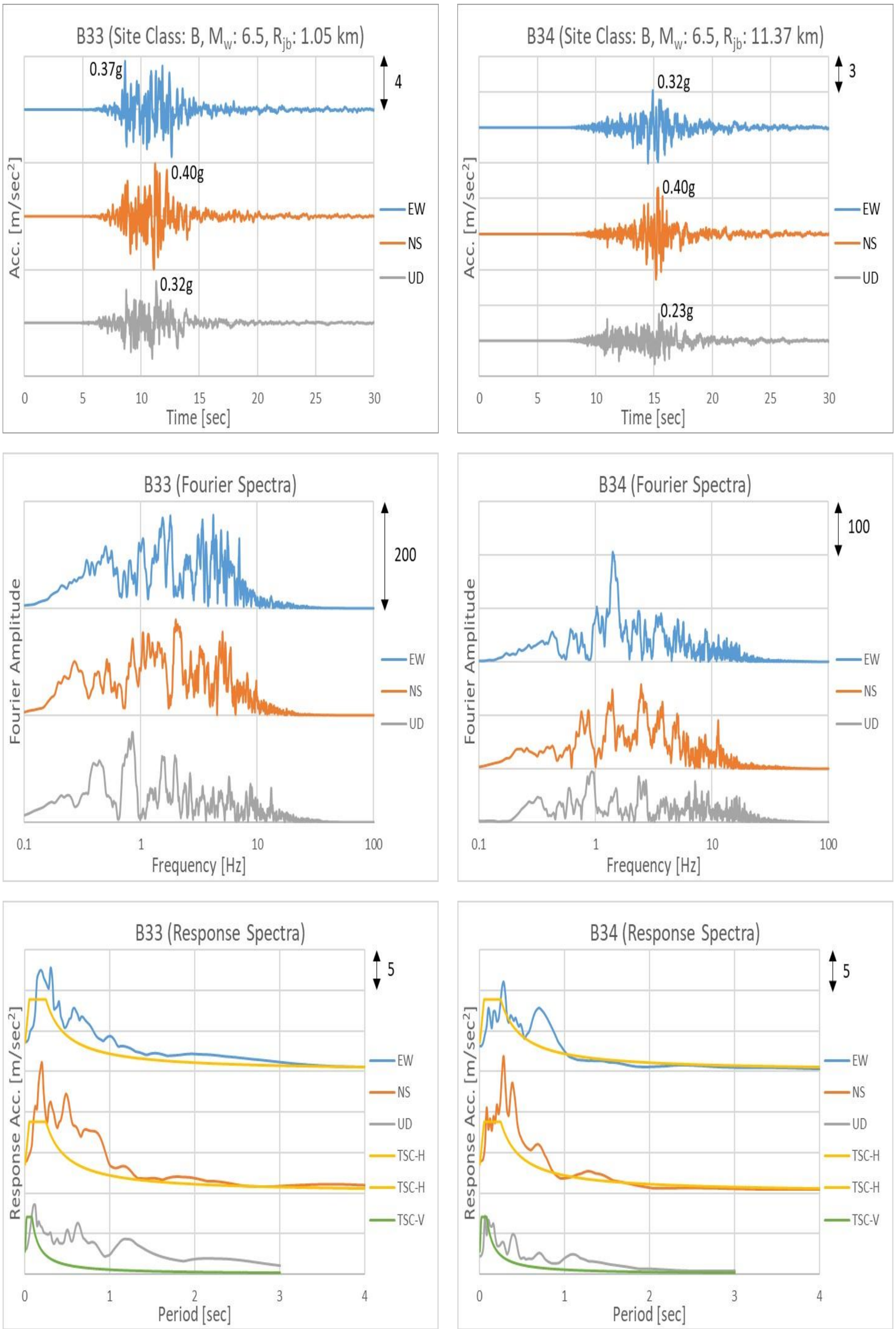

Figure A1. Acceleration Time Histories, Fourier Amplitude Spectra, and Response Spectra of the Selected Data (Cont.)

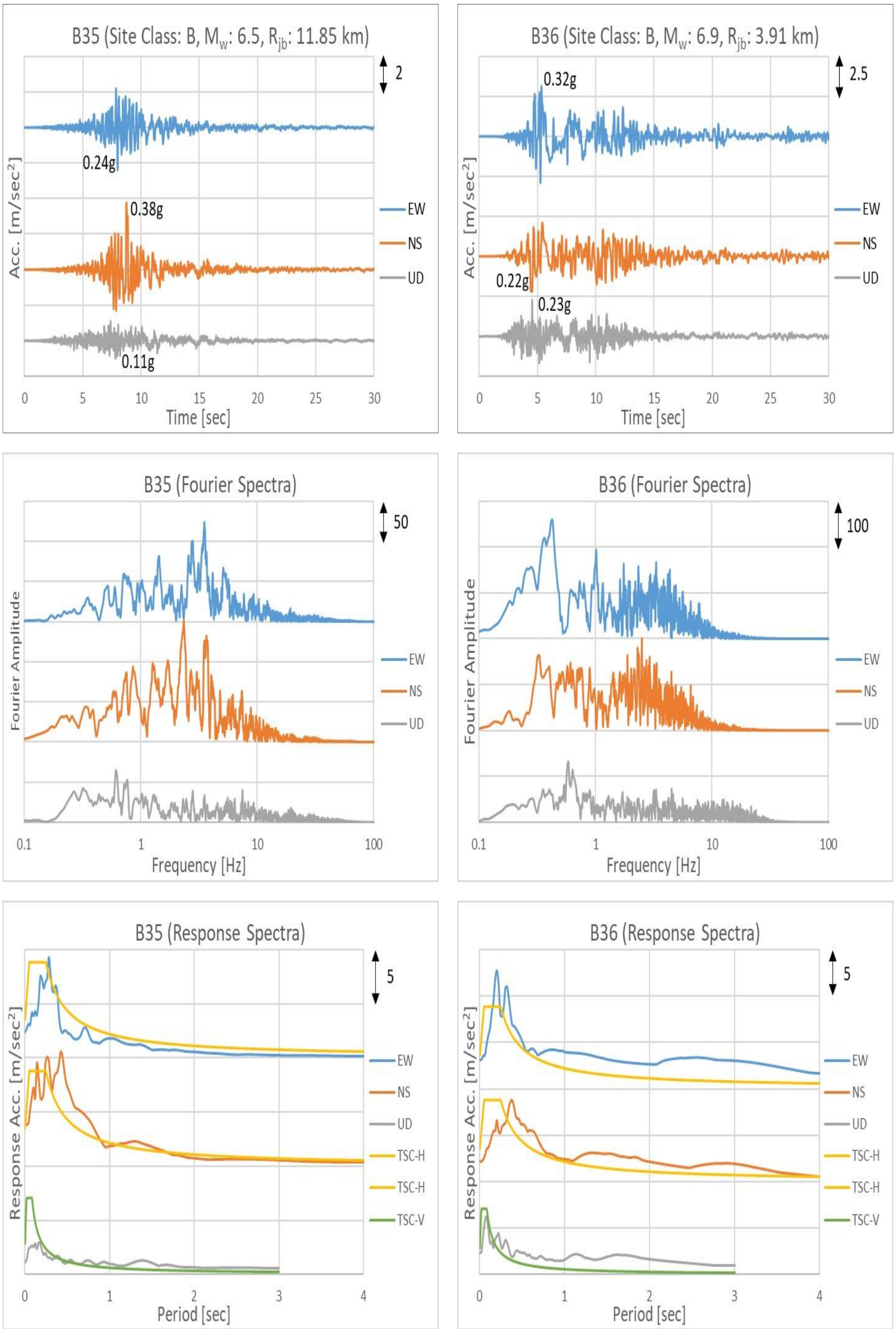

Figure A1. Acceleration Time Histories, Fourier Amplitude Spectra, and Response Spectra of the Selected Data (Cont.)

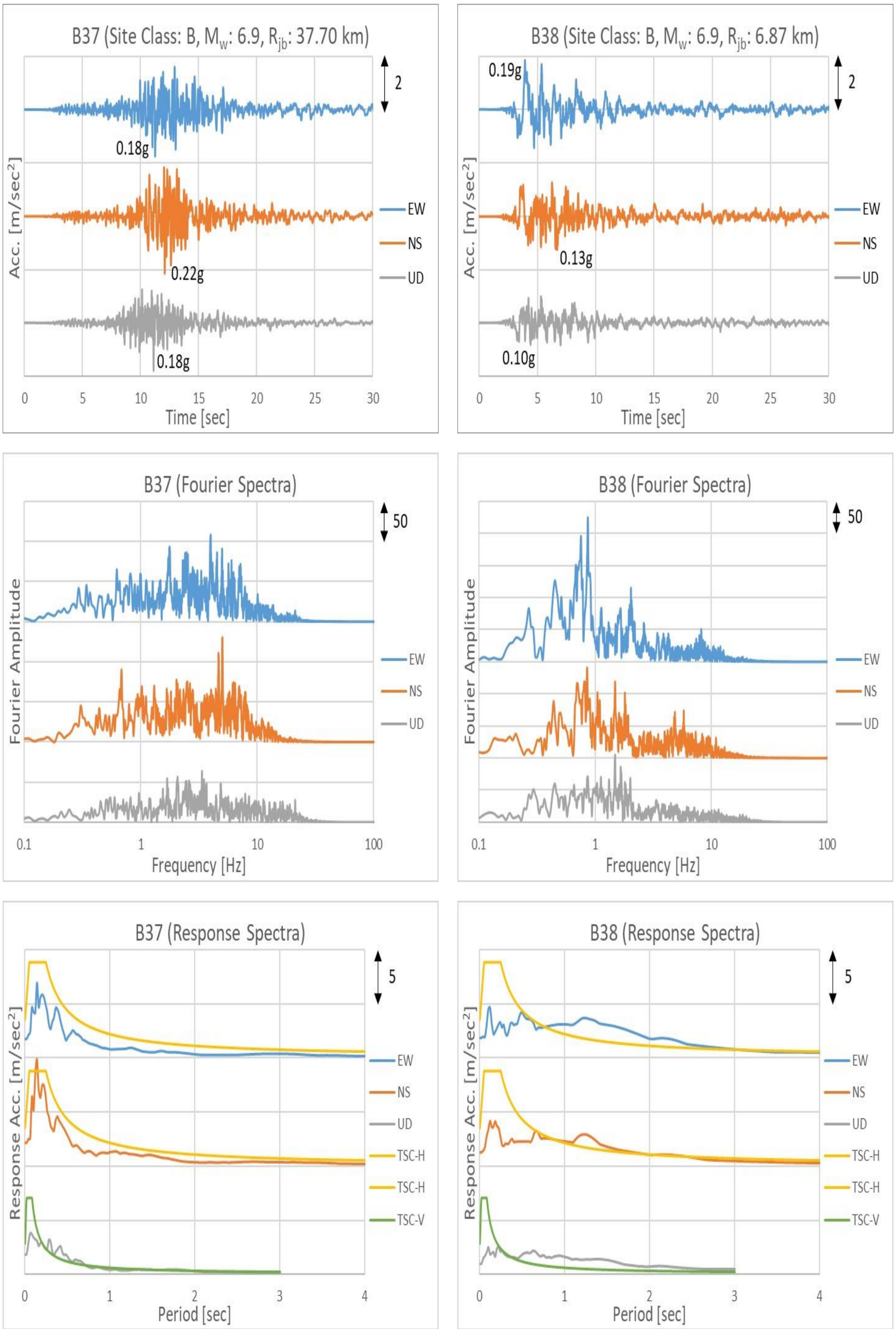

Figure A1. Acceleration Time Histories, Fourier Amplitude Spectra, and Response Spectra of the Selected Data (Cont.)

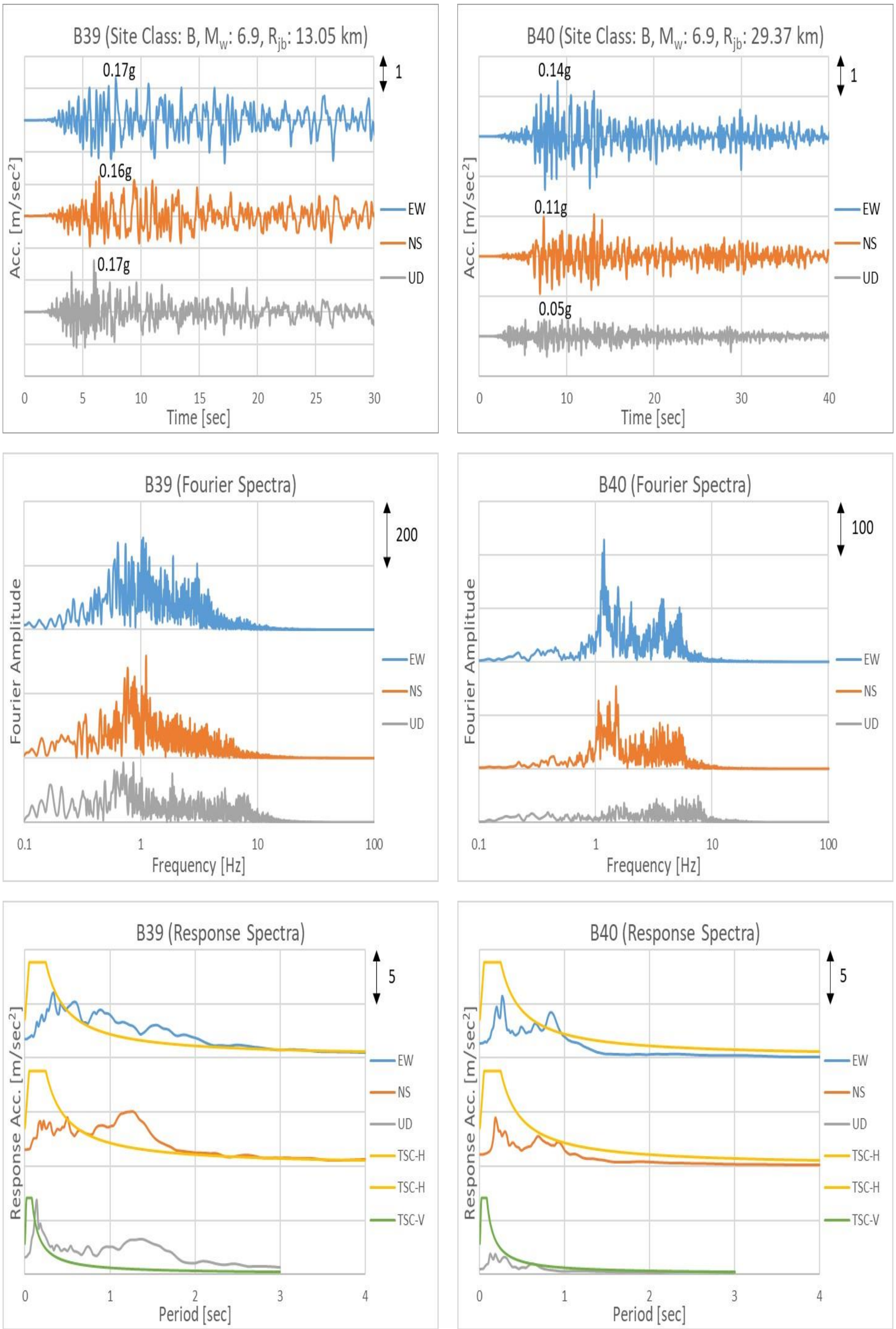

Figure A1. Acceleration Time Histories, Fourier Amplitude Spectra, and Response Spectra of the Selected Data (Cont.)

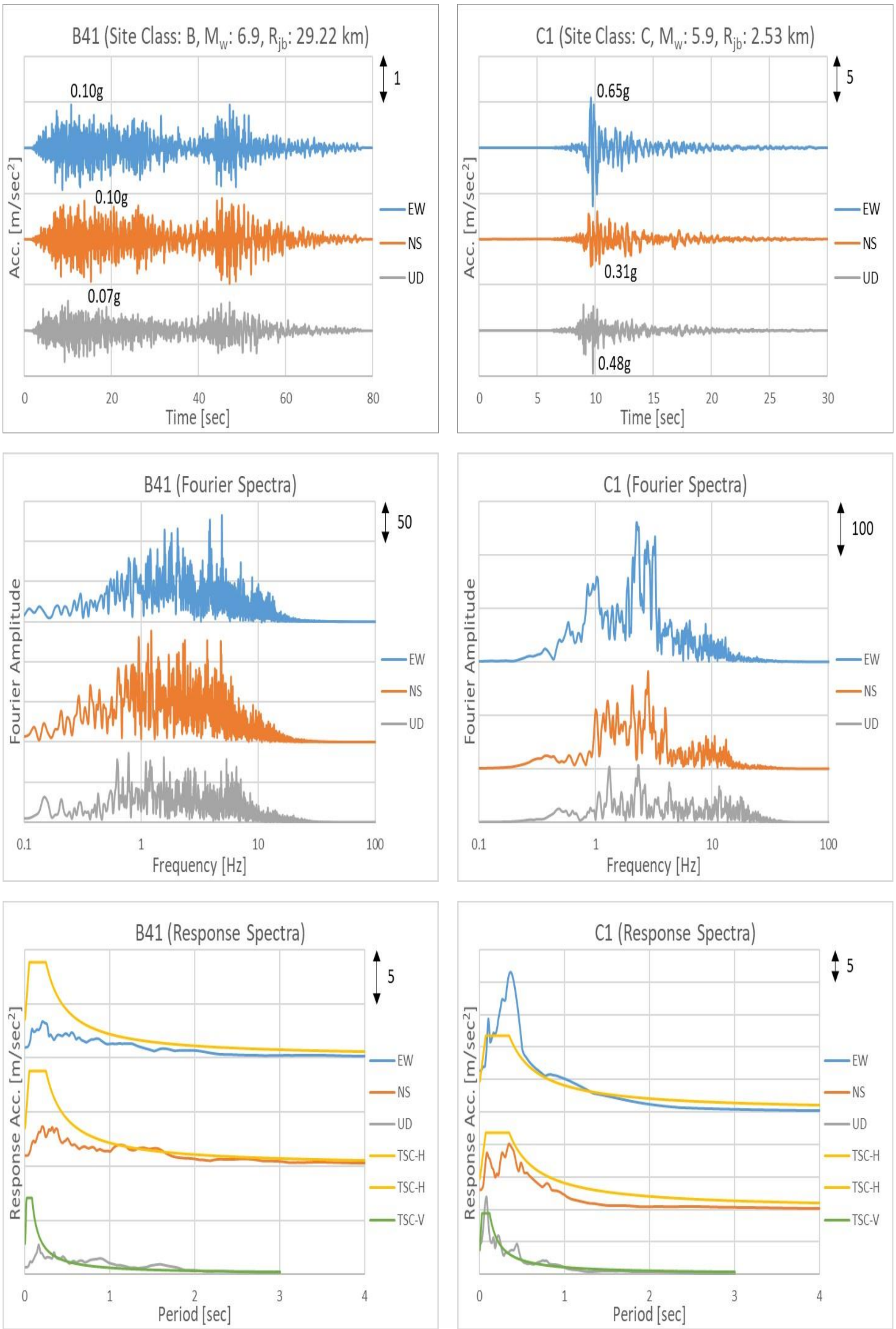

Figure A1. Acceleration Time Histories, Fourier Amplitude Spectra, and Response Spectra of the Selected Data (Cont.)

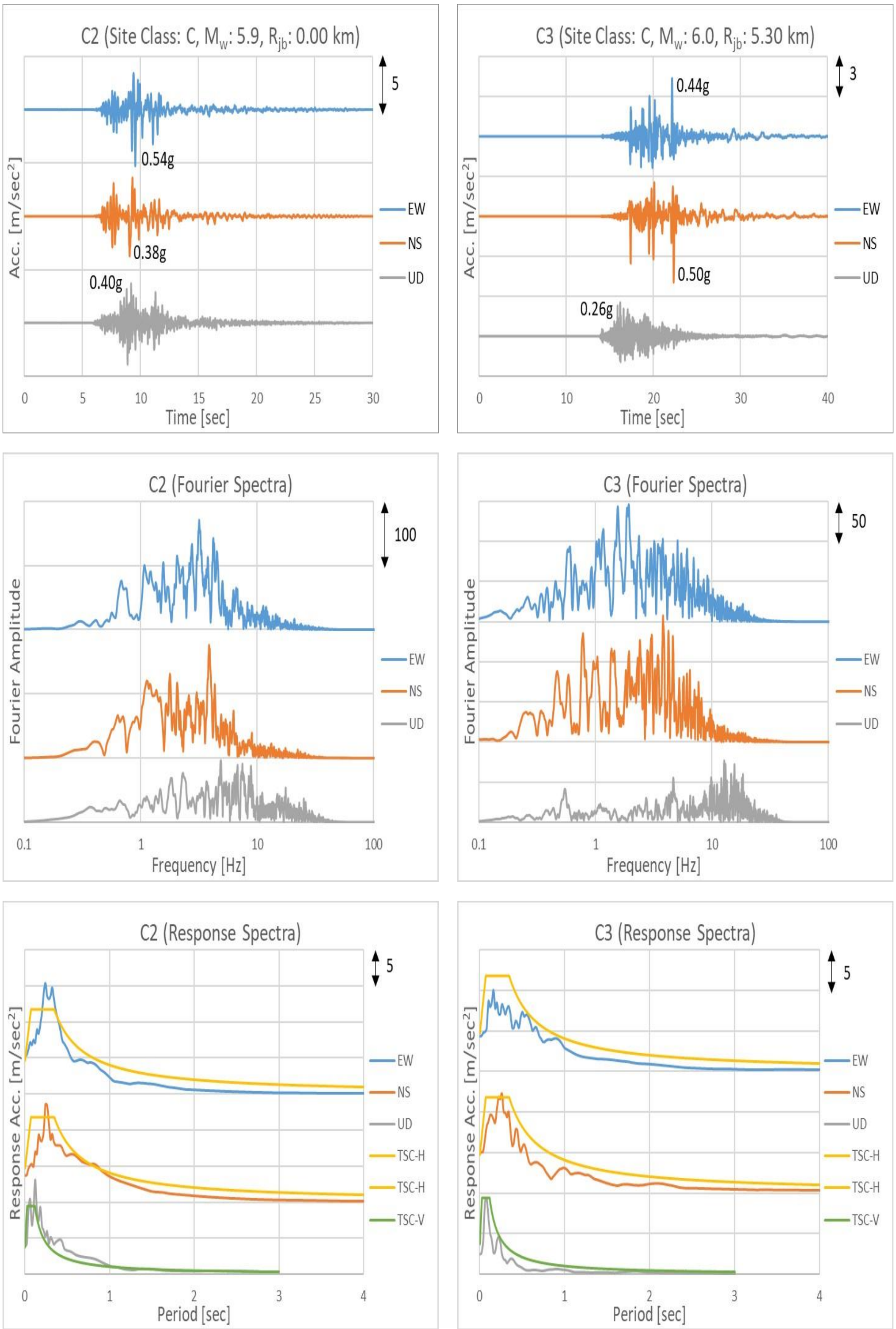

Figure A1. Acceleration Time Histories, Fourier Amplitude Spectra, and Response Spectra of the Selected Data (Cont.)

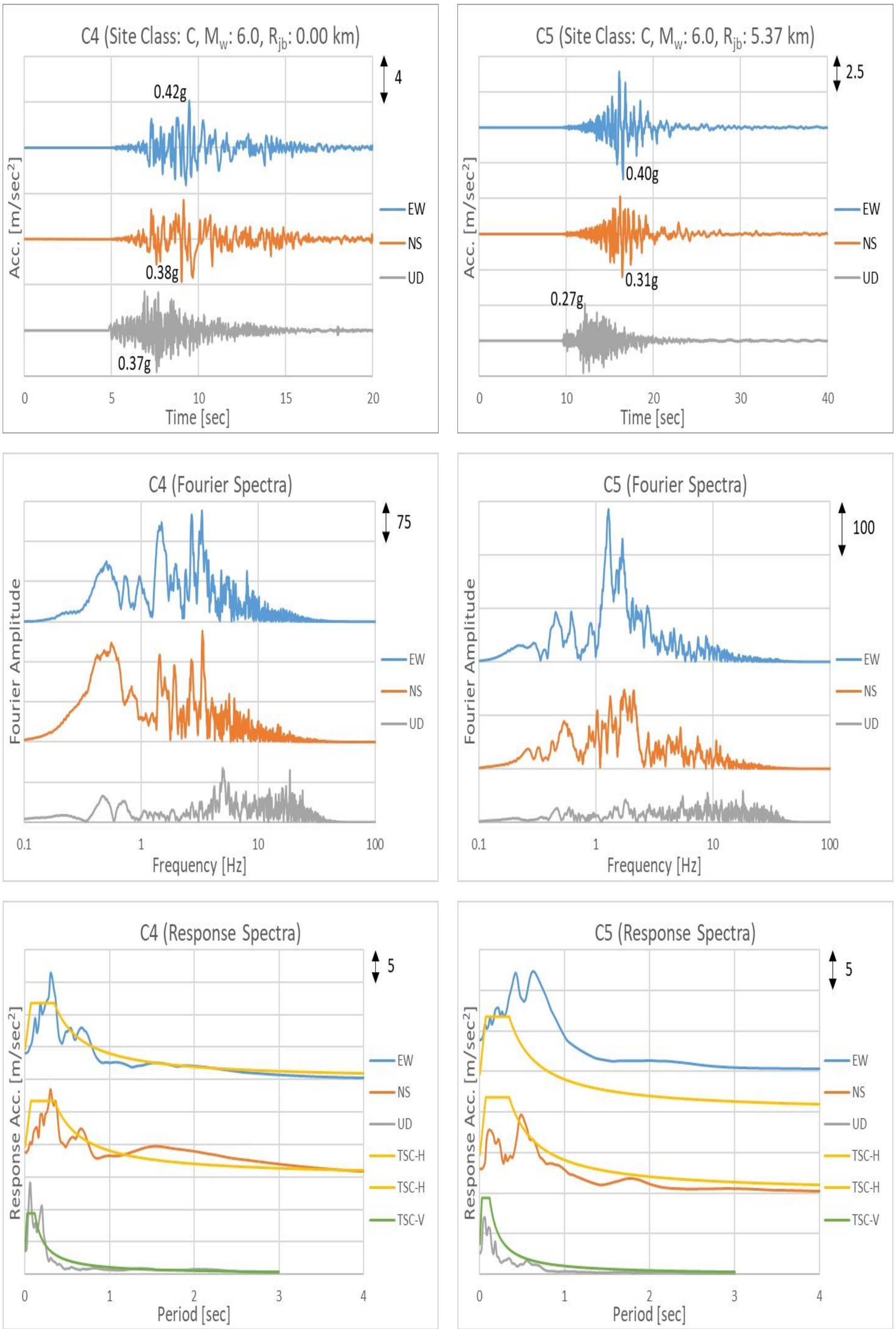

Figure A1. Acceleration Time Histories, Fourier Amplitude Spectra, and Response Spectra of the Selected Data (Cont.)

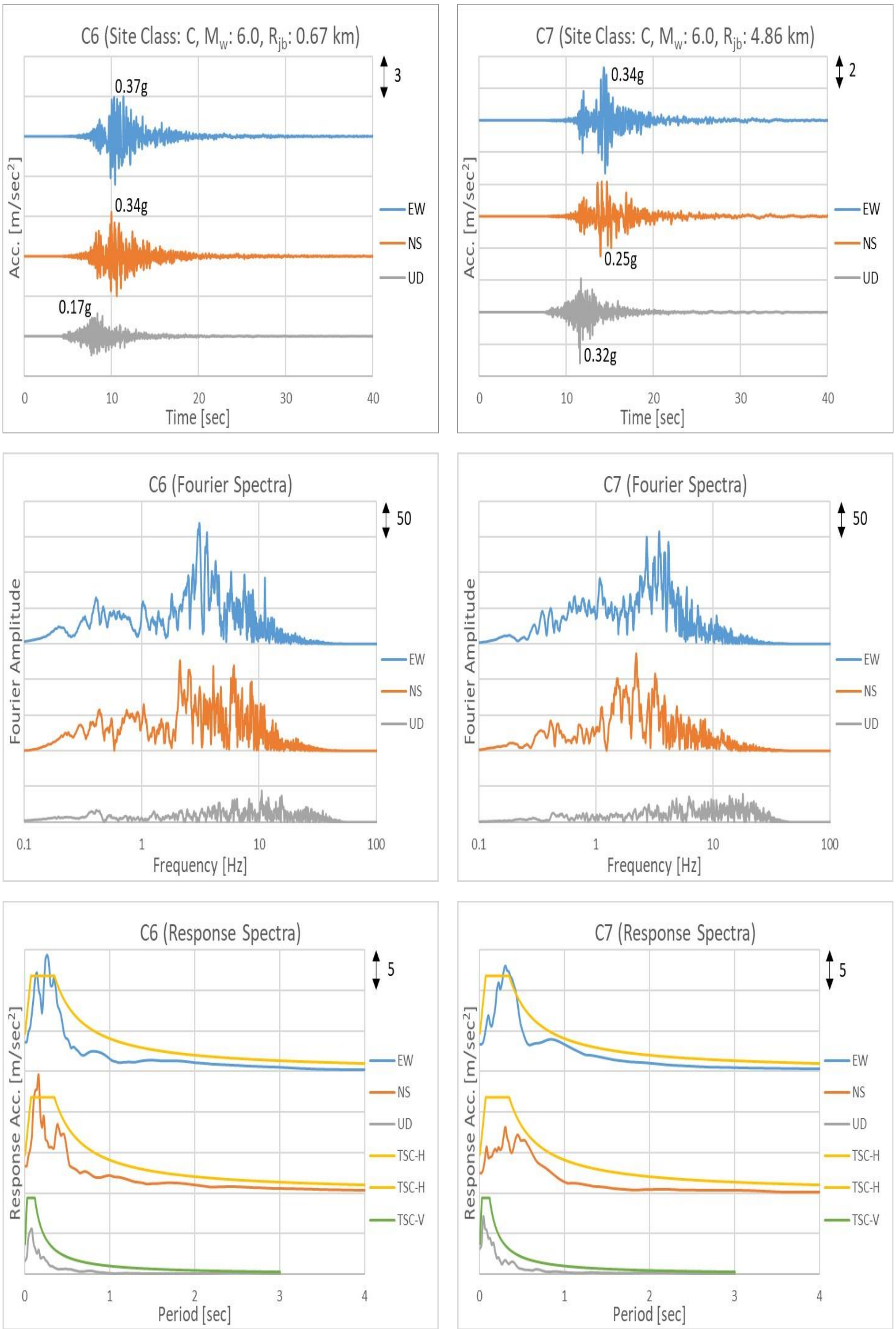

Figure A1. Acceleration Time Histories, Fourier Amplitude Spectra, and Response Spectra of the Selected Data (Cont.)

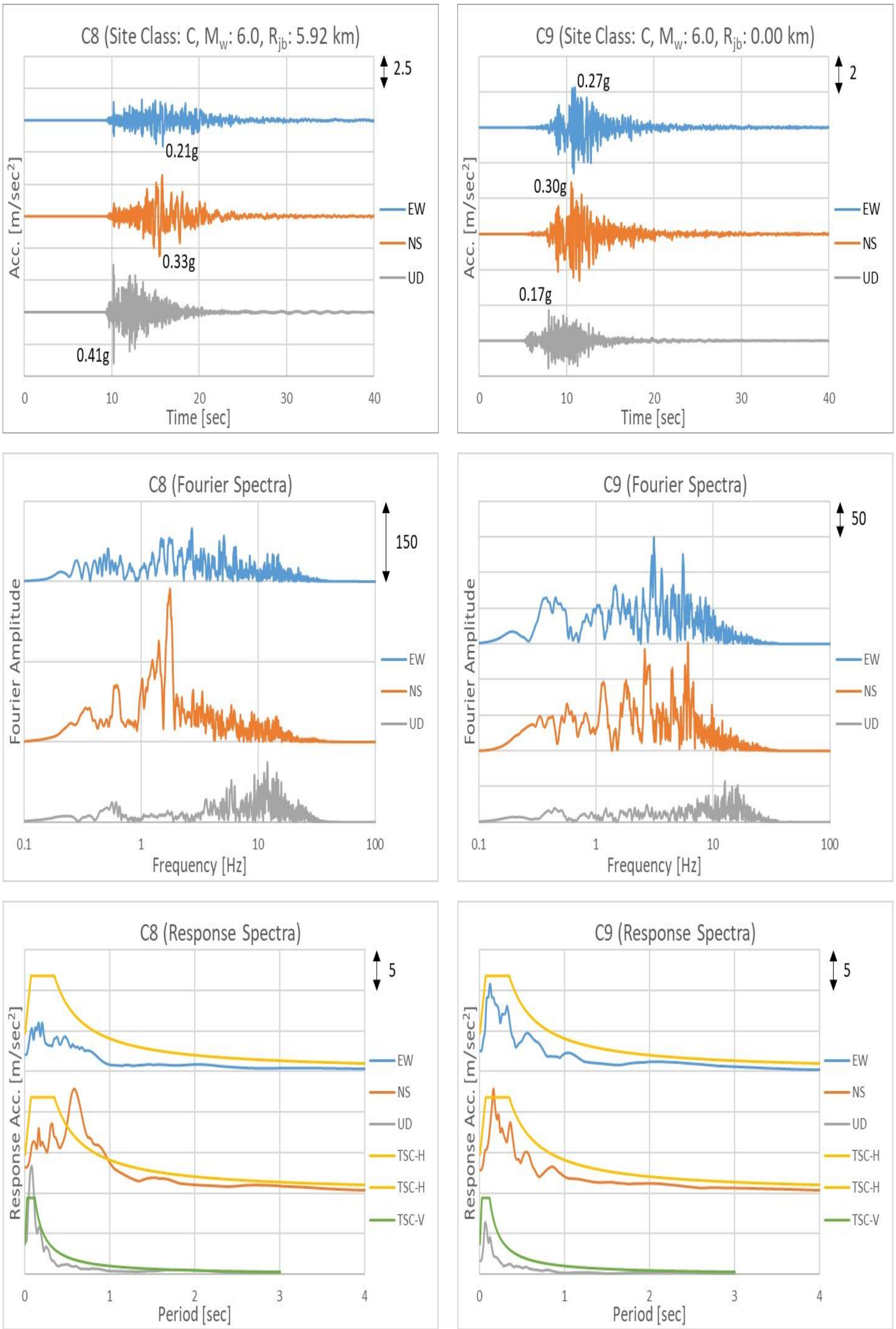

Figure A1. Acceleration Time Histories, Fourier Amplitude Spectra, and Response Spectra of the Selected Data (Cont.)

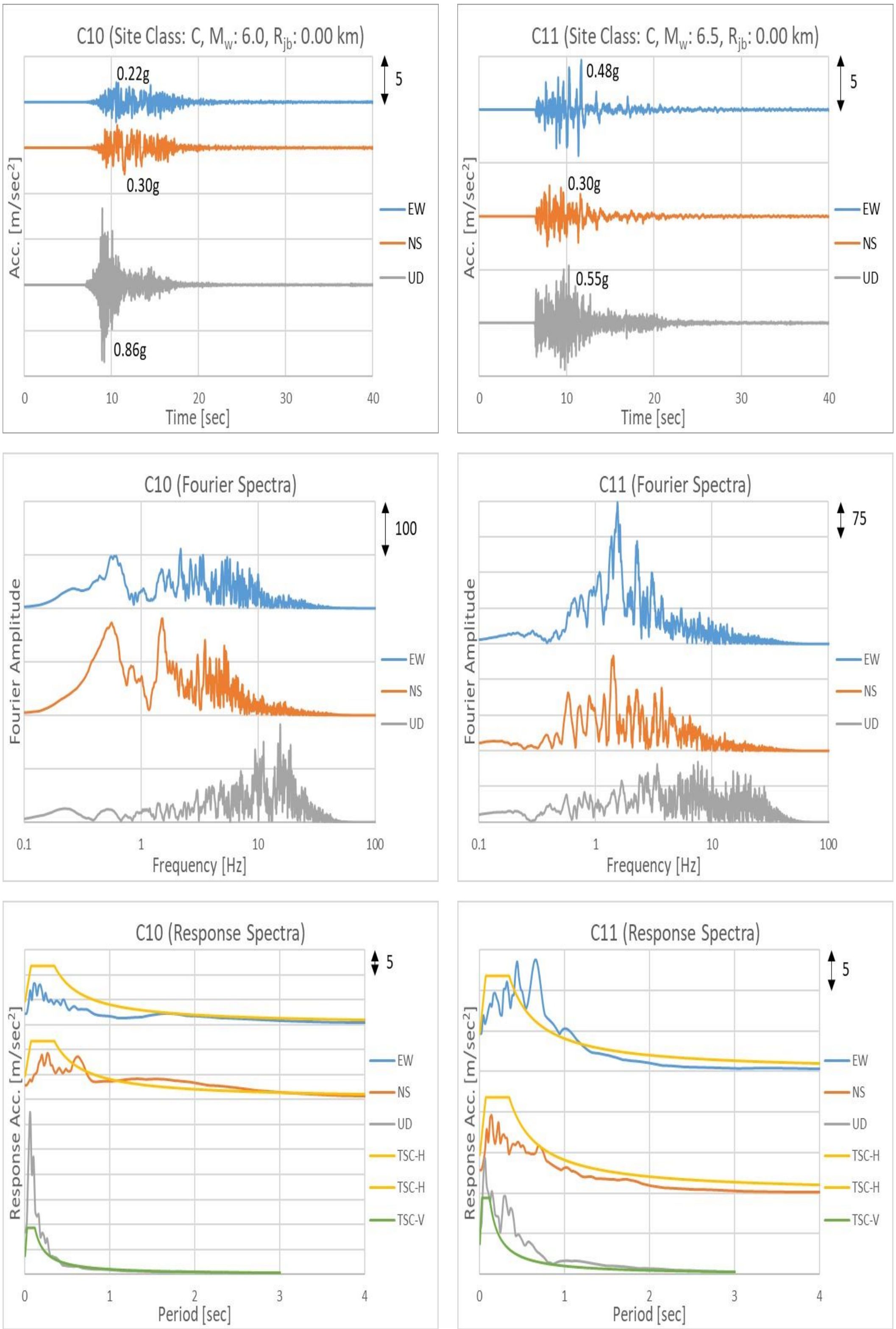

Figure A1. Acceleration Time Histories, Fourier Amplitude Spectra, and Response Spectra of the Selected Data (Cont.)

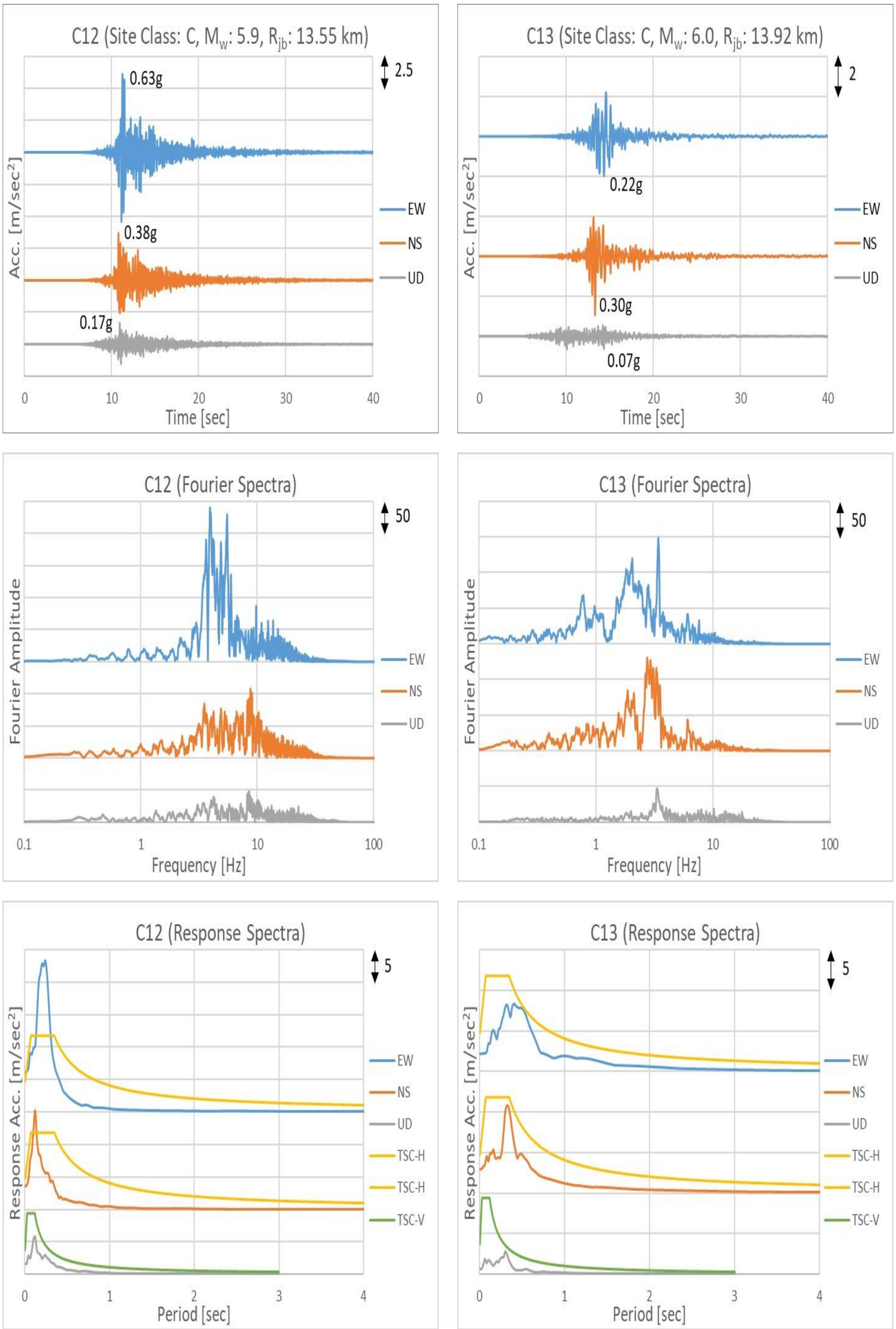

Figure A1. Acceleration Time Histories, Fourier Amplitude Spectra, and Response Spectra of the Selected Data (Cont.)

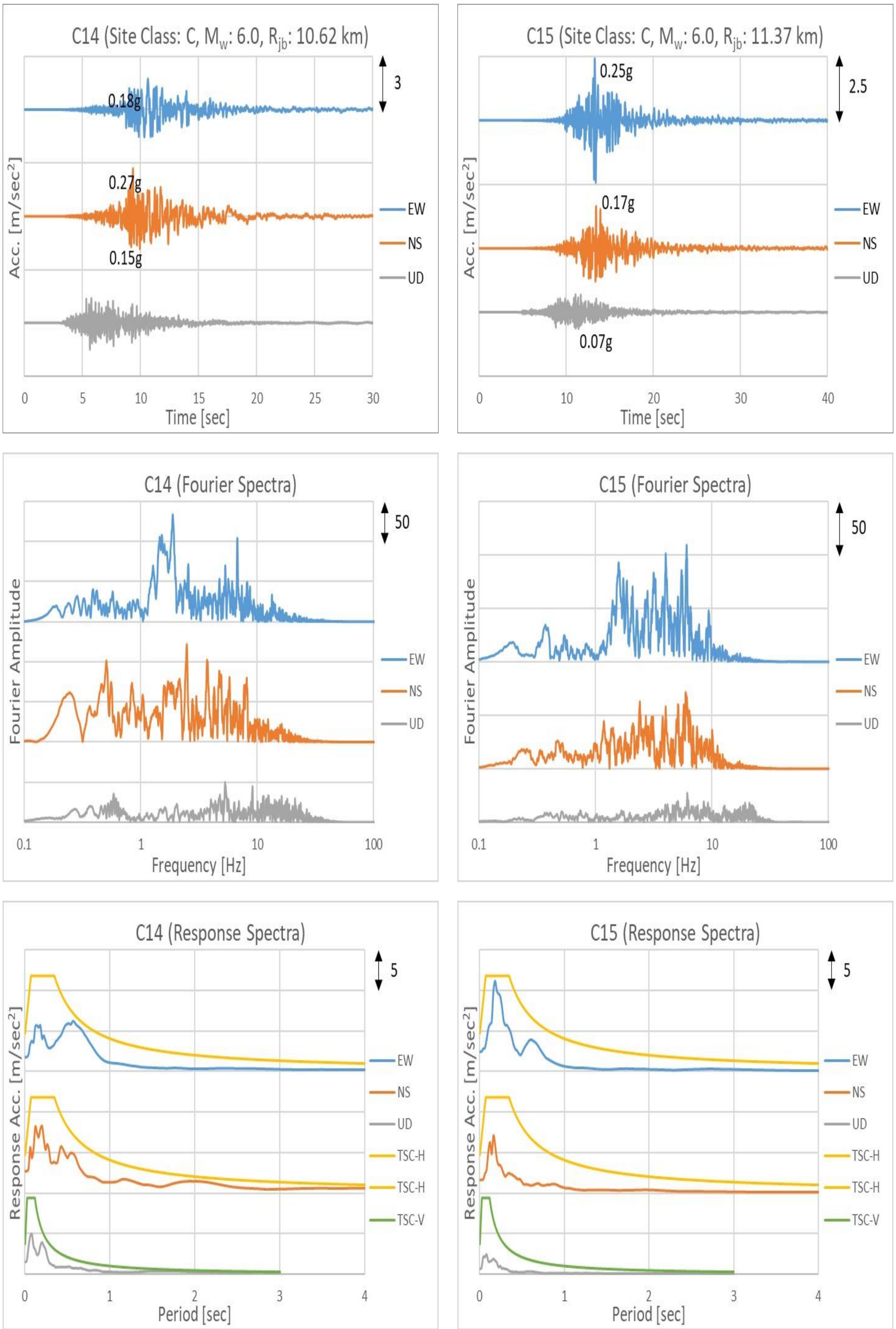

Figure A1. Acceleration Time Histories, Fourier Amplitude Spectra, and Response Spectra of the Selected Data (Cont.)

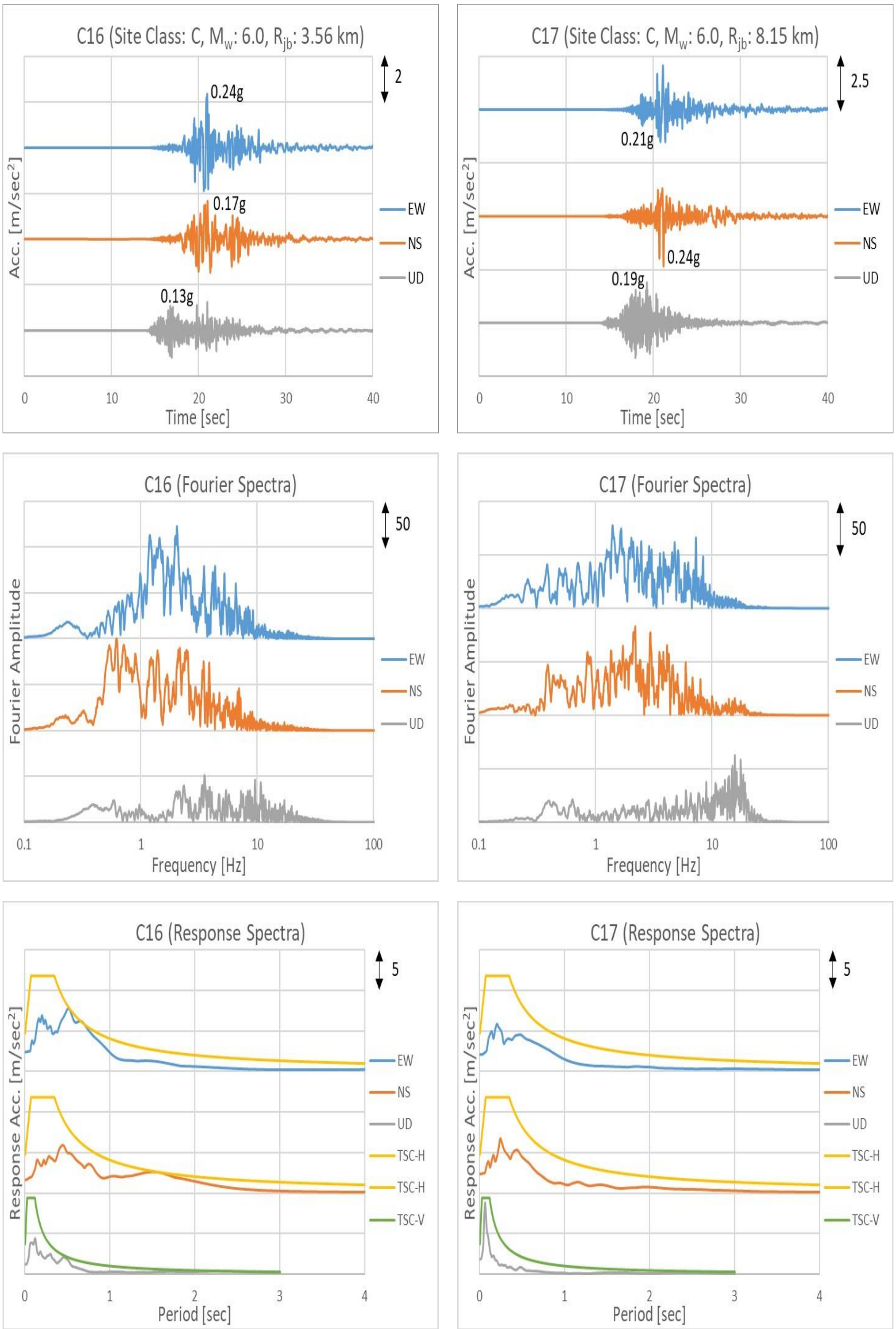

Figure A1. Acceleration Time Histories, Fourier Amplitude Spectra, and Response Spectra of the Selected Data (Cont.)

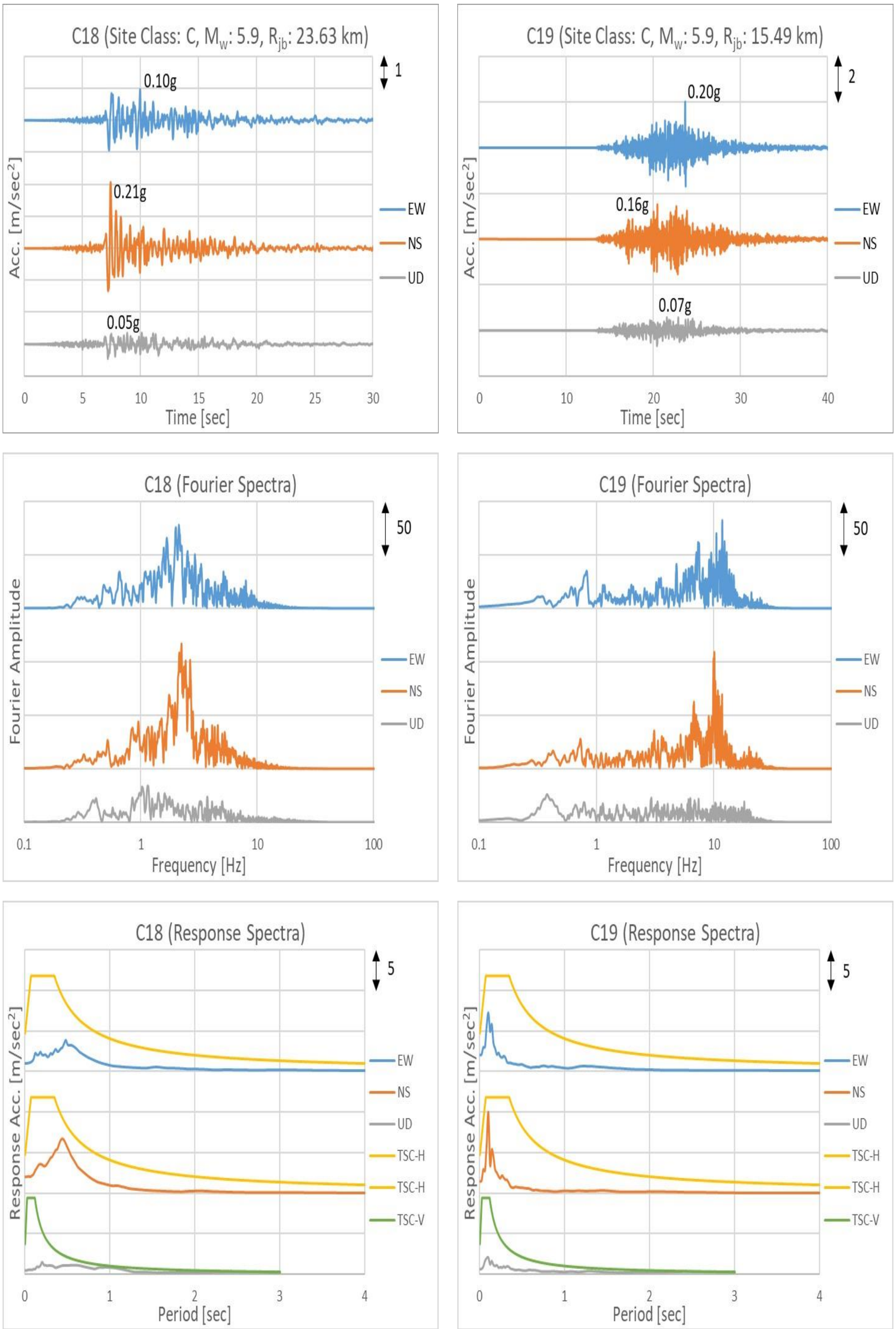

Figure A1. Acceleration Time Histories, Fourier Amplitude Spectra, and Response Spectra of the Selected Data (Cont.)

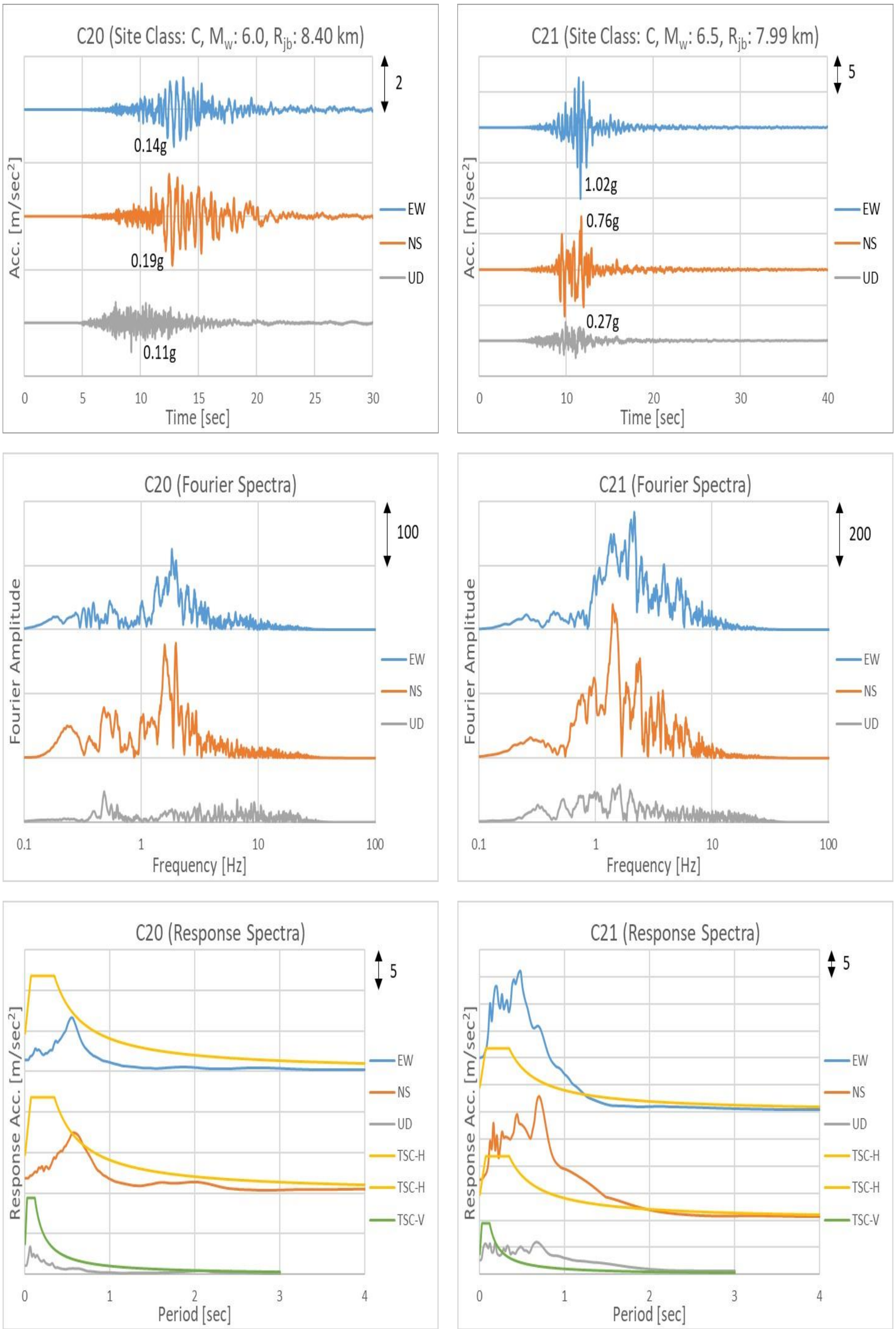

Figure A1. Acceleration Time Histories, Fourier Amplitude Spectra, and Response Spectra of the Selected Data (Cont.)

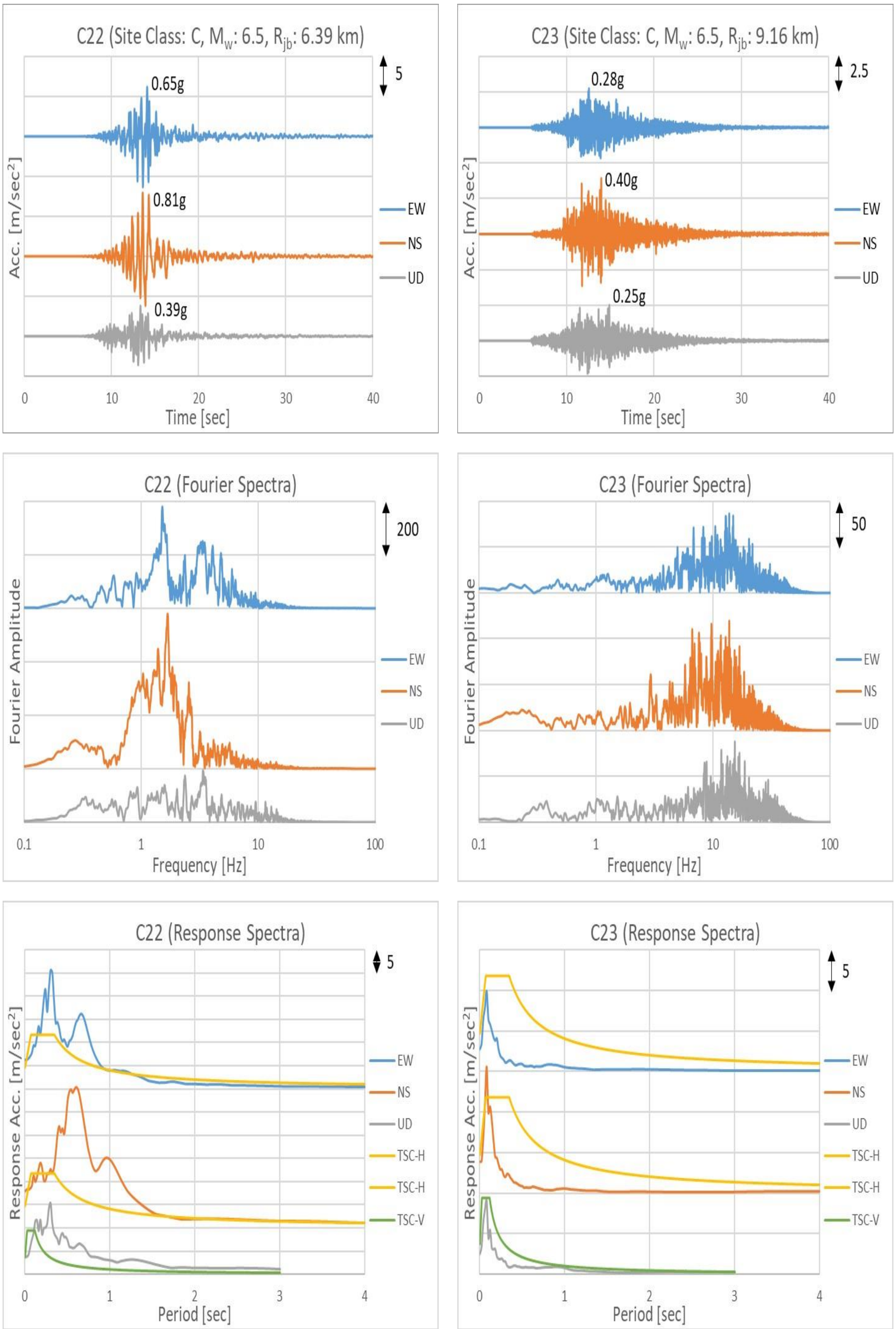

Figure A1. Acceleration Time Histories, Fourier Amplitude Spectra, and Response Spectra of the Selected Data (Cont.)

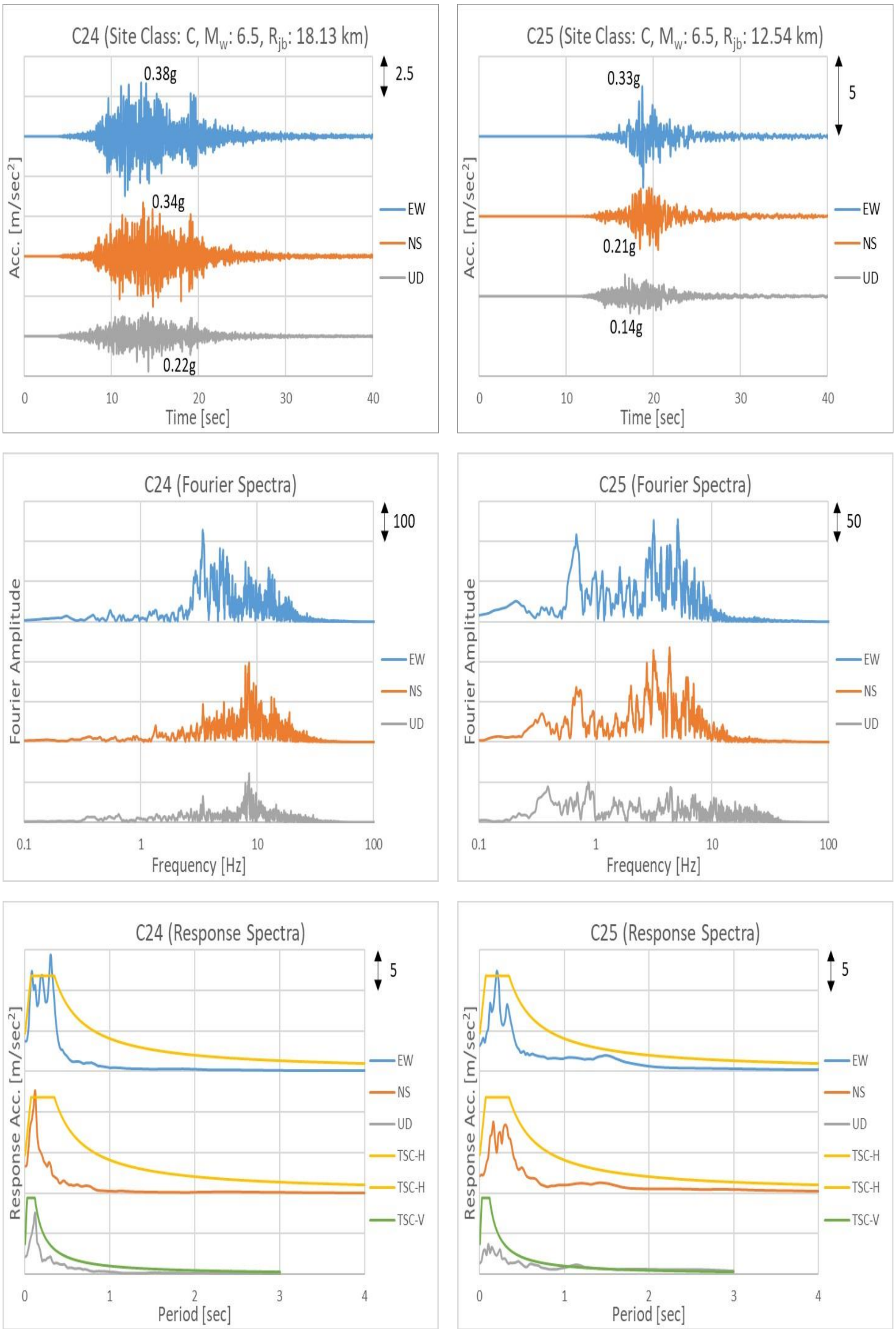

Figure A1. Acceleration Time Histories, Fourier Amplitude Spectra, and Response Spectra of the Selected Data (Cont.)

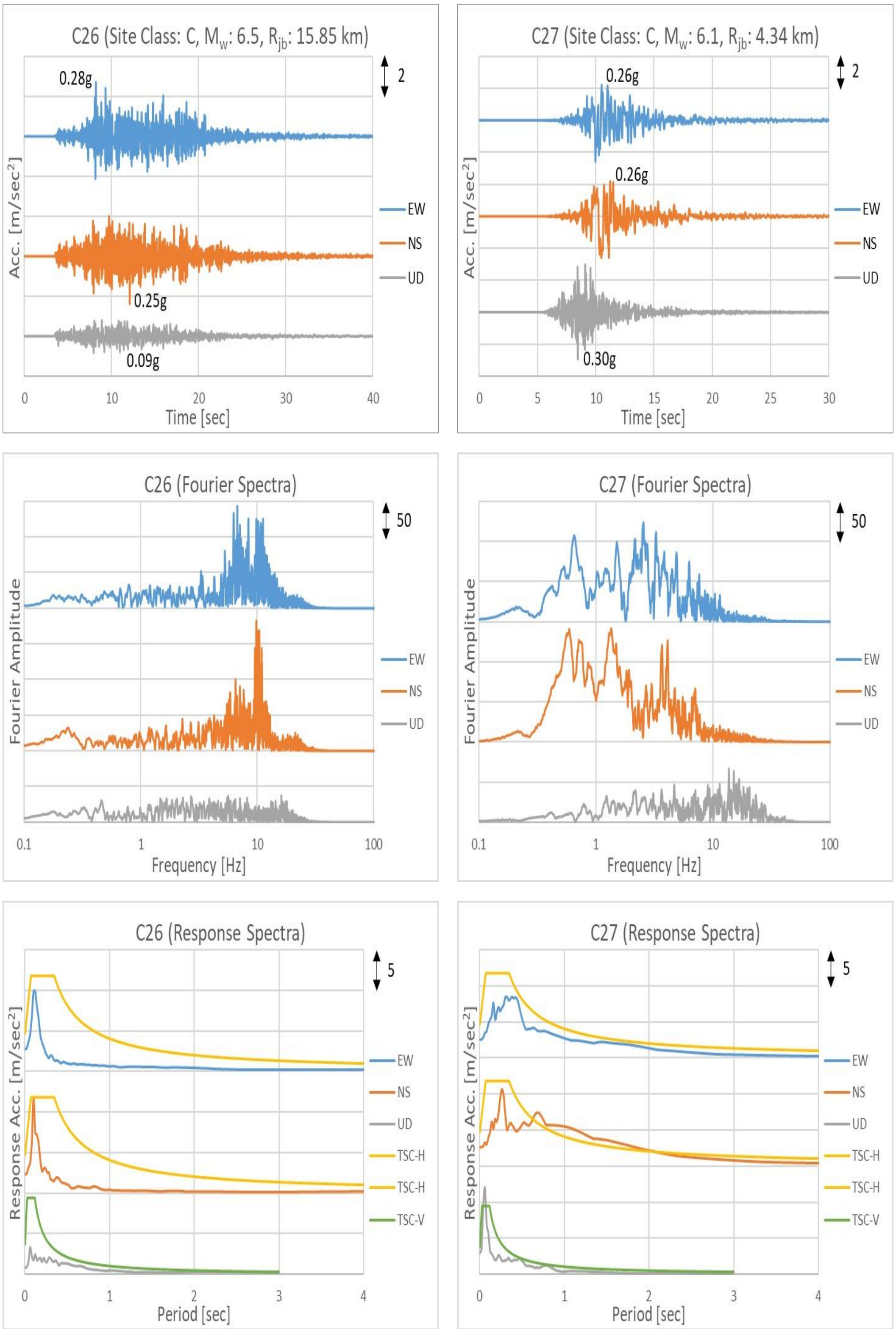

Figure A1. Acceleration Time Histories, Fourier Amplitude Spectra, and Response Spectra of the Selected Data (Cont.)

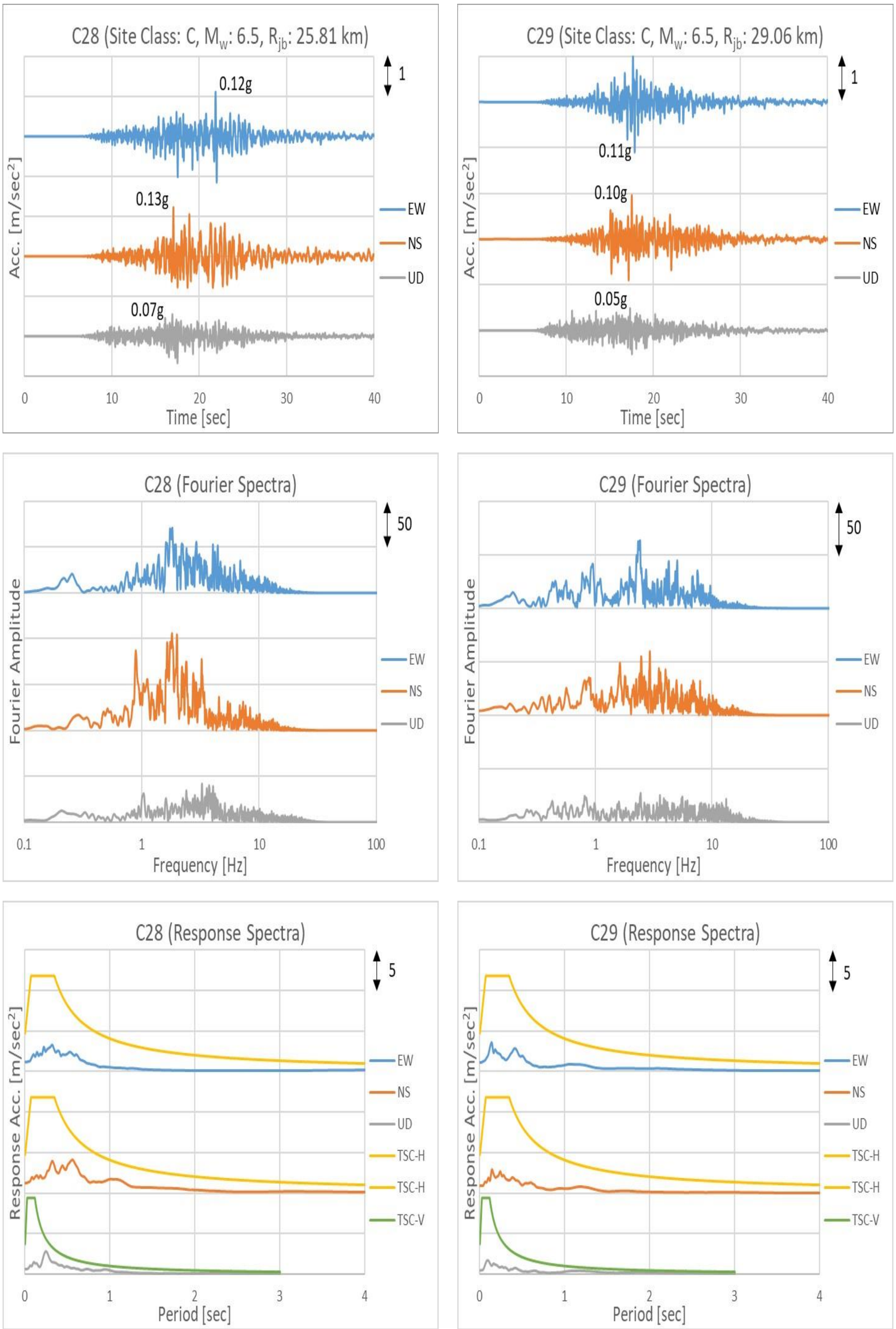

Figure A1. Acceleration Time Histories, Fourier Amplitude Spectra, and Response Spectra of the Selected Data (Cont.)

B. Detailed Analysis Results

The results of the analyses based on inter-story drift ratio, overturning moment, axial force on column, and story shear force are plotted and presented in this section. Each plot is explained in terms of site class and M_w. X axis of each plot represents the R_{jb} (in ascending order) and Y axis represents the amplification factor of response parameter. The exact results can be seen in *Table 5.2*. In inter-story drift ratio, overturning moment, and story shear force plots, *Amp.* represents the ratio of maximum result obtained from the case with vertical component to the result obtained from the case without vertical component whilst in column axial force plots, it represents the ratio of the effect of vertical ground motion to column axial capacity.

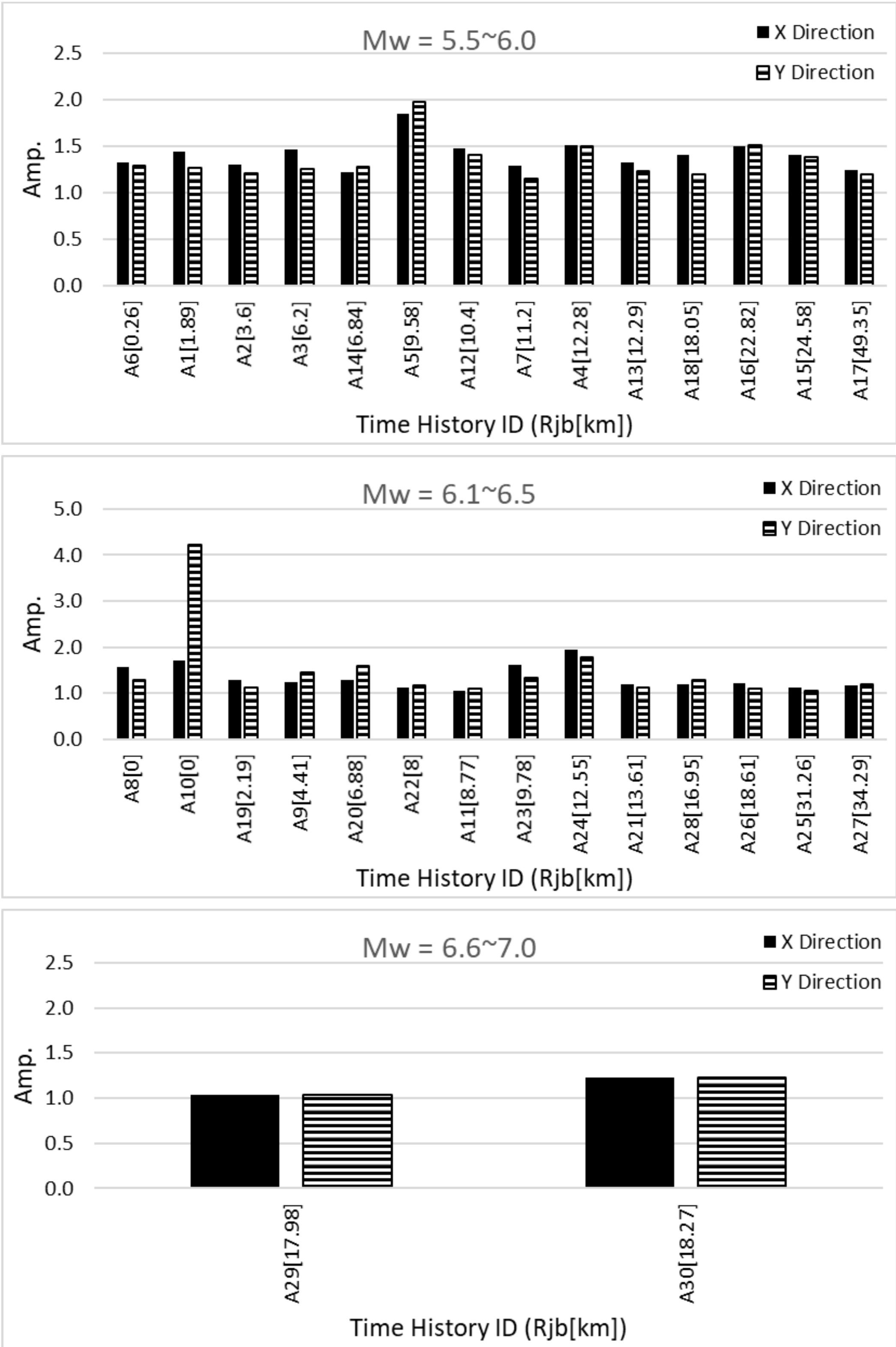

Figure B1. Inter-story Drift Ratio Results for Site Class A

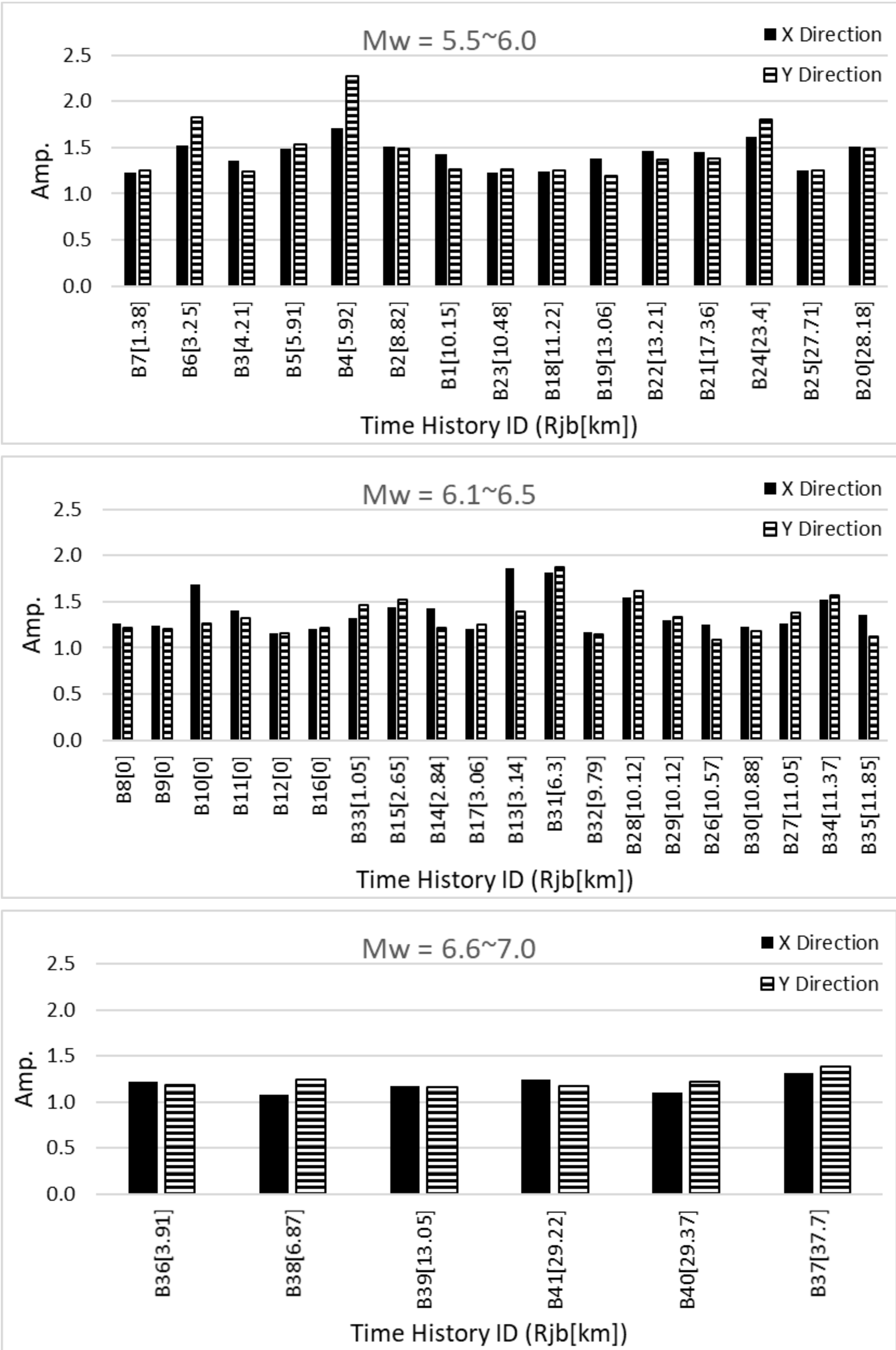

Figure B2. Inter-story Drift Ratio Results for Site Class B

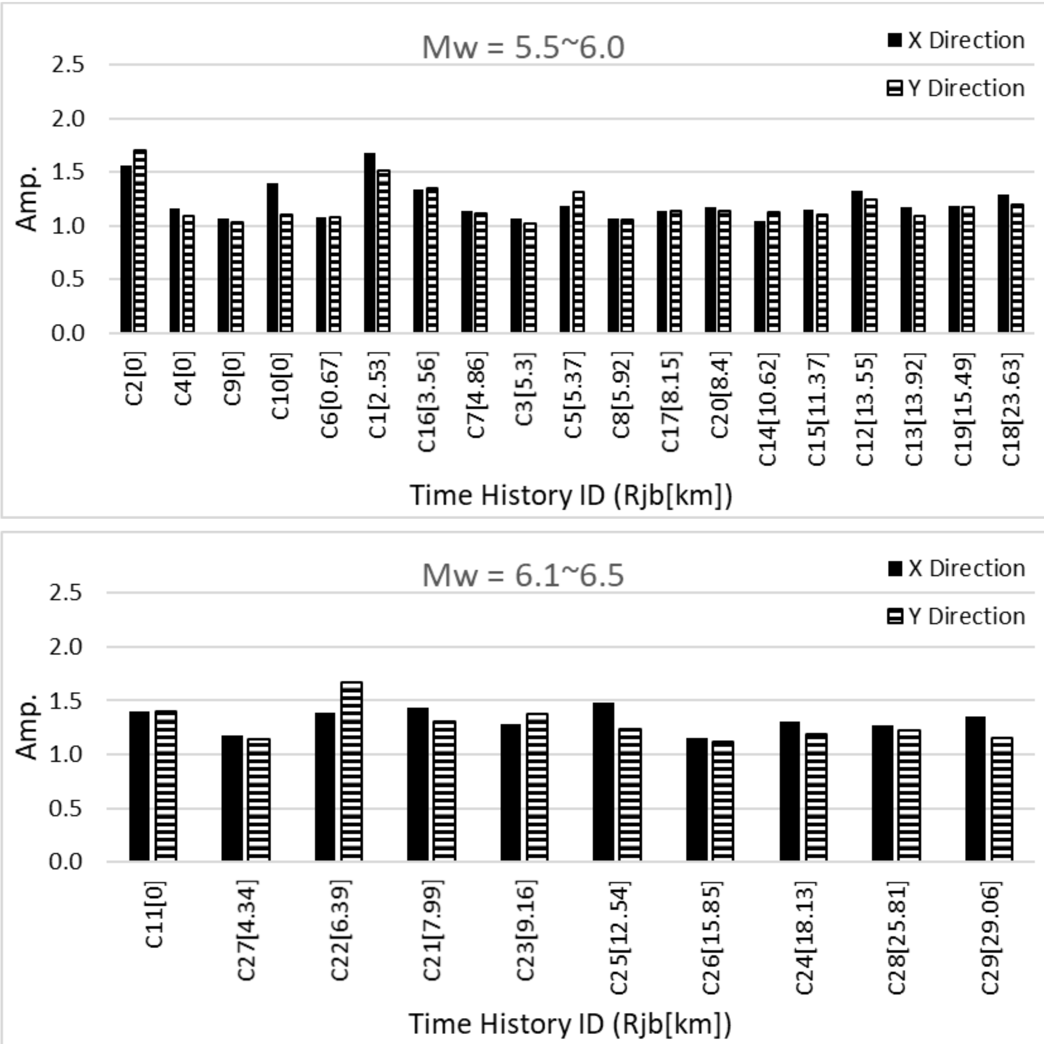

Figure B3. Inter-story Drift Ratio Results for Site Class C

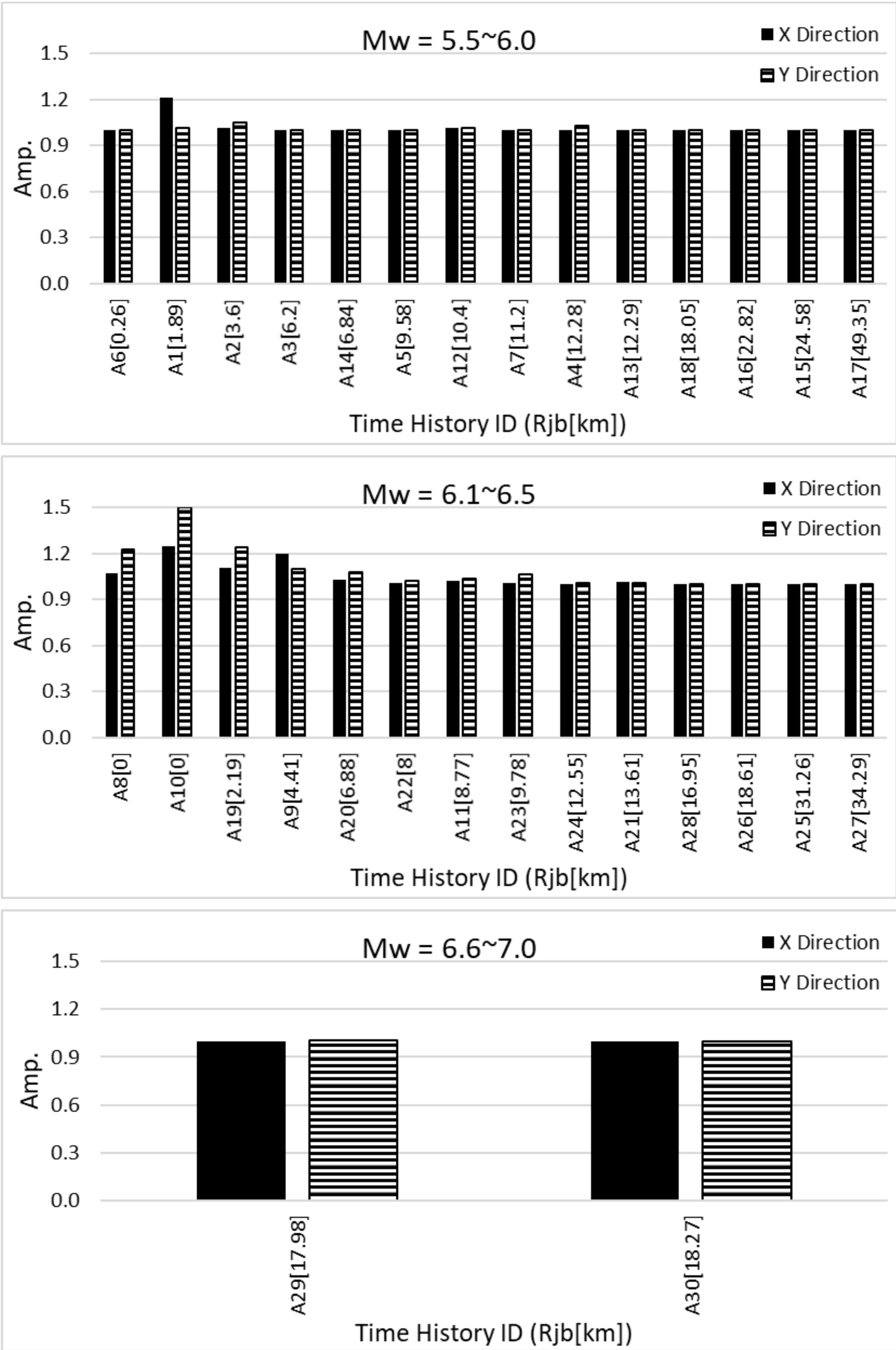

Figure B4. Overturning Moment Results for Site Class A

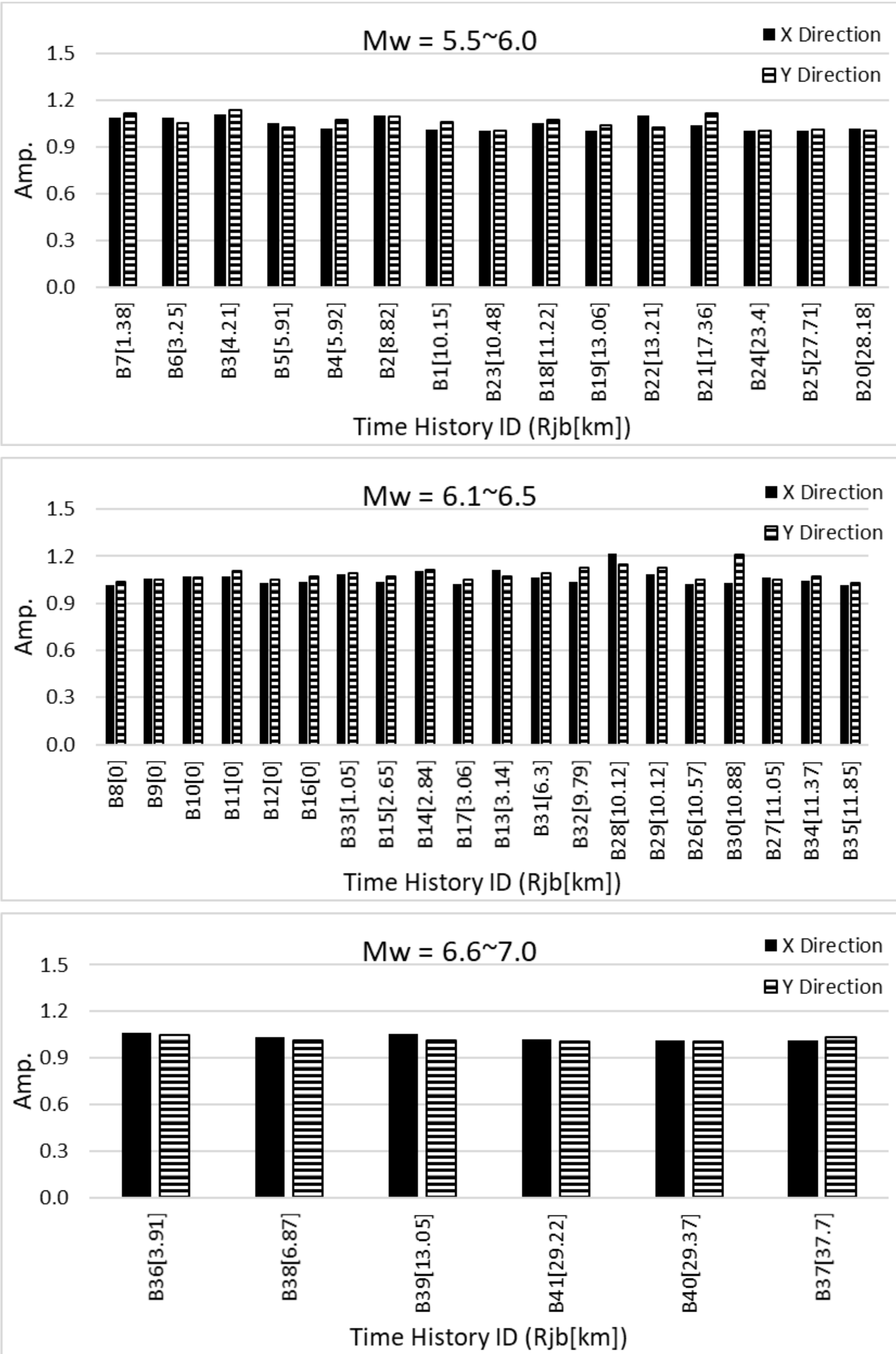

Figure B5. Overturning Moment Results for Site Class B

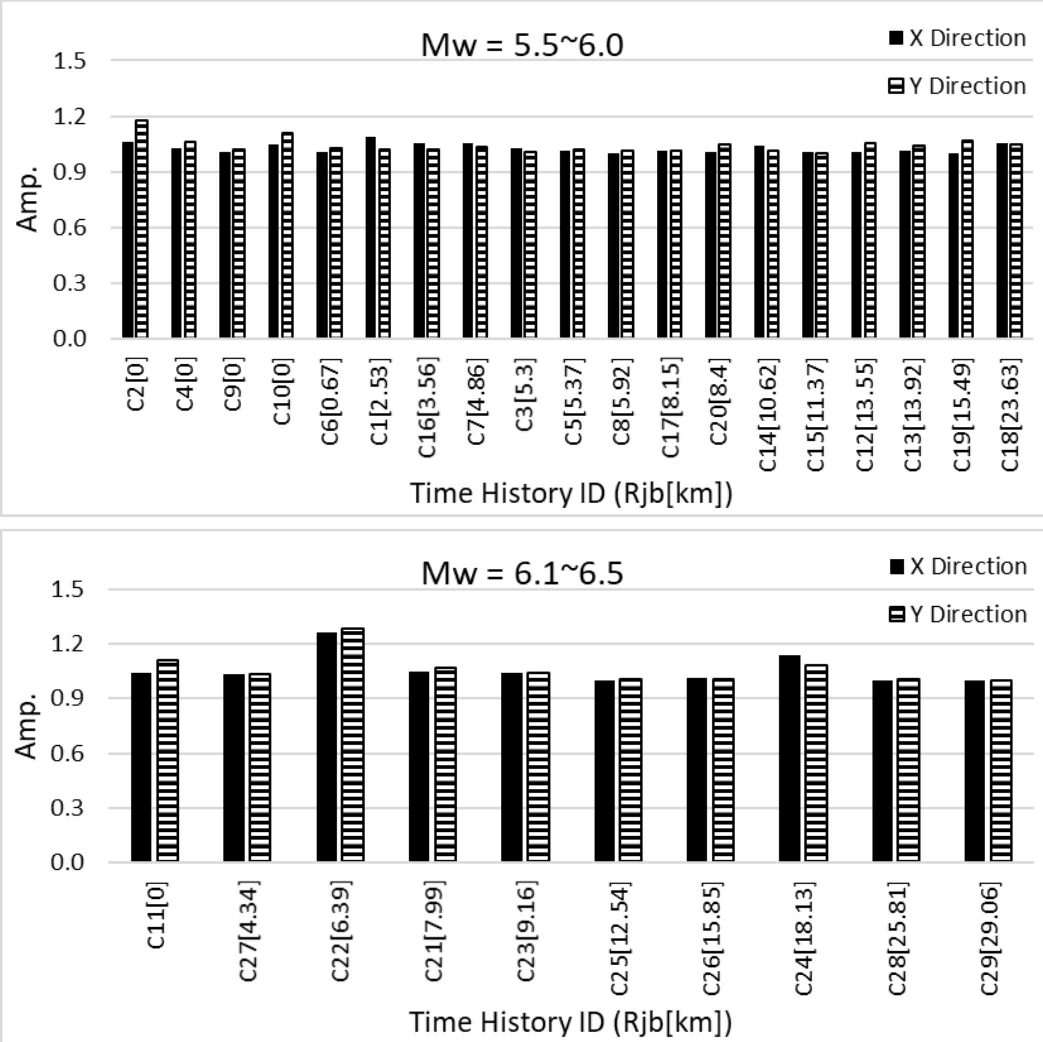

Figure B6. Overturning Moment Results for Site Class C

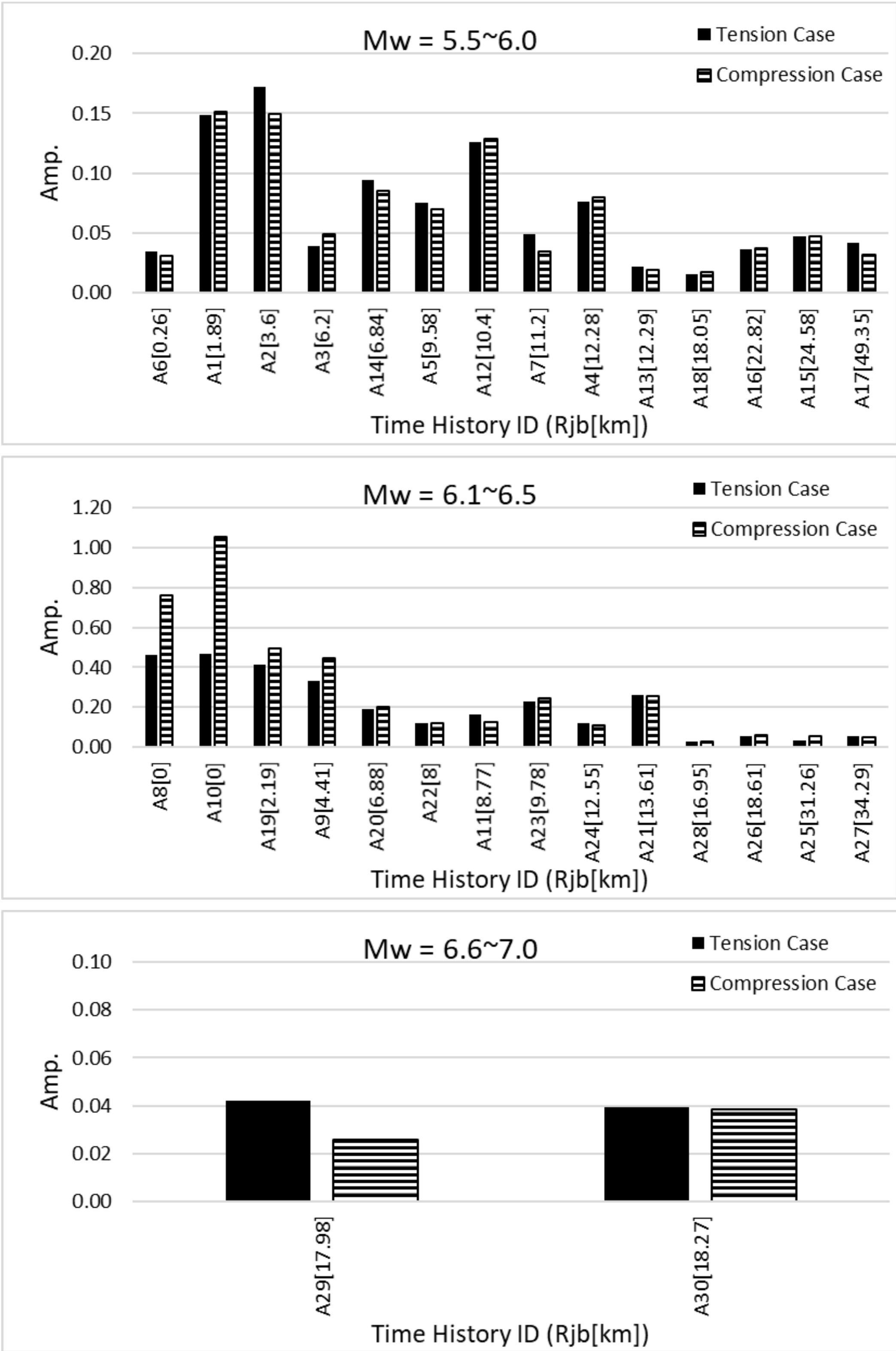

Figure B7. Column Axial Force Results for Site Class A

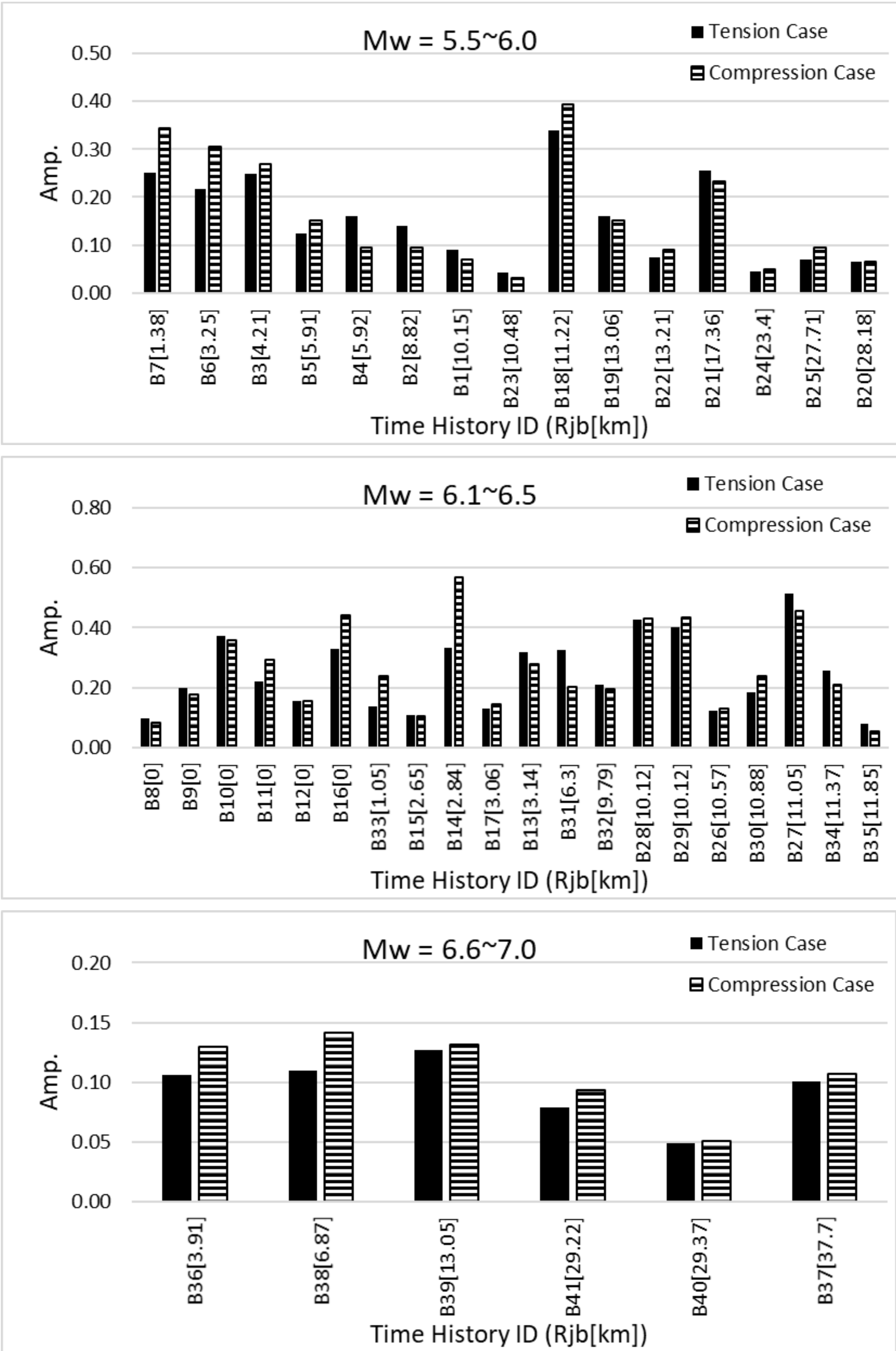

Figure B8. Column Axial Force Results for Site Class B

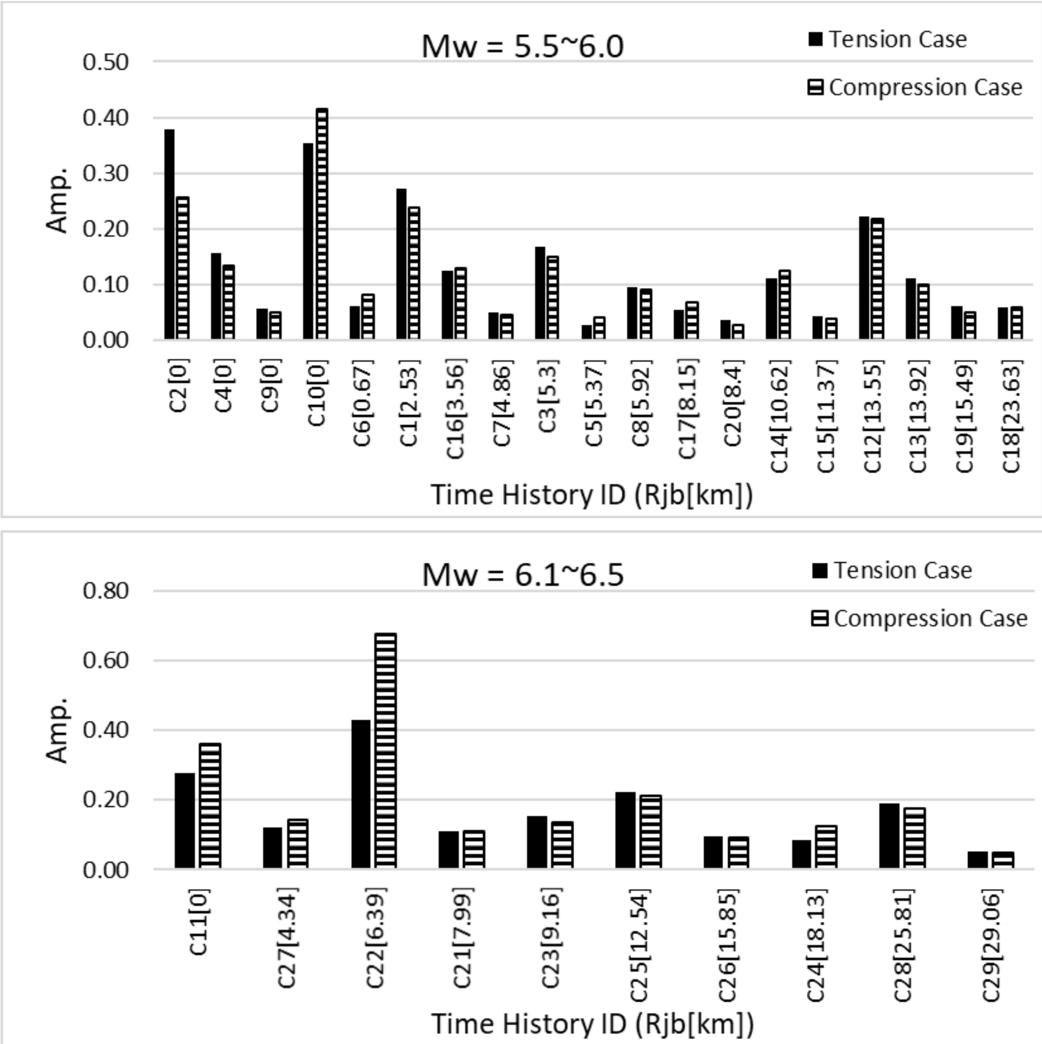

Figure B9. Column Axial Force Results for Site Class C

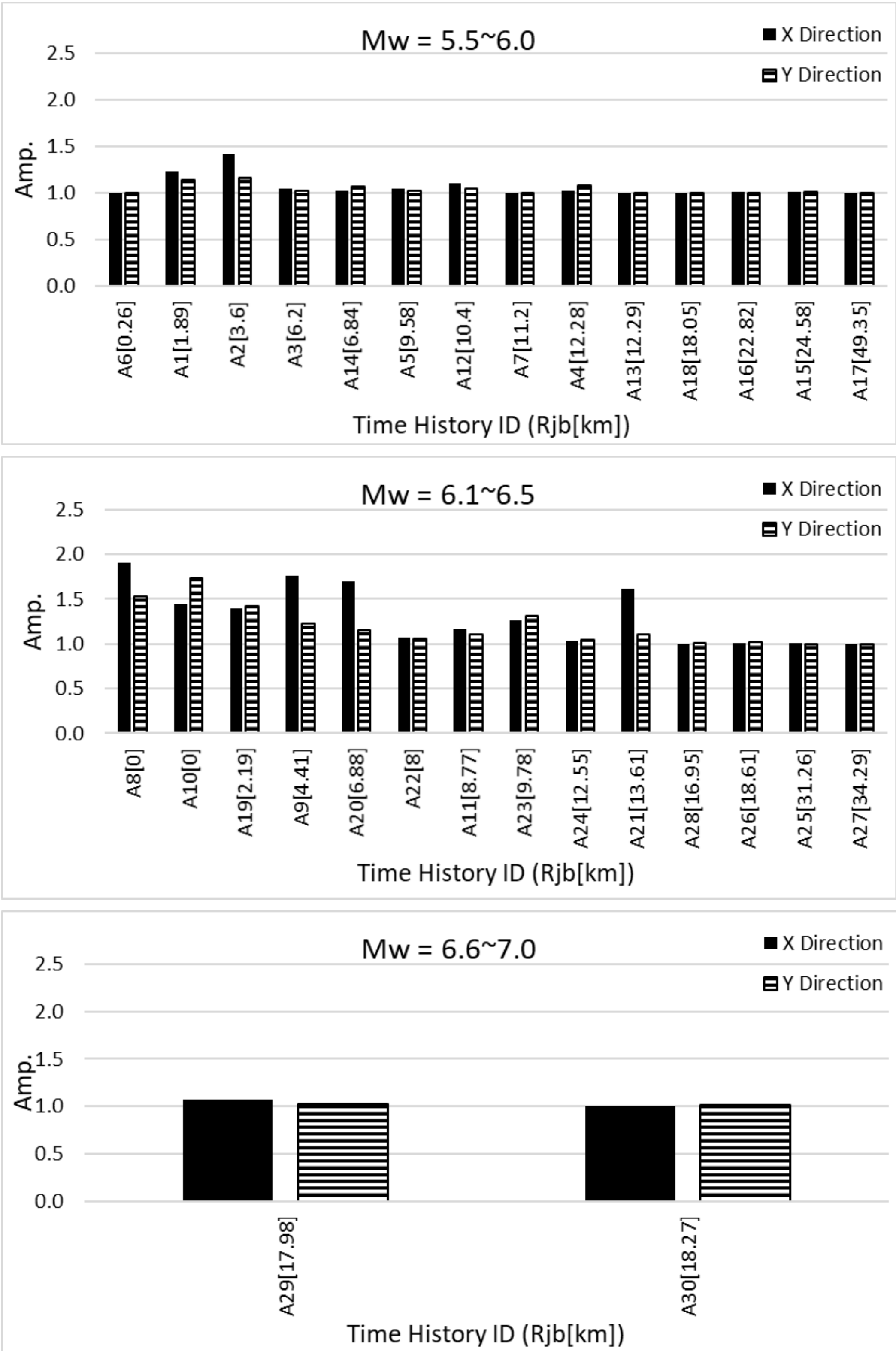

Figure B10. Story Shear Force Results for Site Class A

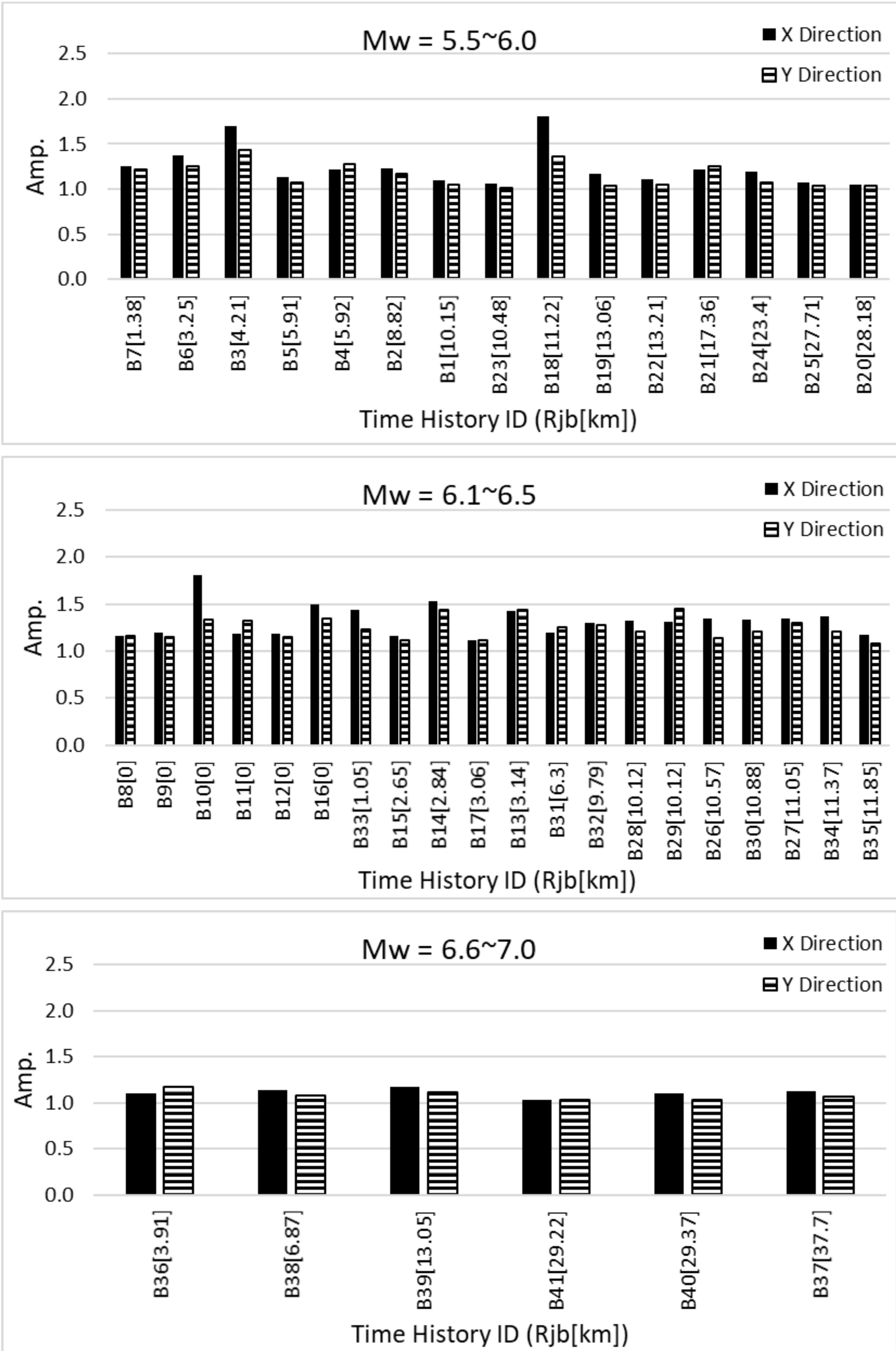

Figure B11. Story Shear Force Results for Site Class B

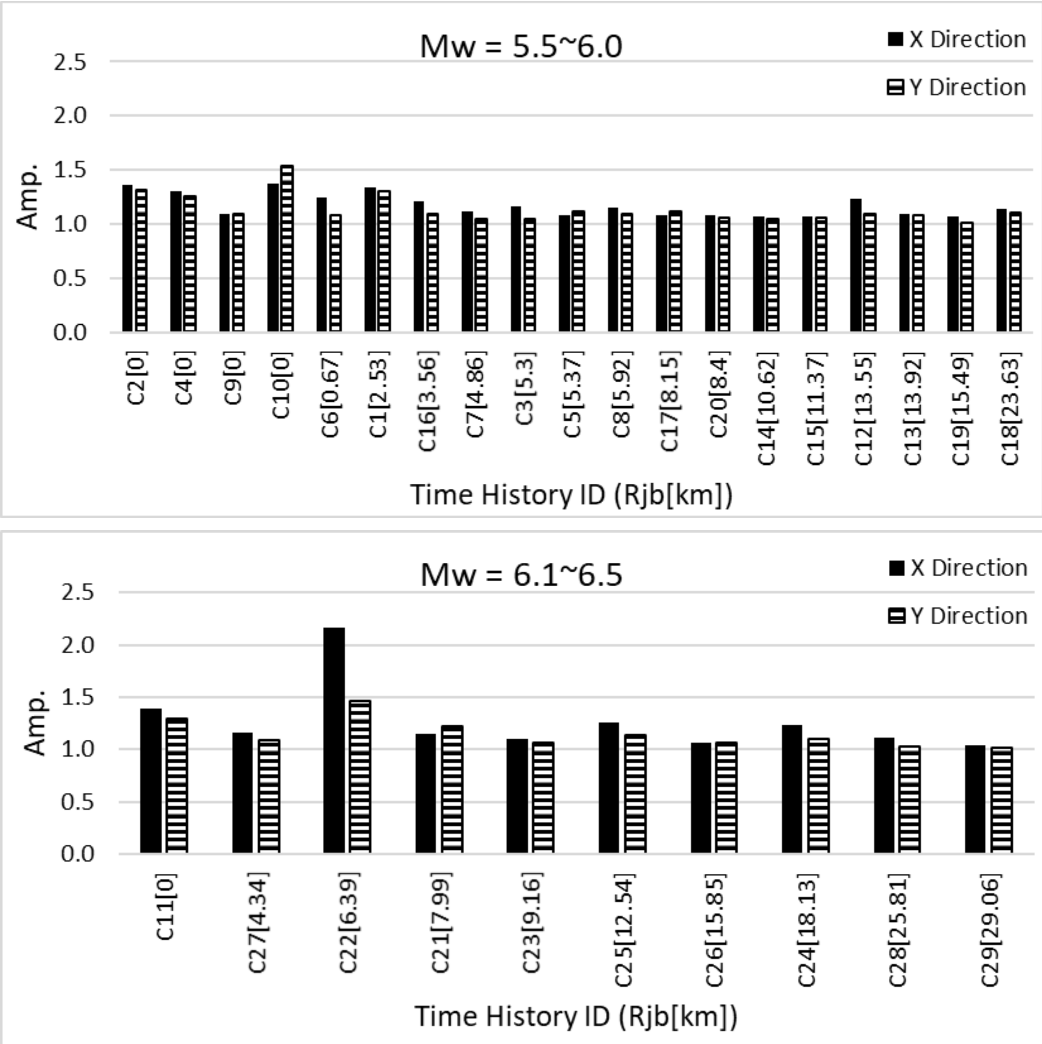

Figure B12. Story Shear Force Results for Site Class C